LUT UNIVERSITY
LUT School of Energy Systems
LUT Mechanical Engineering

Kalle Lipiäinen

FATIGUE OF THERMALLY CUT EDGES ON HIGH STRENGHT STEELS

20.6.2019

Examiners: Professor Timo Björk
M. Sc. (Tech.) Antti Ahola

TIIVISTELMÄ

LUT-Yliopisto
LUT School of Energy Systems
LUT Kone

Kalle Lipiäinen

Termisesti leikattujen reunojen väsyminen suurlujuusteräksillä

Diplomityö

2019

119 sivua, 88 kuvaa, 21 taulukkoa ja 1 liite

Tarkastajat: Professori Timo Björk
DI Antti Ahola

Hakusanat: termisesti leikattu reuna, teräksen väsyminen, 4R-menetelmä, suurlujuusteräs

Termisesti leikattujen reunojen väsyminen on tullut tärkeämmäksi kehittyneiden materiaalien ja hitsaustekniikan takia. Tässä työssä hyödynnettiin 4R-menetelmää leikattujen reunojen väsymiskestävyyden määrittämiseen. Tutkimuksessa mitattiin jäännösjännityksiä ennen koesauvojen kuormittamista ja tehtiin väsytystestejä CO_2 laser, kuitulaser ja plasma leikatuille reunoille S690QL-teräksellä. Kuitulaser leikattuja S1100 Plus teräksisiä koesauvoja väsytettiin vertailukohdaksi. Koetuloksista laskettiin FAT-arvot kaikille tuloksille ja jokaiselle koesarjalle erikseen.

Jokaiselle neljälle koesarjalle tehtiin metallurgia- ja murtopintatarkastelu. Särön ydintymiskohta eri koesauvoille tutkittiin pyyhkäisyelektronimikroskoopilla ja optisella profilometrillä. Laser leikatuille koesauvoille tehtiin alkuaineanalyysi ja löydettiin hapen aiheuttamia muutoksia alkuainekoostumuksessa. Terminen leikkaus vaikutti teräksen mikrorakenteeseen eri tavalla kuin hitsaus.

Olemassa olevia väsymisennusteita vertailtiin leikattujen reunojen väsymistarkastelussa. 4R-menetelmää kehitettiin leikatuille reunoille. 4R-menetelmälle ehdotettiin parametreja sekä suunnitteluvaiheessa että olemassa olevan rakenteen väsymistarkasteluun, mutta itse menetelmä ja siihen liittyvät parametrit vaativat vielä lisätutkimusta.

Tässä tutkimuksessa löydettiin yhteys pinnanlaadun lovivaikutuksen, jäännösjännitystilan ja paikallisten materiaaliominaisuuksien välillä. Leikattujen reunojen väsymiseen vaikuttavien tekijöiden tutkimisen lisäksi tutkittiin leikatun reunan väsymiskestävyyden parantamista.

ABSTRACT

LUT University
LUT School of Energy Systems
LUT Mechanical Engineering

Kalle Lipiäinen

Fatigue of thermally cut edges on high strength steels

Master's thesis

2019

119 pages, 88 figures, 21 tables and 1 appendix

Examiners: Professor Timo Björk
M. Sc. (Tech.) Antti Ahola

Keywords: thermally cut edge, steel fatigue, 4R method, high strength steel

Importance of thermally cut edges fatigue have increased along use of advanced materials and improved welding technology. 4R method for fatigue estimation was used in this thesis for thermally cut edges. Residual stresses were measured from specimens before loading. Fatigue testing for CO_2 laser, fiber laser and plasma cut edges on S690QL steel and for fiber laser cut S1100 Plus. Fatigue test results were analyzed with FAT classes.

Metallurgy and fracture surface examination was done for all four test series. Fatigue crack initiation site was researched and reasons for fatigue characteristics were researched with SEM and optical profilometer. Elemental analysis for laser cut edges were done with EDS-detector and changes close to cut edge was found when oxygen was present at cutting. Thermal cutting also affected microstructure and hardness differently compared to welding

Previous fatigue estimation methods were compared, and 4R method was developed for thermally cut edges. Parameters for both design phase and existing structure were proposed and tested but further measurements and development is still needed for method verification.

In this thesis correlation between surface profile, residual stress state and local material properties were found. Alongside fracture initiation point and fatigue performance affecting parameter research also method for fatigue performance improvement were developed.

ACKNOWLEDGEMENTS

This thesis was done for LUT University Laboratory of Steel Structures. I would like to thank Professor Timo Björk for providing challenging topic and good guidance during project. Antti Ahola and Tuomas Skriko also supported my research work with valuable advices.

I would also like to thank Matti Koskimäki, Jari Koskinen, Mika Kärmeniemi and Olli-Pekka Pynnönen for laboratory work. Antti Heikkinen and Toni Väkiparta helped me a lot of in metallurgy and fracture surface examination.

I want to express my gratitude for Satu who encouraged me during studies. Support especially during this thesis was very important.

Kalle Lipiäinen
Lappeenranta 20.6.2019

TABLE OF CONTENTS

LIST OF SYMBOLS AND ABBREVIATIONS

$area$	$\sqrt{10}$·depth [μm] on single circumferential notch	[μm]
b	fatigue strength exponent	[-]
c	the fatigue ductility exponent	[-]
C_{ref}	mean or characteristic, value, $10^{21.59}$ or $10^{20.83}$	[-]
C_σ	surface quality reduction factor	[-]
FAT	stress variation at $2 \cdot 10^6$ cycles	[MPa]
E	modulus of elasticity	[GPa]
f_u	tensile strength	[MPa]
$H_{HAZ/soft}$	local hardness	[HV]
H_{bm}	base material hardness	[HV]
m	slope of SN-curve	[-]
m_{ref}	slope of reference curve, 5.85	[-]
N_f	estimated life time	[-]
R	stress ratio	[-]
R_z	surface quality value	[μm]
R_m	material tensile strength	[MPa]
$R_{m,HAZ/soft}$	local tensile strength calculated from hardness	[MPa]
$R_{m,bm}$	base material tensile strength	[MPa]
R_{local}	local stress ratio	[-]
$R_{p0.2}$	yield strenght	
ε_f'	fatigue ductility coefficient	[-]
$\Delta\varepsilon/2$	strain amplitude	[-]
σ	stress	[MPa]
σ_f'	fatigue strength coefficient	[-]
CO_2	Carbon dioxide	
DT	Destructive testing	
FEA	Finite element analysis	
HAZ	Heat affected zone	

HCF	High cycle fatigue
HFMI	High-frequency mechanical impact treatment
HSS	High strength steel
IIW	International Institute of Welding
UHSS	Ultra high strength steel
LCF	Low-cycle fatigue
LEFM	Linear elastic fracture mechanics
MC	Thermo-mechanically treated and cold formable
MSSPD	Minimum square sum of perpendicular distances
NDT	Non-destructive testing
QL	Quenched and low temperature tough
QT	Quenched and tempered
QC	Quenched and cold formable
SDT	Semi destructive testing
SEM	Scanning electron microscope
SN-curve	Stress-cycle curve, also known as Wöhler curve

1 INTRODUCTION

High-strength-steels (HSSs) and Ultra-high-strengthsteels (UHHS) are used in weight critical applications. Automotive and crane industries are typical users of high-strength materials because of possibility to lower CO_2 footprint of product during its lifetime. Automotive and crane manufacturers use HSSs to maximize net lifting or transporting capacity due to weight restrictions. To utilize the potential of advanced materials the manufacturing, structural design and design codes should be also updated to meet potential of materials.

Welded joints made of high-strength materials have been main interest in previous studies. In this thesis, fatigue properties of cut edges are examined as phenomena instead of statistical evaluation of fatigue testing that has been done previously. Research work of Peippo (2015) was used as a basis of this thesis to give ideas for further research and better adaption of the 4R method. Also research from Timo Björk and Timo Nykänen was adapted for cut edges. Assumptions regarding fatigue were made during research process from literature data and from own research. These assumptions were tried to be validated with measurements and microscopic investigations when possible.

In this research work the fatigue strength of thermally cut S690QL and S1100 Plus steels are studied. Specimens are cut with CO_2 laser, fiber laser and plasma cutting. Oxy-fuel cutting was not considered in this research because it has significantly lower fatigue resistance on cut edges than laser or plasma cutting and different characteristics of cut edge. Residual stresses and surface quality of edge was measured for comparison of different processes and parameters, but also in order to compare with results from previous studies.

The study consists of literature review, experimental tests and fatigue design code adaption for thermally cut edges. In literature review, the cutting methods are characterized by the surface quality, hardness and residual stresses. Static test for laser cut S690QL specimen was performed to obtain static strength characteristics of the base material. Fatigue test results from previous studies are researched to find comparison for LUT University fatigue testing. Also the alternative methods for fatigue strength assessment are presented for comparison. Experimental tests results are compared to the computational fatigue lives obtained using

different approaches. Local and global stresses are used and notch effect of surface defect has been considered as an extra notch factor or defect size by Murakami's *area* parameter (Murakami 2002). This thesis includes re-analysis of existing studies because of only straight cut edges were tested and 4R method was wanted to be applicable to curved edges also.

The 4R method is applied to estimate fatigue life of thermally cut edges. Following parameters are utilized in the 4R calculations. Stress range $\Delta\sigma_k$ from FEM (finite element method) or strain gauges, external loading stress ratio R estimated or obtained from strain gauges, material tensile strength R_m from material certificate or estimated by local hardness, and residual stress σ_{res} from recommended values or measured by X-ray diffraction. 4R method can be utilized on design phase or for existing structure.

Correlation between surface quality and local stress was studied. Residual stresses were characterized for the different cutting methods and steel grades. In the experimental part of the thesis, residual stresses are measured with X-ray diffraction only from cut and rolled surfaces but in literature review the residual stress profile along the thickness is researched as hardness profile also. Crack propagation starting from the weakest point of detail and on thermally cut edges is researched with various failure modes.

Research questions in this thesis are:

- Which location on thermally cut edge is the most critical to crack nucleation?
- What are the main parameters to assess the fatigue strength of a thermally cut edge?
- Which of the fatigue strength assessment method is the most suitable for the thermally cut edges?
- What are the main characteristics for a high quality cut edge in terms of fatigue strength capacity
- How the 4R method can be used to estimate the fatigue life of a cut edge?
- How fatigue performance of thermally cut methods could be improved?

Schematic thermal cutting process is presented in figure 1 with terminology used this thesis. Term cutting direction was used for cutting head travel direction. Plate top side was starting side of jet while bottom side was leaving side of jet. Plate top and bottom surfaces are determined as rolling surfaces and for S690QL material rolled surfaces are also described as blasted surfaces due to delivery condition of plate material. Burr was attached in the plasma and fiber laser cutting to bottom side of plate.

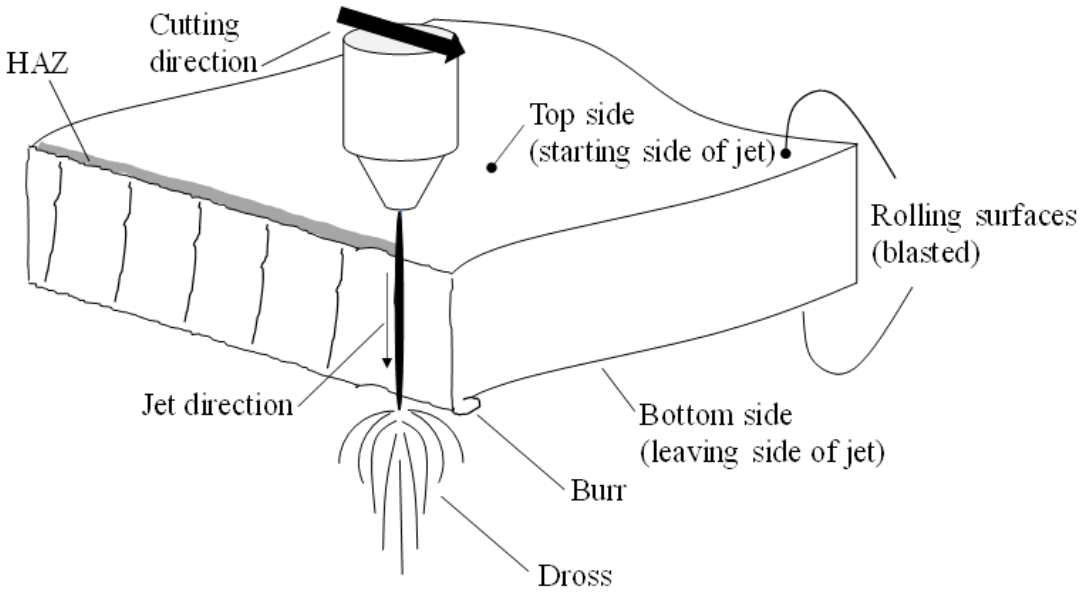

Figure 1. Schematic thermal cutting process with terminology used in this thesis.

2 LITERATURE REVIEW

Fatigue of welded structures have been studied and different fatigue strength assessment methods have been developed. Most of the known methods take only few aspects into, account such as fatigue capacity of critical detail, stress range and different treatments for critical detail. For HSSs and UHSSs, these basic parameters are not enough to utilize the full potential of material. Eight-step template (Figure 2) was originally made for welded joints but all steps are relevant also for cut edges. For example, structural stress can be low for straight cut edge but small flaws in designed geometry or global geometry influence fatigue strength by stress concentration factors thus reducing fatigue strength.

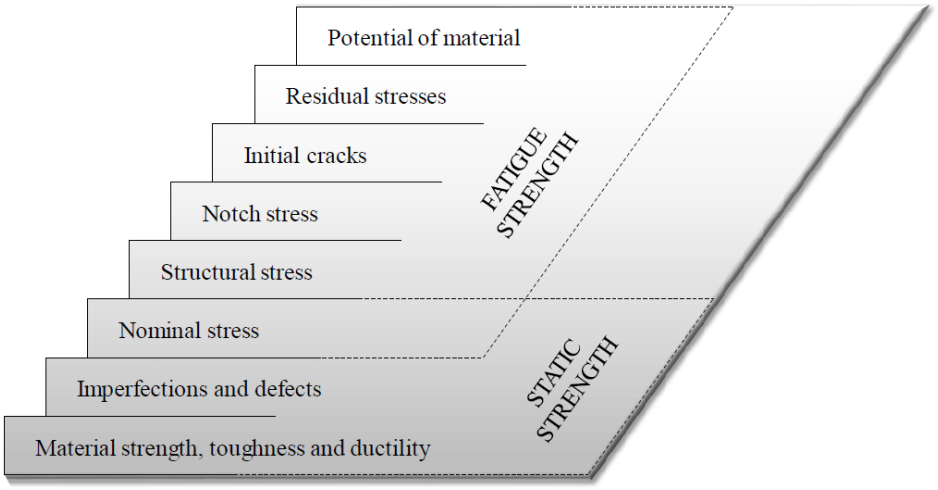

Figure 2. Eight-step template for fatigue strength for welded joint (Skriko 2018 p. 35, original Björk et al. 2008).

In this research, the term fatigue limit is used. Fatigue limit does not mean absolute limit of stress where no fatigue failure would happen but the knee point before 5─10 million cycles on welded structures where run out -level on fatigue testing is experienced and 2 million cycles on cut edge testing. Fatigue limit itself have been researched widely and Murakami approach was considered for 10^7 cycles in this thesis because of its simplicity for parameter determining for regular defects like shot blasted surface and cut edge (Murakami 2002). More advanced theories are available for example Rabb's probability-based fatigue limit theory but usability of the advanced theory is limited due to more complex parameters (Rabb 2012).

2.1 Steel grades

HSS in 690 MPa yield strength are usually hot rolled and quenched (Q) or thermo-mechanically treated (M). Quenched steels are classified to C (cold formable) and L (low-temperature tough) classes. In 700 MPa yield strength grade, thermo-mechanically treated sheets are limited to thicknesses below 12 mm while quenched plates are available up to 160 mm thickness. Different alloying elements are used on manufacturing processes. (SSAB 2006 & SSAB 2009) On 1100 MPa yield strength class all available material are hot rolled but differed heat processing is done. Depending on material strength and manufacturing process, the grades are available either coils or cut to length sheets. Chemical composition influence weldability of steels. Effect of steel grade on weldability has been researched widely but chemical composition and manufacturing process effect on thermally cut edges is not reported widely.

2.2 Thermal cutting methods

Thermal cutting of welded structures is defined in the EN1090 standard by execution classes from EXC1 to EXC4. On more demanding structures better perpendicularity and mean height of the profile are demanded. The most demanding class EXC4 qualifies only R_z value below $70 + 1.2 \cdot t$ and perpendicularity of $0.4 + 0.01 \cdot t$ where t is plate thickness in millimeters. For a 12 mm sheet, these values are for R_z 85 μm and 0.52 mm for perpendicularity. Execution classes also defines maximum allowable hardness values of cut edges. For S235-S460 the maximum permitted hardness is 380HV and with S700 grade the maximum hardness is 450 HV measured with HV10 hardness test. The hardness of heat affected zone (HAZ) with standard procedure is challenging to measure and may give conservative results due to narrow HAZ compared to measurement point size. Surface quality is concern when using fiber laser cutting on thick sheets and perpendicularity and hardness especially with plasma cutting.

Laser cutting can be done with different types of laser source. Two of the most common types are CO_2 and fiber laser. The main difference between laser types is wavelength. The wavelength of CO_2 laser is 10.6 μm while fiber laser has wavelength of 1.07 μm. Wavelength changes material absorption factor and different wavelengths and laser type affects surface quality. Cutting quality of fiber laser is usually worse than CO_2 laser and on thicker sheets, the surface quality of fiber laser decreases because of harder material removal from kerf.

Nitrogen is used as a cutting gas on thinner sheets and oxygen with thicker sheets. The power of laser restricts nitrogen usage while it offers better cutting quality and prevents cut edge from oxidizing. Usage of nitrogen as an assist gas prevents edge from oxidizing. Oxidized layer should usually be removed after cutting. (Mahrle & Beyer 2009 p. 8)

The cutting with laser is fusion cutting and the process is called as reactive fusion cutting if active assist gas is used. Active gas reacts exothermally with the cut material and another heat source is added to the cutting process. Optical energy transfer and mass transfer are presented in figure 3. Use of oxygen supplies 60% more heat than laser alone on mild steel and 90% with more reactive metals like titanium. Faster cutting speed provides narrower HAZ because lower diffusion time of heat. Shorter wavelength of fiber laser provides more energy for penetration of sheet but absorption factor of fiber laser reduces along cutting depth. (Steen 2010 p.156-182)

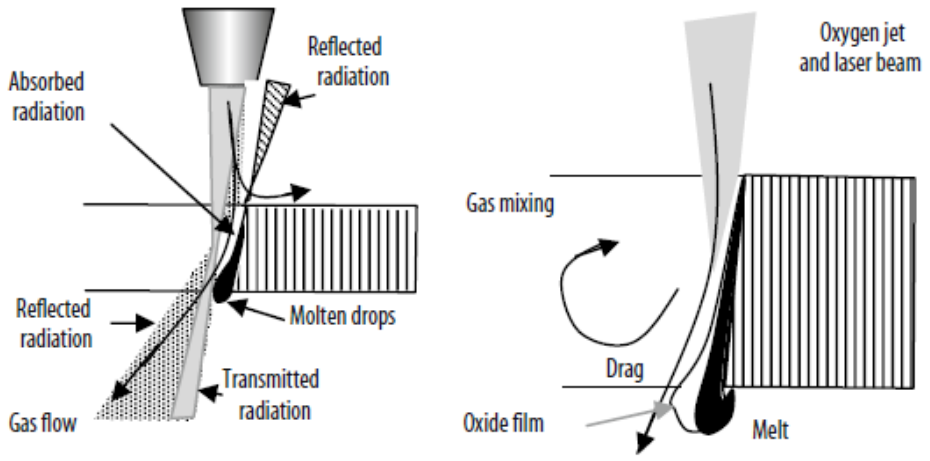

Figure 3. Optical energy transfer and mass transfer in laser cutting (Steen 2010 p.161).

Regular striations in laser cut edge are on laminar assist gas flow area and they end after flow turns turbulent. This is called as flow separation depth. Assist gas flow is important for dross free cut edge. Gas flow is controlled by nozzle size and gas pressure. Cut quality is the best with inert assist gas when cutting speed is reduced from maximum and assist gas pressure and flow is set to high level. With high flow and pressure of assist gas regular striation pattern can be achieved. Focal point position is important factor on thick sheet, over 6 mm, laser cutting. Focal point position determines the width of kerf and together with assist gas material removal from kerf is controlled. Fiber laser cutting benefits from locating

focal point inside the work piece or even to bottom of the sheet if power is sufficient to penetrate the top surface. (Wandera, 2010)

The power of fiber lasers have been increasing and 10─12 kW lasers have become available while CO_2 lasers are usually limited to 6 kW due to limitations of optics. Fiber laser with 10 kW power is able to cut 15 mm thick steel sheets with nitrogen as an assist gas. With oxygen cutting the capacity increase to 25─30 mm thick sheets. Maximum cutting speed of 60 m/min is achieved with 1 mm sheet thickness. Versatility of fiber laser cutting systems has increased due availability of high power machines. Cutting maximal thickness sheets with fiber laser reduces the quality of cut surface because focal point must be moved up and material removal from kerf becomes more difficult.

Plasma arc cutting is widely used thermal cutting method that as an alternative to laser cutting. Plasma- and shielding gas is blown from the nozzle. Plasma arc (figure 4) is created by electric current between the electrode and work piece. Temperature in plasma arc can increase to 30 000 K. Plasma cutting can be done submerged in water. (Fridman, 2008)

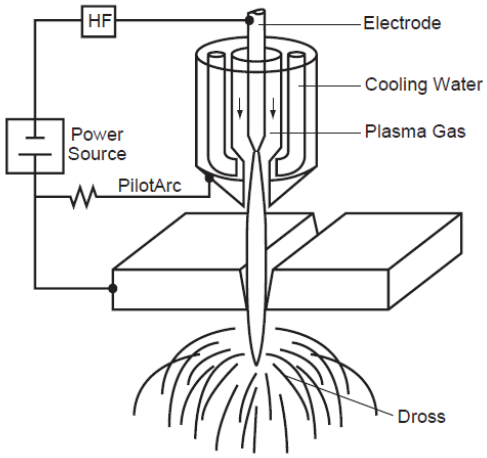

Figure 4. Principle of plasma cutting. (Fridman, 2008)

Material removal from the kerf is challenging with short wavelength lasers. The dross may form stress concentration to bottom of the cut surface. Pessoa et al. (2017) examined crack initiation location on laser cut stainless steels. AISI 304 stainless steel with thickness of 4 mm were cut by a disk laser with 1030 nm wavelength and 3 kW power. Nitrogen was used as cutting gas with 14 bar pressure, focal point was positioned 2.6 mm below top surface and 5000 mm/min cutting speed was used. Similar specimens were tested as cut condition

and with trimmed cutting edges without burr. Trimming the burr increased the fatigue strength by 33%. In figure 5, the burr and the crack initiation from notch effect of burr is presented in a SEM-image. When burr was removed the crack initiation location moved away from bottom corner of cut to initiate from striation on cut surface. The SEM-images were taken from specimens failed at $1.9 \cdot 10^6$ (burr) and $4.2 \cdot 10^6$ cycles (burr removed) with equal 370 MPa loading. Crack initiation from burr-removed specimen was at the surface near a pore between the recast layer and HAZ.

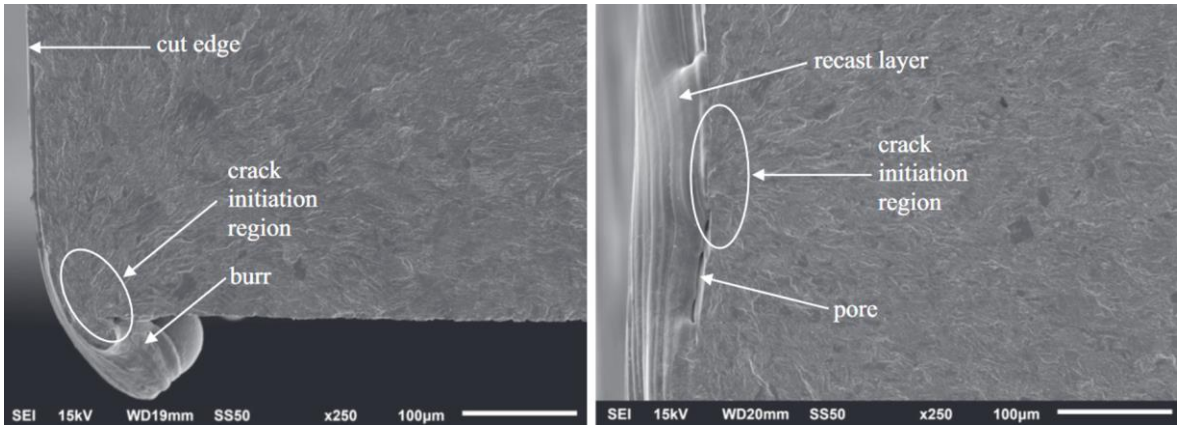

Figure 5. Laser cut edge and crack initiation location from burr and burr removed specimens. (Modified Pessoa et al. 2017)

2.3 Residual stresses and hardness of cut surface

Residual stresses are inner stresses form by cooling or phase deformation. Residual stresses may be relaxed at least partly during cyclic loading. Their influence on fatigue life is greater on HSSs because of higher stability than on lower tensile strength steels and higher stress values on HSSs. Compressive residual stresses have positive impact on fatigue strength and tensile residual stresses reduce the fatigue performance. Overloading of a structure or detail may relax residual stresses and it should be considered on fatigue analysis.

Residual stresses can be measured by non-destructive testing (NDT) with e.g. X-ray diffraction or semi- or destructive testing (SDT & DT) for e.g. by hole drilling. Without any treatments the X-ray diffraction only measures residual 1─10 micrometers under the surface but using electro-polishing or removing material by etching measurements up to 1 mm can be done. 1 mm measuring depth is enough for thermally cut edges because HAZ is usually

significantly narrower. With hole drilling the complete residual stress distribution over the plate thickness can be measured.

Remes et al. (2013) measured residual stresses from plasma cut specimens in as cut, ground and sandblasted edges from rolled and cut surface. Both rolled and cut edge had compressive residual stresses as cut, although on plasma cut edge had only small compressive stresses were measured from -8 MPa (S460) to -64 MPa (S690Q) parallel to the loading. Grinding increased compressive residual stresses and sandblasting relaxed residual stresses. Lillemäe-Avi et al. (2017) researched same type of specimens than Remes et al. (2013) and compressive residual stresses were measured from S690Q plasma cut edges after grinding. Sandblasting relaxed residual stresses from rolled surface but not from cut edge.

Stenberg et al. (2016) researched S700 steel cut edges residual stresses from 16 mm thick specimens (6 mm with water jet cutting). Results of the Stenberg's research are presented in figure 6. Residual stresses were highest at the middle of the cut surface on thermal cutting in both tensile and compressive directions. Laser and oxygen cut surfaces had compressive residual stresses while plasma cut edge has small tensile stress.

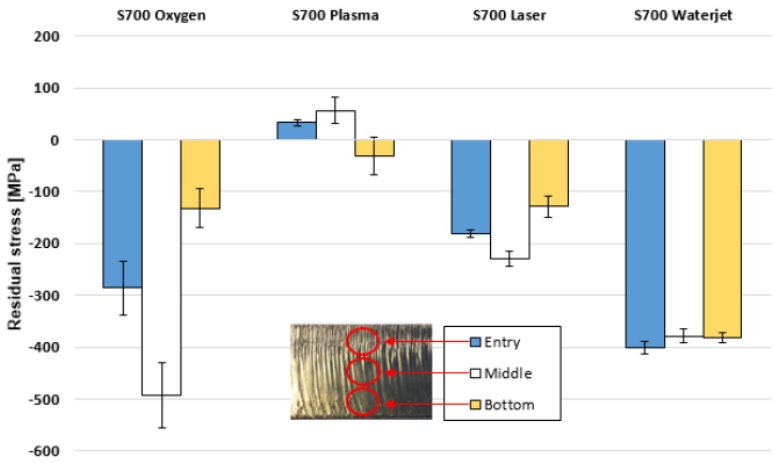

Figure 6. Residual stresses at cut edge. (Stenberg et al. 2016)

Riski (2017) researched S960QC steel with t = 8 mm low cycle fatigue (LCF) and residual stresses were measured from edges of laser cut, waterjet cut and machined specimens. Tensile residual stresses of 126 MPa, with 9 MPa variation, were measured from middle of cut edge on machined while fiber laser cut edges had average 190 MPa tensile residual stresses with 48 MPa variation. Water cut edges had high compressive residual stresses with

average of -319 MPa with 7 MPa variation. Surface quality or hardness was not measured from cut edge specimens. Also measurements from laser cut specimen was done on the center point of specimen from the rolled surface. Parallel to the loading, 48 MPa tensile and transverse to the loading -89 MPa compressive residual stress was measured.

Laitinen, Valkonen & Kömi (2013) measured residual stresses from CO_2 laser cut S900 QC steel made from several thicknesses. High concentration of both longitudal (0 deg), parallel to loading, and through thickness (90 deg) direction tensile residual stresses was found 0.2─0.4 mm below the cut edge from soft zone. Compressive residual stresses of -130 to -280 MPa were found through thickness direction from edge to 0.2 mm depth. Residual stress profile from 0─0.5 mm depth from laser cut edge is presented in figure 7. Depth of measurements were defined by etching and measuring was done with X-ray diffraction.

Hardness was also measured in Laitinen et al. (2013) research. Vickers hardness of cut edge was 455 on HAZ and 323 on soft zone after HAZ where 700 MPa tensile residual stresses were measured. Crack propagation was expected from soft zone instead of hardened zone on the edge.

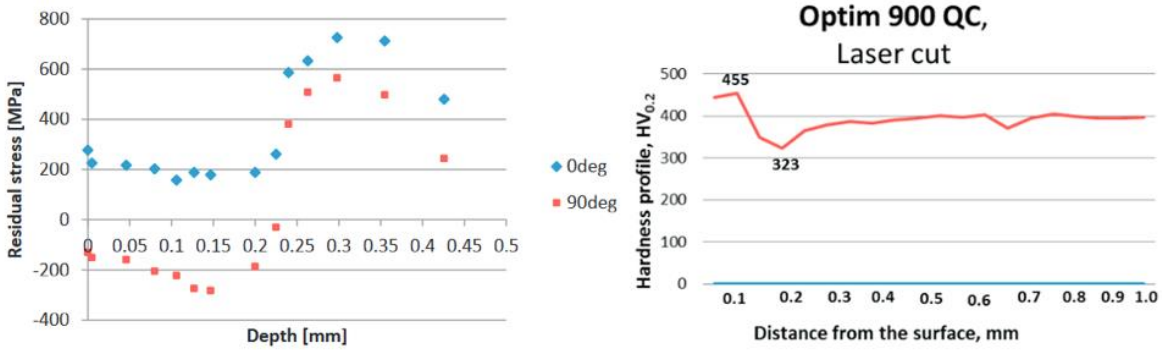

Figure 7. Residual stresses and $HV_{0.2}$ hardness from CO_2 laser cut edge of Optim 900 QC (Modified Laitinen et al. 2013)

In the HIPERCUT (2016) project, residual stresses were measured and residual stress distribution was made for different steel grades and for plasma and laser cut edges. Electro-polishing was used to measure residual stresses from various depths. Residual stresses from the 100 µm and 500 µm depths are presented in table 1. Residual stresses were compressive under 100 µm in as cut condition except S700MC with laser cut edge. In laser cut edges, tensile residual stress increase after 250 µm depth and on plasma cut edges after 500 µm.

The HAZ of plasma cutting and measurement ended to 700 µm where plasma cut edges had tensile residual stresses from 200 MPa to 800 MPa. On 700 µm depth the tensile residual stresses in laser cut edges were generally lower than on plasma cut edges. Residual stresses on S700MC and on S690Q steels were completely different. S700MC was thermo-mechanically treated and S690Q quenched and tempered. Fatigue test for S700MC were not conducted so fatigue performance of these two steel grades could not be compared.

Table 1. Residual stresses in longitudal direction (HIPERCUT 2016 p. 96).

Grade	Thickness [mm]	Cutting method	Long. Residual stress depth 100 [µm]	Long. Residual stress depth 500 [µm]
S700MC	8	Plasma	-24	-167
S700MC	8	Laser	193	612
S690Q	15	Plasma	-471	-537
S690Q	15	Laser	-149	590
S890Q	15	Plasma	-479	-569
S890Q	15	Laser	-97	772

In figure 8, all the measurements are reported graphically, and general trend evaluation could have been done. From residual stress data should be noted that compressive residual stresses measured from plasma cut edge from table 1 turned highly tensile with increasing steel grades at the end of measuring range at 700 µm. In measurements only an approximative residual stress distribution was determined because of high, 100─200 µm, material removal between measurements steps occurred. Highest values of residual stresses may not have been found in some specimens due to high step increment between measurements.

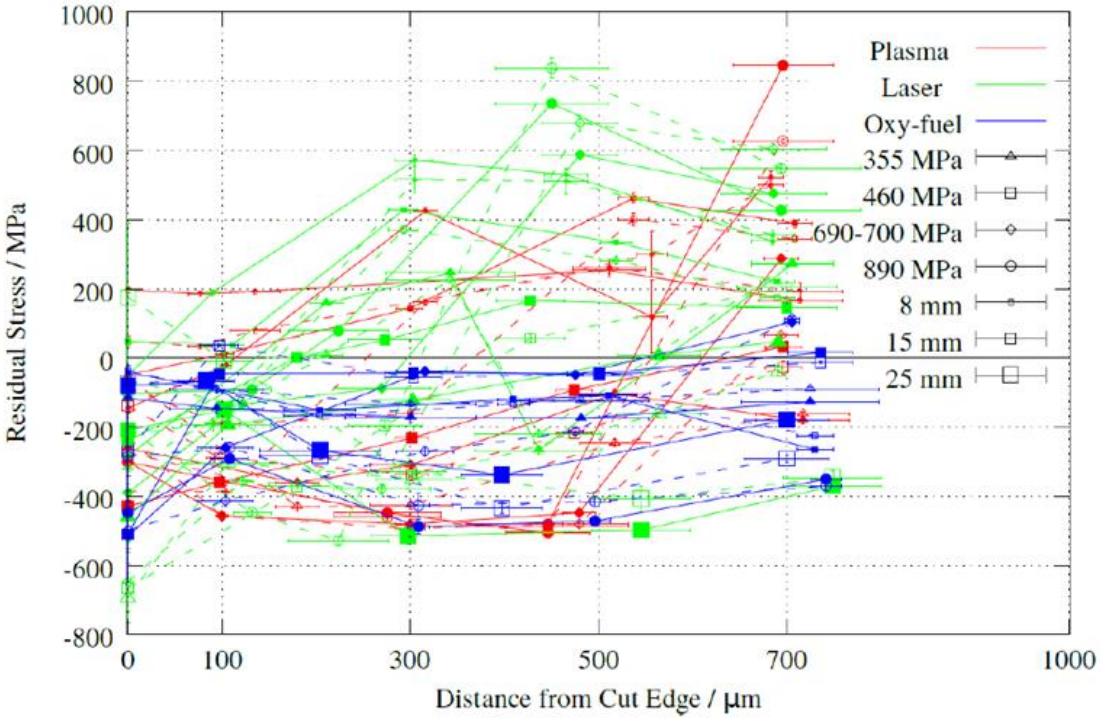

Figure 8. All residual stress data from the HIPERCUT project (HIPERCUT 2016 p. 92).

In the HIPERCUT project, the grinding turned compressive residual stresses to tensile residual stresses. The result of grinding was contrary to the results found in Remes et al (2013) and Lillemäe-Avi (2017) results where grinding induced compressive residual stresses. Residual stresses and surface roughness values could have not explained fatigue characteristic of specimens because both were better on plasma cut specimens but laser cutting had better fatigue resistance.

Zanon et al. (2017) researched fatigue characteristics of S355N laser cut edge. Residual stresses were measured from S355N with CO_2 laser cut edge with oxygen as assist gas. Hardness of HAZ was 300 HV while base material hardness was below 200 HV. Residual stresses were measured in three directions at the middle of cut surface. The measurements were conducted by X-ray diffraction and by removing material layers to measure various depths. Residual stress measurements from 5 mm thick sheet and measurement directions are presented in figure 9. Tensile residual stresses equal to yield strength were measured after HAZ at 125 µm below cut surface.

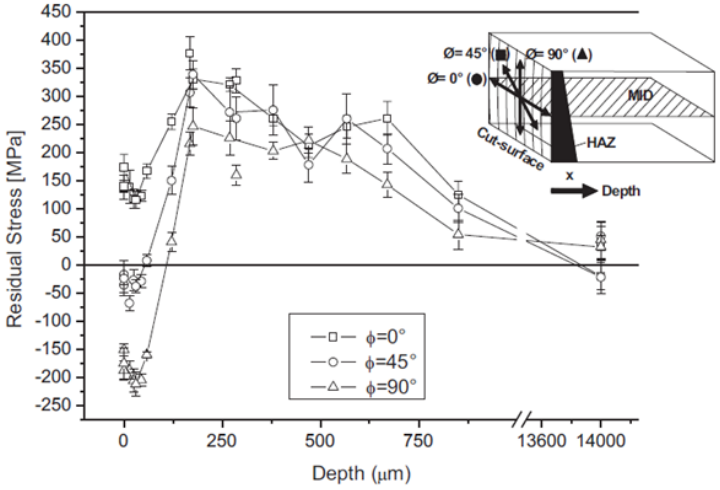

Figure 9. Residual stress profile in three directions on laser cut S355N edge. (Zanon et al. 2017).

Residual stress relaxation measurements were not available from literature for thermally cut edges, but Torres & Voorwald (2002) researched residual stress relaxation on shafts on AISI 4340 steel. Shot peening was used to produce compressive residual stresses for surface. Residual stress profile was measured with X-ray diffraction and electrolytic polishing. Compressive residual stresses had influence on fatigue life and on medium to high cycles moved fracture initiation point inside the shaft instead of surface. Residual stress relaxation was found to be relative to number of fatigue cycles and applied stress. Figure 10 shows the residual stress relaxation as a function of depth and with unstressed and run out tested specimens. The relaxation was most significant inside the shaft with 700─1000 MPa compressive residual stress relaxation.

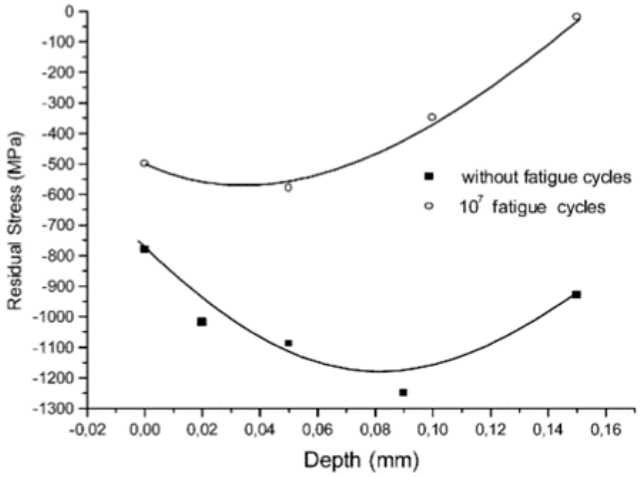

Figure 10. Residual stress relaxation on shot peened shaft. (Torres & Voorwald 2002).

The relaxation of residual stresses can be studied from post-weld treated welds, such as HFMI treatment. Leitner, Khurshid & Barsoum (2017) researched the stability of residual stresses with S355 and S960 steels by measuring residual stress with X-ray diffraction from the weld toe of HFMI-treated longitudal stiffener plate. On both material HFMI-treatment improved fatigue life and reduced the slope of SN-curve close to base material SN-curve. Residual stress relaxation was found to have two modes; first cycles and high cycle fatigue (HCF). The specimens were loaded with 250 MPa (S355) and 275 MPa (S960) stress range with stress ratio of 0.1 to run out -level at $5 \cdot 10^7$ cycles.

During first cycles there was significant residual stress relaxation. Then there was slow residual stress relaxation until the cycles representing the run out limit. Before loading -400 MPa residual stress was measured from the S355 specimen and after $5 \cdot 10^7$ cycles -100 MPa residual stress was measured. From the S960 specimen -700 MPa and -200 MPa corresponding values were measured. Results are shown in figure 11. Based on this research, the stability of residual stresses, when mild and HSS steel are compared, is complicated. The residual stress absolute value change was higher at the surface on HSS steel but still there was residual stresses left after $5 \cdot 10^7$ cycles and below the surface, the residual stresses were remained the same level. From S355 specimen the residual stress relaxation was measured after the first cycle and almost the half of compressive residual stress were relaxed. The measurement was repeated after five cycles and result remained steady. In the S960 steel grade, measurements of the residual stress relaxation was most significant near weld toe where local stress range was higher than inside material.

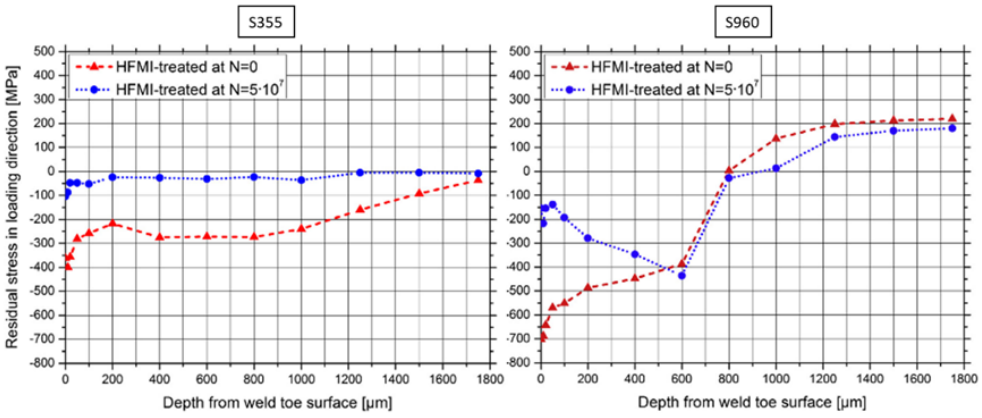

Figure 11. Relaxation of residual stresses from HFMI-treated weld. (Modified Leitner, Khurshid & Barsoum 2017)

The different characteristics of as welded (ASW) and treated weld residual stresses influence on residual stresses in data analysis because of opposite effect on fatigue life. On HFMI-treated welds compressive residual stresses have positive impact and on ASW-joints tensile residual stress have negative influence. The relaxation of residual stresses follows also these characteristics by decreasing the performance of HFMI-treated welds performance and improving ASW-joints on HCF-area.

Nano-hardness was measured also in the HIPERCUT-project and the CO_2 laser cut S690Q. The pores with fiber laser cut surface research carried out by Pessoa et al. (2017) were not visible in CO_2-laser cut edge SEM-image. The hardness had high peak to 5─7 μm depth for laser cut and to 30-50 μm depth it was measured with stable 600 HV hardness. Two measurement arrays were measured similarly and results from both arrays are shown in figure 12.

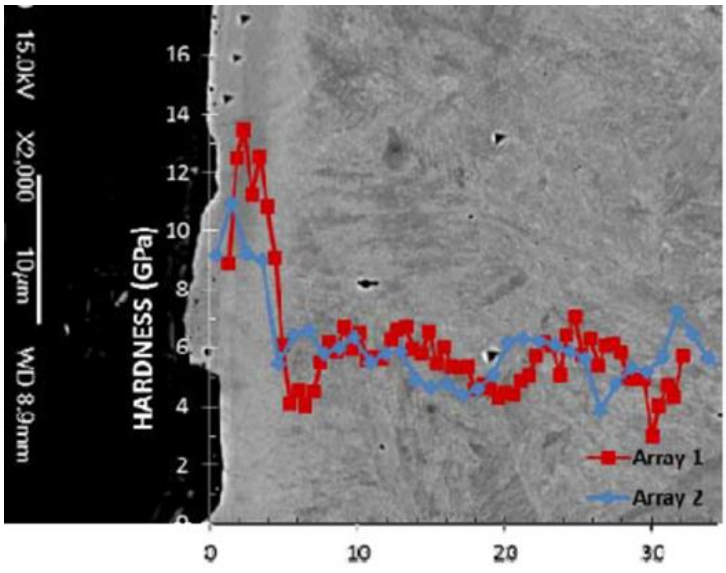

Figure 12. Nano hardness of CO_2 laser cut S690Q edge. (HIPERCUT 2016, p.87)

Novel mini tensile test specimens were cut from laser, plasma and oxy-fuel cut S460 specimens in the HIPERCUT project from several depths relative to cut edge. Close to cut edge, material had significantly increased yield strength and the yield strength decreased as a function of depth to nominal level of material. Plasma cutting had the highest heat input to specimen, widest HAZ and the highest yield strength on mini tensile specimens. These yield strength values follow hardness trend of nano and micro hardness tests and are presented in figure 13.

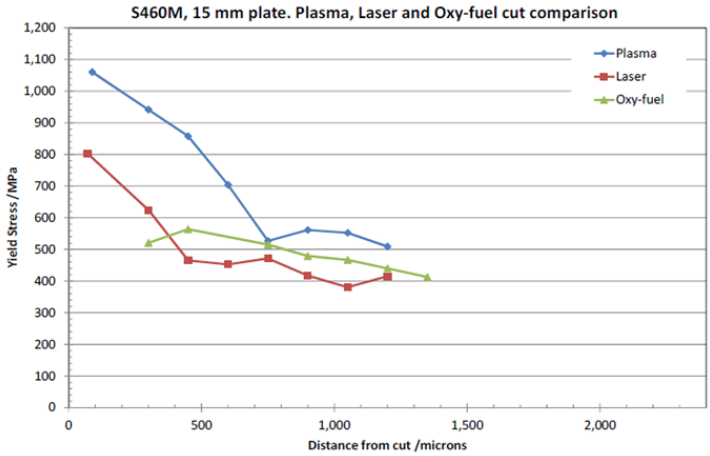

Figure 13. Trend of yield strength of mini tensile specimens (HIPERCUT 2016).

Peippo (2015) measured micro hardness of plasma and laser cut S355 steel. S355 hardness distribution with plasma and laser cutting are presented in figure 14. The first measurements were from 0.05 mm perpendicular distance to cut edge. These first points are usually excluded from measurements due to the challenges in measurements. Knowledge of material properties is still essential because of notch factor reduces along distance from edge.

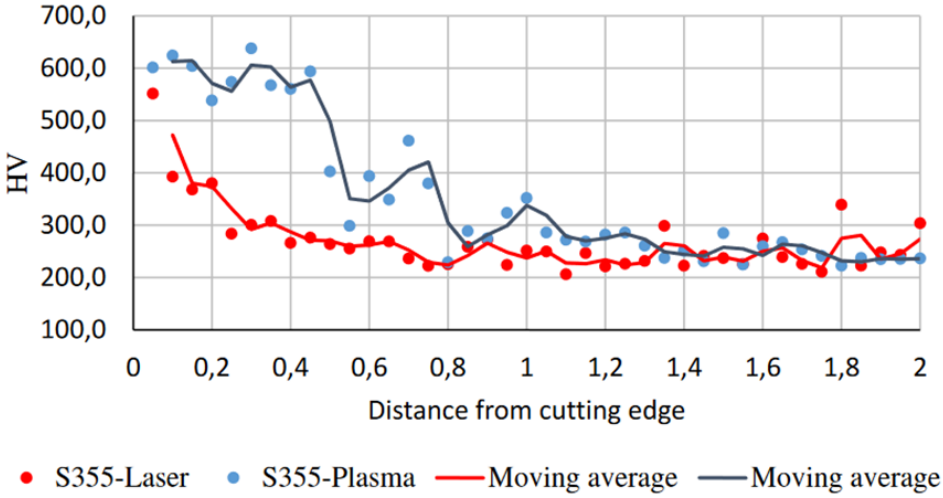

Figure 14. S355 hardness distribution with plasma and laser cutting. (Peippo 2015 p. 109)

Diekhoff et al. (2019) measured hardness profile of S690Q oxygen, plasma and laser cut edges. HAZ of laser cut edge was narrow and increased hardness was measured only from one point. Plasma cutting exceeded EN1090 standard permitted hardness value with $HV_{0.1}$ 510 and the HAZ was significantly wider than on laser cut edge. Residual stresses were also measured with X-ray diffraction method from cut surface. The results are presented in table 2. All residual stresses from laser and plasma cut edges were tensile for S690Q steel.

Residual stresses from thermo-mechanically rolled S355M and normalized S355N were also measured. Thermo-mechanically rolled plates were 8 mm thick while normalized plates were 20 mm thick but still difference in residual stresses can be seen. Residual stresses in thermo-mechanically rolled plates were highly tensile on both laser and plasma cut edges.

Table 2. Residual stress measurements from Diekhoff et al. (2019)

Grade	Cutting method	Thickness [mm]	Cut surface residual stress [MPa]
S690Q	Plasma	8	39
S690Q	Laser (low speed)	8	540
S690Q	Laser	8	147
S690Q	Plasma	20	99
S690Q	Plasma	20	100
S355M	Plasma	8	208
S355M	Laser (Low speed)	8	728
S355M	Laser	8	320
S355N	Plasma	20	-36
S355N	Plasma	20	-16

2.4 Estimations for fatigue life

Fatigue life of steel structures can be estimated by different methods. Fatigue life can be expressed with a mean or characteristic value. Mean values are fitted to points with 50% survival probability while characteristic values represent 97.7% survival probability. Mean values can be estimated to characteristic values from IIW recommendations with safety factor of 1.37. FAT-values are given at two million cycles. (Hobbacher 2007)

2.4.1 Fatigue testing

Fatigue testing of structure is the most accurate way to determine structures fatigue properties although it is the most expensive and slowest method. Fatigue life verification by testing may be economical on weigh concerned applications like aerospace industry. Verification by testing allows possibility to use 40─50% higher stress in design phase with respect to the design codes (Hobbacher 2007).

2.4.2 Nominal stress method

Standards and design codes offers various FAT-classes for thermally cut edges. FAT-classes for nominal stress method varies between 125 and 280 MPa with m = 3 and m = 5 values.

Definition of FAT-classes is difficult and design codes may be conservative about FAT-classes. Fatigue life can be calculated with nominal stress method after defining *m*-value and FAT class. Nominal stress can be difficult to define on structures and it does not consider structural detail or residual stresses that has effect on fatigue life especially on high strength steels.

$$N_f = \left(\frac{FAT}{\Delta\sigma}\right)^m \cdot 2 \cdot 10^6 \quad (1)$$

Where

$\Delta\sigma$	Nominal stress variation	[MPa]
N_f	Estimated life time	[cycles]
FAT	Stress variation at $2{\cdot}10^6$ cycles	[MPa]
m	Slope of SN-curve	[-]

2.4.3 Critical distance approach

Fatigue estimation can be done by several different stress obtaining approaches. Nominal or maximum stress can be used and then critical distance method can be used where material strength and notch sensitivity are determined the distance from notch bottom to stress obtaining depth. In critical distance method, higher stress is used for HSS than mild steel because of notch sensitivity. The method does not consider changing material parameters due to heat input and it is correlated with base material properties not actual properties on detail.

2.4.4 Surface quality reduction

In FKM-Guideline, the surface roughness factor have been presented. For steels the equation for axial stress is shown in equation 2. Equation does not take width or form of striation into account and it utilizes notch sensitivity of higher strength material although high strength material benefit from slower crack nucleation.

$$C_\sigma = 1 - \ 0.22 \cdot \log(R_z) \cdot \log\left(\frac{2 \cdot f_u}{400\ \text{MPa}}\right) \quad (2)$$

Where

C_σ	Surface quality reduction factor	[-]
R_z	Surface quality	[µm]
f_u	Tensile strength	[MPa]

2.4.5 Strain-life method

Strain-life method is developed to reduce fatigue testing by creating parameters from material properties. Low-cycle fatigue tests are made to fit strain-life curve. Plastic and elastic strains are summed to total strain. Strain-life fatigue strength is calculated with equation 3. The local strain can be measured from real structure, calculated with analytical equations or obtained from FEA. Elastic strain will be dominant when LCF regime is passed.

$$\frac{\Delta\varepsilon}{2} = \frac{\sigma_f'}{E} \cdot \left(2 \cdot N_f\right)^b + \varepsilon_f' \cdot \left(2 \cdot N_f\right)^c \quad (3)$$

Where

Δε/2	strain amplitude	[-]
σ_f'	fatigue strength coefficient	[-]
E	modulus of elasticity	[GPa]
b	fatigue strength exponent	[-]
ε_f'	fatigue ductility coefficient	[-]
c	fatigue ductility exponent	[-]

Potiris & Mettänen (2018) used strain-life –method to evaluate fatigue life of thermally cut and ground edges. S690QL steel with 60 mm plate thickness was used with macro geometrical rounding with radius of 120 mm. Factors of 0.75 and 0.92 were used to reduce surface quality of ground edge and size of machine element from fatigue strength exponent. Mean results from fatigue analysis with strain-life –method estimated 15 times longer fatigue life than IIW standard with 140 FAT-class and 7.5 times higher than the EN13001 –standard with 200 MPa FAT-class. FAT classes were obtained from design codes according to material strength and surface quality. The strain life diagram from case study is presented in figure 15.

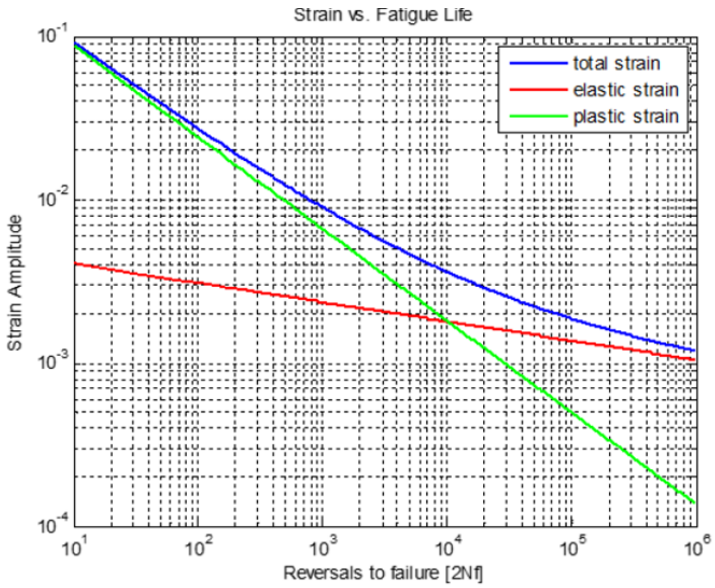

Figure 15. Strain-life curve for S690QL (Potiris & Mettänen 2018)

2.4.6 Linear elastic fracture mechanics

Linear elastic fracture mechanics (LEFM) estimates crack growth time as a function of stress intensity factor by Paris' law presented in equation 4. LEFM can be used typically for practical applications by finite element method (FEM). Crack growth is simulated by updating element mesh in FEM to estimate the stress intensity factor.

$$\frac{da}{dN} = C \cdot K^m \tag{4}$$

Where

a	Crack length divided by depth
K	Stress intensity factor
C	Material parameter
m	Material parameter

LEFM may be conservative on small under 0.5mm long cracks (Suresh & Ritchie, 1984). LEFM may not be suitable for fatigue estimation of small under 100 µm that represents R_z value of cut surface. However further analysis in this thesis prove the short crack behavior in notches of laser cut edges with fiber laser cut edges where pores or burr located on bottom of the notch have recuced fatigue life that figure 16 estimates.

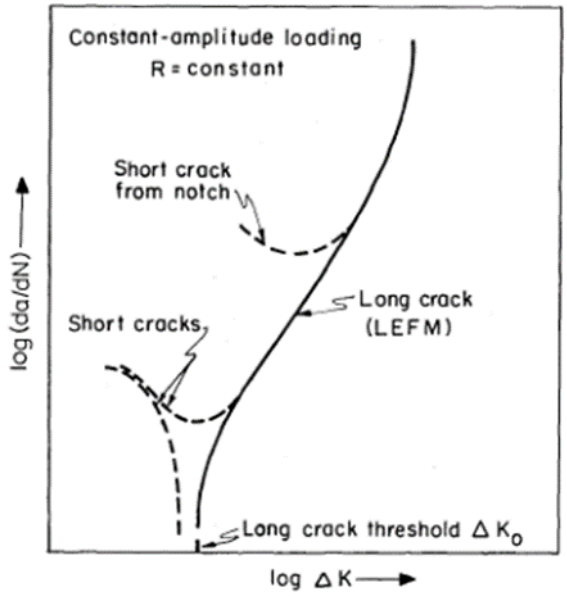

Figure 16. Propagation of short cracks compared to LEFM. (Suresh & Ritchie 1984)

Barmicho (2015) used LEFM analysis with the commercial AFGROW (Air Force Grow) software. Crack depth was set to R_z value of cut edge. When two million cycle fatigue life was was expected with 10 μm crack length, the stress was below 200 MPa and with 100 μm crack which is typical for laser cut edge, the stress was significantly lower, below 150 MPa.

Figure 17 presents Kitagawa – Takahashi (KT) diagram that include the EI-Haddad modification for low and high-strength structural steels. HSS have higher notch sensitivity and their fatigue limit is effective on shorter crack lengths. In the KT diagram, the first horizontal line represents the fatigue limit of smooth material and the second sloped line the LEFM prediction of fatigue life. El-Haddad have modified the diagram to be suited for short cracks with transition curve between smooth specimen and notched specimen with LEFM by modifying effective crack length. Sperle (2008) presented diagram for different steel grades crack nucleation and growth. HSS have longer crack nucleation time than lower strength steels but equal crack growth rate.

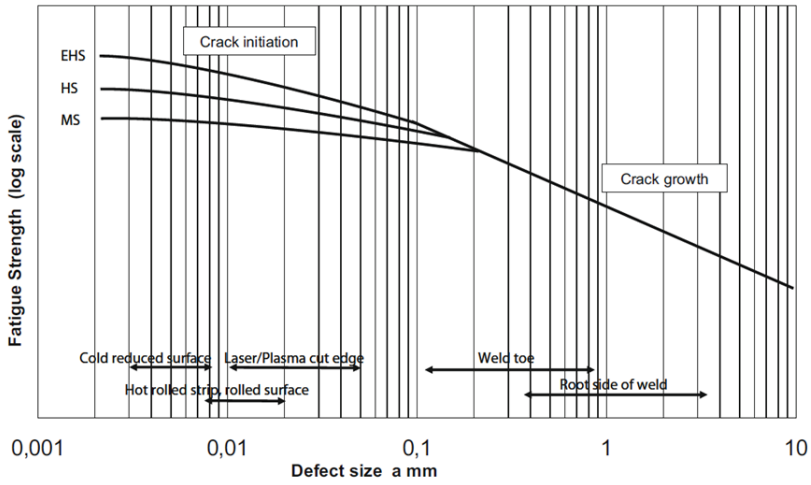

Figure 17. Kitagawa- Takashi diagram for different steel grades and defect conditions (Sperle 2008).

2.4.7 Hardness based fatigue limit

Fatigue limit of base material can be estimated from hardness. On cut edges, there is softening of material after HAZ. The softened base material can be the crack nucleation point even though the stress concentration of notch effect on cut edge. The equations from Garwood et al. (1951) shows correlation between base material fatigue limit and hardness. These equations are tested with base material specimens and residual stress influence is not considered. In thermally cut or welded specimens, the residual stresses have negative effect on obtained fatigue limits.

$$\sigma_w \sim 1.6 \cdot HV \pm 0.1, HV < 400 \quad (5)$$
$$\sigma_w < 1.6 \cdot HV \pm 0.1, HV > 400$$

Where

σ_w Fatigue limit for smooth specimen [MPa]

Tensile strength has been found to correlate with hardness also.

$$0.5\sigma_u = 1.6H_v \quad (6)$$

Where

σ_u Tensile strength [MPa]

Based on hardness profile of thermally cut edges relative to cut edge, the material parameters on thermally cut edge changes with hardness profile presented in figure 18. To understand fatigue phenomena of thermally cut edges material model for 3─5 hardness zones should be developed. Within this thesis, nano hardness profile was not possible be measured and based on FEA the high hardness area after 5 µm layer the second 30 µm layer is more critical and material model should be developed from this layer to estimate fatigue phenomena on global notch stress cases. After thin surface layer on cut edge, the regular hardness HAZ layer material parameters should be considered. Softened zone is not as significant concern on cut edges as on welded structures.

Murakami (2002) developed model that estimate fatigue limit by hardness and defect area parameter. Stress ratio was also included to model. On Murakami approach the maximum value of area parameter is around 1000. When defect size is over critical threshold the behavior of material follows Paris' law for crack propagation.

For surface defects the estimation follows equation

$$\sigma_w = \frac{1.43(H_v + 120)}{(\sqrt{area})^{1/6}} \cdot \left[\frac{1-R}{2}\right]^{\alpha} \quad (7)$$

For internal defect hardness factor increases.

$$\sigma_w = \frac{1.56(H_v + 120)}{(\sqrt{area})^{1/6}} \cdot \left[\frac{1-R}{2}\right]^{\alpha} \quad (8)$$

Where

area	$\sqrt{10}$·depth on single circumferential notch, max depth 300	[µm]
R	stress ratio	[-]
α	$0.226 + H_v \cdot 10^{-4}$	[-]

Equations 7 and 8 are similar to the defects inside material and on surface with variating hardness coefficient. In thermally cut edges the surface is not polished, and it probably have greater *area* parameter than defects inside material. For thermally cut edges critical location

is on rolled or on cut edges. The defect size for area parameters is different for cut and rolled edges but still calculated by same method because of similar regular notch pattern. *Area* parameter calculation for regular pattern can be done differently including stress reducing effect from notch interference but estimation with single notch approach is conservative and on safe side.

Full micro hardness profile was available on Peippo (2015) research for S355 and S960QC materials with both laser and plasma cut edges. Results were averaged from four measurements with two materials and cutting methods. These measurements miss data from 50 µm surface layer but high hardness under 0.2 mm distance from cut edge is included. Averaging the results increase the reliability and shows also that high hardness surface is not dependent of base material strength. Averaged results are shown in figure 18. Hardness profile can be divided to zones at averaged hardness profile; 540HV at 0.05─0.2 mm, 450 HV at 0.2─0.5 mm and 350 HV after 0.5 mm.

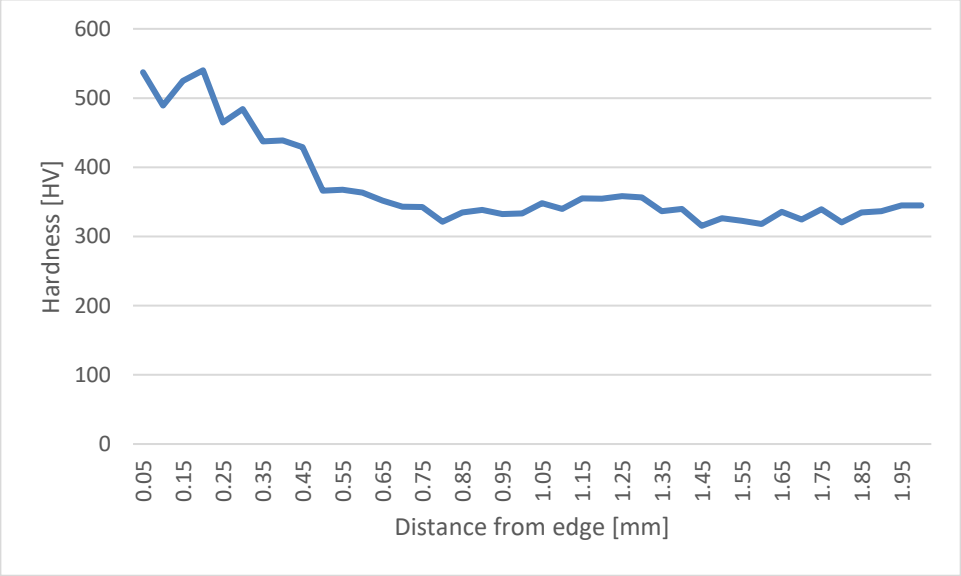

Figure 18. Averaged micro hardness from plasma and laser cut S355 and S960QC (Data from Peippo 2015)

Equation 5 and 7 were used to calculate fatigue limits for these hardness zones are presented in table 3. Higher fatigue limit from Garwood approach was calculated for smooth specimen and lower from Murakami approach for area with 30 µm deep circumferential notch.

Table 3. Hardness zones with estimated material parameters.

Hardness zone [HV]	Fatigue limit [MPa]	
	Garwood, smooth	Murakami, 30 μm notch
540	865	520
450	720	450
350	560	375

Fatigue zone-based approach was tested with the results of Peippo (2015) where the stress from global geometry variated as a function of distance over hardness zones. For stress ratio 0.1 and 30 μm, 50 μm and 100 μm notch depth fatigue limits are presented in figure 19 with local hardness values. Notch depth of 30 μm could estimate shot blasted surface or good quality thermally cut edge while notch depth of 100 μm represent harsh striations on cut surface.

Fatigue limits are also presented to HAZ hardness of different steel grades and surface layers. Calculated fatigue limits are valid only when cut surface is uniform and should be compared to nominal stress on straight cut edges or ideal shape notch factor on curved edges because fatigue limits include local notch factor via *area* parameter. Run out -result from Peippo (2015) from S235 and S355 materials was added for a comparison of extreme case of curved thermally cut edges. The intersection point of curves move to direction of high hardness cut surface area when high global notch factor was added to thermally cut edges and failure point moves towards higher hardness zone with better fatigue capacity.

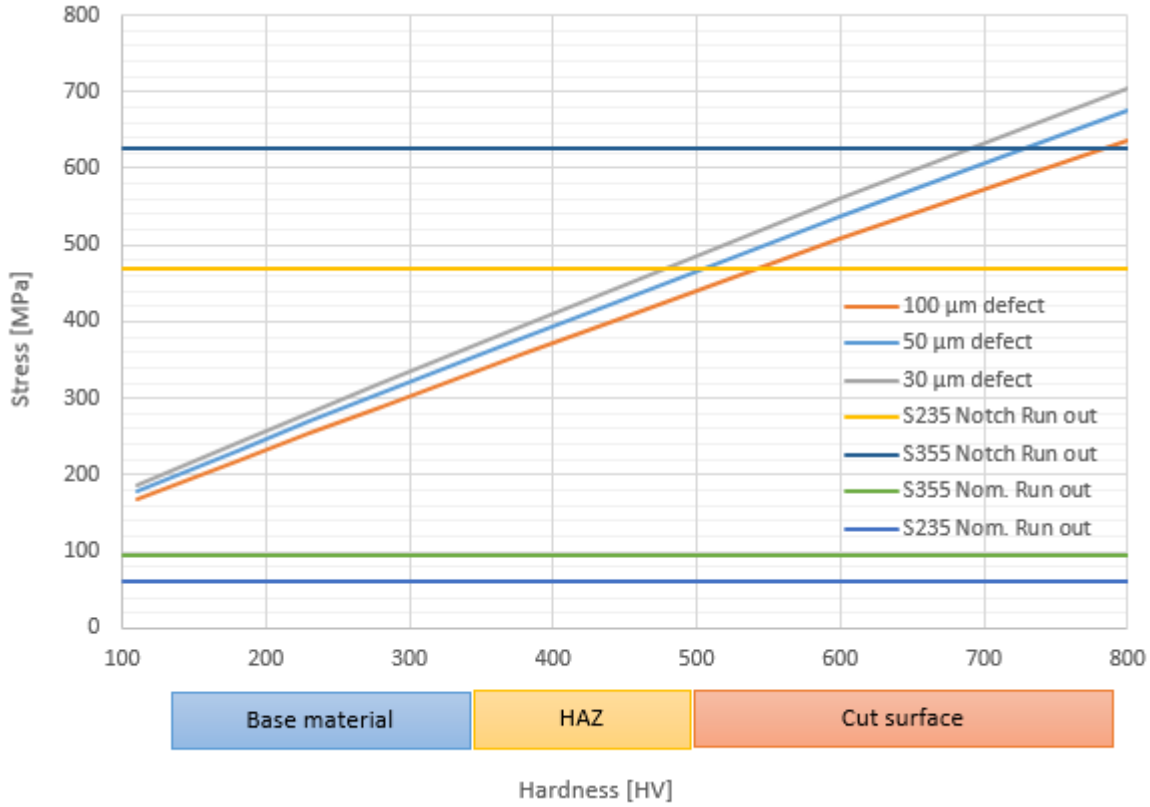

Figure 19. Fatigue limits and tested run outs as a function of notch depth and hardness.

2.4.8 4R method

4R method is originally developed by Timo Nykänen and it combines conventional fatigue theories and experimental results. Juha Peippo developed similar method for thermally cut edges called as FATmod. Parameters in the 4R method are $\Delta\sigma_k$, R, R_m and σ_{res}. The parameters are selected so that they can be measured with normal engineering practice. The method is not highly sensitive to residual stress measurements rather the magnitude should be known. Utilization of parameters for design stage and existing structure is presented in table 4. Palmgren-Miner damage accumulation theory can be used if the structure is loaded with variable amplitude loading. 4R method is originally developed for welded structures but applicability of the method for machine elements is under investigation. (Nykänen et al. 2017; Peippo 2015)

Material model of the method has been kept as simple as possible. The change of material parameters is supposed to be made with modifying tensile strength, R_m, value. In welded structures the material properties can be changed by strain hardening due to hammer peening

or softening from heat input. (Nykänen et al. 2017) 4R method can be used simultaneously for different material parameters with local affecting loading and lowest fatigue life can be chosen for estimation.

The 4R method have relation to ENS (effective notch stress) method. ENS-method is shown in equation 10. The loading in the 4R method can be obtained from similar FEA than in ENS method but additional parameters are used for stress ratio, material properties and residual stresses.

$$N_f = \frac{C}{(\Delta\sigma_k)^m} \tag{10}$$

Table 4. Parameters of 4R method for fatigue life estimation on both design stage and existing structure. (Modified Björk et al. 2018)

4R parameter	Design stage	Existing structure
$\Delta\sigma_k$ (ENS)	Designed geometry with standard imperfections Simulation of loading	Measured geometry and loading
R	Effect of global residual stresses included	Global residual stresses and geometrically non-linear behavior included
R_m	Nominal or material certificate	On the basis of local hardness
σ_{res}	Default values	Measured values
Geometry	Default values	True, measured or scanned

Material strength, residual stresses and applied stress ratio are taken into account in the 4R method. Stress values are measured with strain gauges or obtained from FEA. Residual stresses are included in input stress ratio and local cyclic behavior is calculated. Residual stresses can be measured or standard values for different type of joint or can be used. In joints in the ASW condition, residual stresses of $+f_y$ is used for as welded detail and $-0.255 \cdot R_m$ for HFMI-treated detail. On basis of local hardness the material strength can be estimated with for example Pavlina's equations. In welded details residual stresses are

known to affect weld toe directly on surface of sheet. Failure point can locate on cut surface or on softened zone. Also behavior of residual stresses for LCF-region is under development.

Ramberg-Osgood and Neuber equations are combined to obtain maximum local stress and equation of Masing-type material combined in second phase to calculate stress variation in order to solve minimum local stress. With maximal and minimal local stress the local stress ratio can be calculated. R_{local} can be calculated when local cyclic behavior is known. In order to use 4R method the following equations should be solved numerically in particular order. Usage of equations base on hysteresis loop of cyclic loading.

$$\sigma_k = \frac{\Delta\sigma_k}{1 - R} \tag{11}$$

Where

R	Applied stress ratio	[-]
$\Delta\sigma_k$	Applied stress range	[MPa]
σ_k	Maximum stress without residual stress on first loading cycle	[MPa]

$$\frac{\sigma_{max}}{E} + \left(\frac{\sigma_{max}}{H}\right)^{\frac{1}{n}} = \frac{(\sigma_k + \sigma_{res})^2}{\sigma_{max} \cdot E} \tag{12}$$

Where

σ_{max}	solved maximum local stress	[MPa]
E	modulus of elasticity	[GPa]
H	$1.65 \cdot R_m$	[MPa]
n	coefficient, 0.15	[-]
σ_{res}	residual stress from measurement or assumption	[MPa]

$$\frac{\Delta\sigma}{E} + 2 \cdot \left(\frac{\Delta\sigma}{2 \cdot H}\right)^{\frac{1}{n}} = \frac{\Delta\sigma_k{}^2}{\Delta\sigma \cdot E} \tag{13}$$

Where

$\Delta\sigma$	local stress range	[MPa]

$$\sigma_{min} = \sigma_{max} - \Delta\sigma \quad (14)$$

Where

σ_{min}	minimum local stress	[MPa]

With local minimum and maximum values the local stress ratio can be calculated and fatigue life can be estimated with equation 15.

$$N_f = \frac{C_{ref}}{\left(\frac{\Delta\sigma_k}{\sqrt{1 - R_{local}}}\right)^{m_{ref}}} \quad (15)$$

Where

C_{ref}	mean or characteristic reference curve, value $10^{20.83}$ or $10^{21.59}$	[-]
m_{ref}	slope of reference curve with value of 5.85	[-]
$\Delta\sigma_K$	stress obtained from FEA	[MPa]
R_{local}	local stress ratio	[-]

The 4R concept is presented in figure 20. The method is constructed from fatigue testing and residual stress relaxation is embedded to master curve. However, on fatigue testing HFMI treated joints with Duplex steels, the residual stress relaxation was found with stress ratio of 0.5. The relaxation of compressive residual stresses from HFMI-treatment can be seen from strain gauges as increasing strain values while difference between minimum and maximum remains steady.

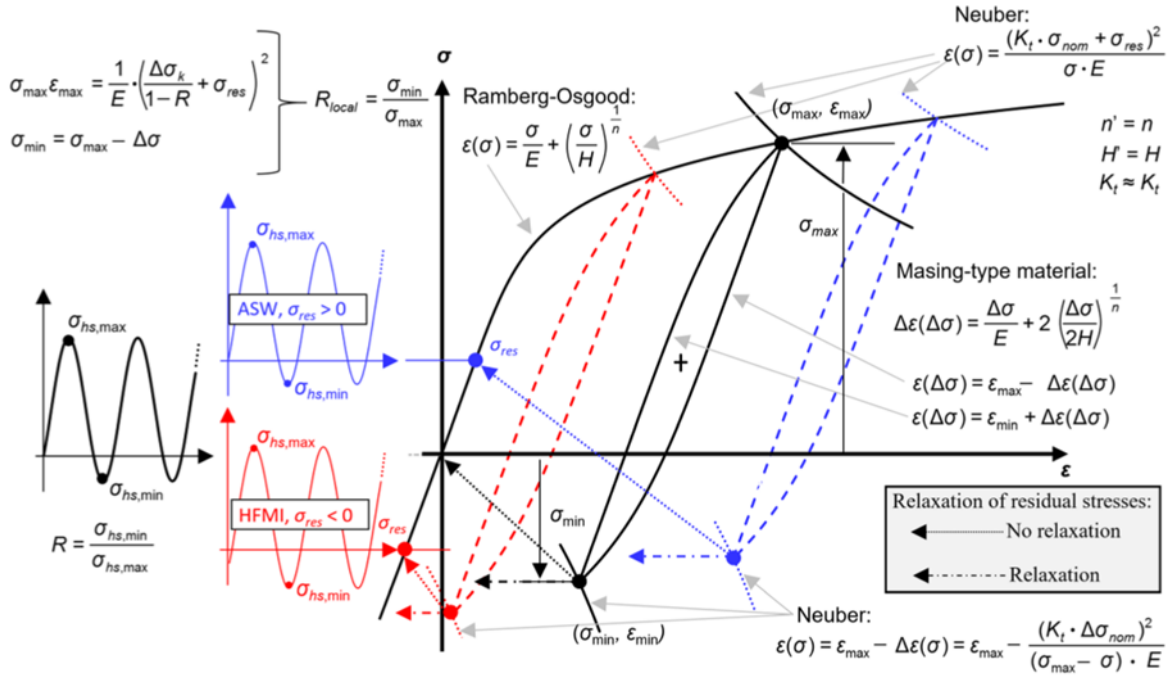

Figure 20. Master curve and principle of 4R method. (Björk et al. 2018)

2.5 Fatigue test results from previous research

Figure 21 presents the data for 4R master data for fatigue capacity of welded joints. The data from run out -testing was not included in the data analysis of slope and fatigue capacity. The stress in butt welds have been calculated by reported or default factors. The materials used for data had yield strength of 225 MPa to 1100 MPa. Most of the fatigue testing was at the regime between 10^5 and 10^6 cycles. Total 775 test were included to master data of which 196 were run outs.

From visual analysis of data can be seen that trend of test results is changing after 10^6 cycles. The slope of fitted SN-curve decreases and less failures happened between 10^6 cycles and run out -level. Number of failures is most likely influenced by residual stress relaxation and when loading is approaching fatigue limit. Both of these qualities are different for each test series and are not as visual in generalized data than on individual test data for single test series where knee point of SN-curve is visible.

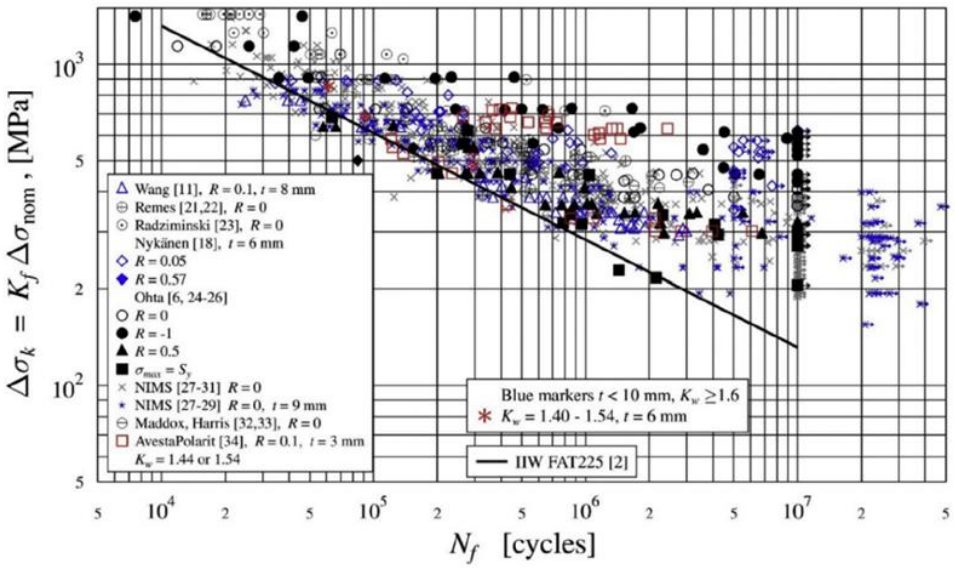

Figure 21. The master data of 4R method for fatigue capacity. (Nykänen & Björk 2015)

Strength of material described by hardness has the most significant effect on fatigue performance. Murakami (2002) presented a fatigue limit estimation compared to fatigue test results. Single notched specimen has the lowest fatigue limit while regularly notched specimens located between smooth and single notched specimen. Hardened and notched specimen fatigue limit was its own magnitude with 549 MPa fatigue limit. The results are shown in figure 22. Material A was annealed and residual stresses were not affecting fatigue life. Residual stress from QT specimen could have not been measured but tensile residual stresses between 0 and 150 MPa were measured from similarly prepared electro polished specimen.

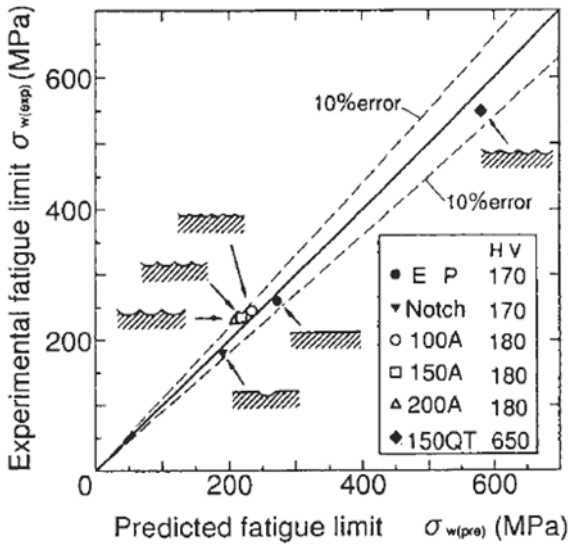

Figure 22. Notched, smooth and hardened specimen fatigue limit. (Murakami 2002 p. 317)

Specimens in Murakami (2002) research were made by turning in the lathe and had very repeatedly pattern. When turned pattern was compared to single notch, it was found out that regular patter had 30% better fatigue life than single notch. In turning the surface pattern is regular, but on thermal cutting surface pattern could have random factor in striation formation especially on long straight cut edges. On notch stress calculations of thermally cut edges, this phenomena from interference should be considered if striations are regular. The 4R method for machine elements should include interference in master curve or in notch stress calculation. By the theory on regular notches, notch stress should be decreased by 10% if stress is obtained from single striation FEA or analytically on straight cut edges.

In the HIPERCUT project, the 15 mm thick S690Q specimen cut by CO_2 laser were fatigue tested. The run out -level of 230 MPa was low compared to similar researches but here were significant striations also on bottom of the cut. Plasma cut S690Q edge had fatigue limit of 250 MPa with good quality cut. Also S890Q was tested with better cut quality run out -stress for laser cut 15 mm thick S890Q specimens 449 MPa, while plasma cutting had 374 MPa. Oxy-fuel cut edge was also tested and had run out -stress of 324 MPa. In figure 23 the tested cut quality is shown for laser and plasma cut edges. Specimen coding in figure present cutting method with L (laser) and P (plasma) and material strength by 6 (S690) and 8 (S890) while 15 represent plate thickness.

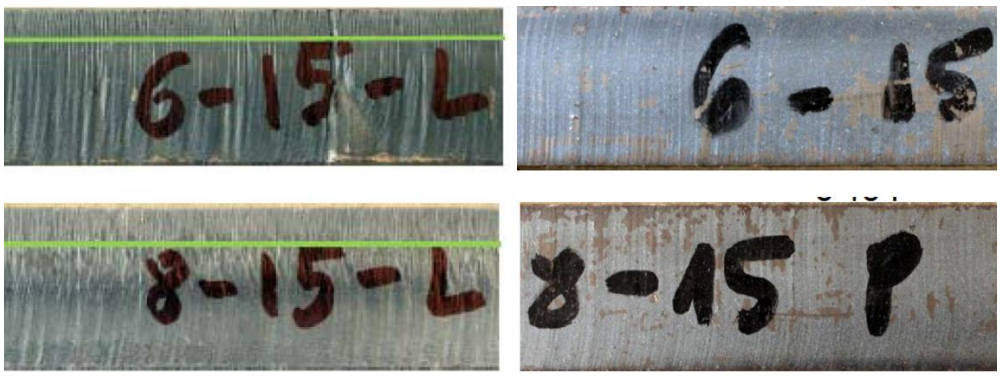

Figure 23. S690Q and S890Q with 15 mm thickness CO_2 laser and plasma cut surface. (HIPERCUT p. 44)

Laitinen, Valtonen & Kömi (2013) researched plasma and CO_2 laser cut steels from S355 to S1100 with 6─12 mm test specimen thickness. Fatigue strength and yield strength correlated on plasma, CO_2 laser cut and machined specimens. Test results for plasma, CO_2 laser and

machined edges are presented in figure 24. Plasma cut edges had lower fatigue strength than laser cut on high strength steels. In this research where 6─12 mm thick specimens were cut, CO_2 laser cutting quality was better than plasma cut. The design value FAT 280 MPa with m = 5 was too high for thermally cut edges below 700 MPa yield strength and S700 steel with plasma cut edges failed also.

Laser cut specimens S700, S900, S960 and S1100 performed better than FAT 280 with m = 5. Laser cut specimens had shallower SN-curve than m = 5. In the laser cut S900 QC edges the slope of SN-curve was 8.42. The measured surface quality was very good on laser cutting due to only 6 mm thick sheets. Surface quality by R_z measurement on S900QC specimens was 8─20 µm on laser cut specimens and the notch effect small compared to thicker sheets. The run out -level on S900QC specimens was around 520 MPa in fatigue testing.

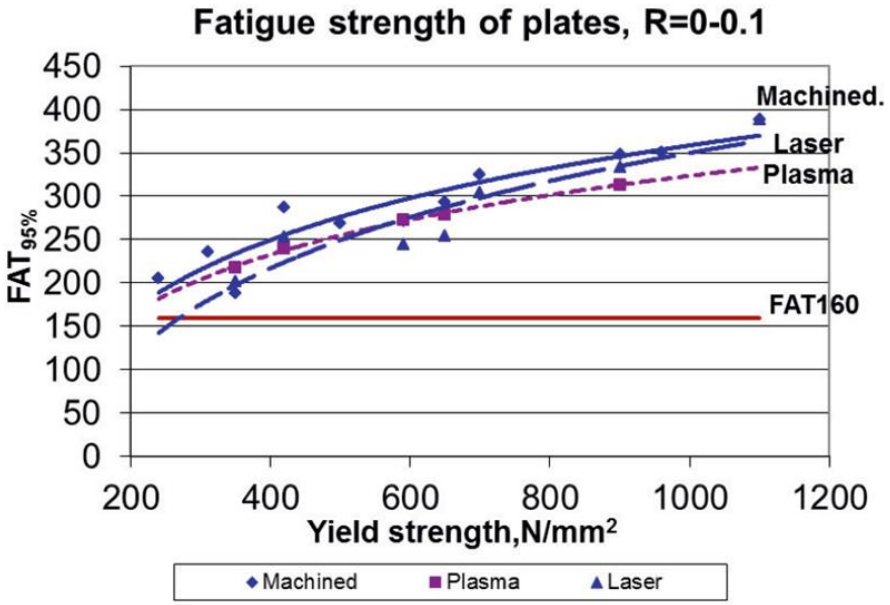

Figure 24. CO_2 Laser cut, plasma cut and machined edge compared to material yield strength (Laitinen et al. 2013)

In the study by Laitinen et al. (2013), the crack initiation point was not found out but the softened zone crack initiation was considered. With categorizing measured hardness, residual stresses and surface quality, there was three competitive solutions for fatigue limit estimation. Possible crack nucleation locations would have been base material with high residual stresses and notch effect from rolled surface, soft zone with low tensile residual stresses and notch effect from rolled surface and surface with high notch effect from cut edge

and low tensile residual stresses. Depending of cut quality and relative distances between areas the combination of notch stress from cut edge and rolled edge is possible.

Stenberg et al. (2016) researched HSS with plate thickness of 16 mm and stress ratio of 0.1. S700 steel with thermally cut edges exceed FAT 250 with m = 5 and S960 steel could match FAT 280 with m = 5 with oxygen, plasma and laser cut edges. Results are shown in table 5 and test series is also presented in figures 24 and 25. Plasma cut S700 and S960 had lower fatigue resistance than laser cut samples although surface quality were better with standard measuring. Plasma cut specimens had tensile residual stresses while compressive residual stresses were measured laser cut specimens. 15 specimens were tested to run out –level of 5 million cycles and only one runout was below 300 MPa stress level. Calculated mean FAT classes were below 300 MPa level which indicates knee point before two million cycles.

Table 5. Fatigue test results of Stenberg et al. (2016).

Cutting method	Grade	Natural slope	Log C	Mean fatigue strength [MPa]	Char. fatigue strength P_f = 2.3% [MPa]
Plasma	S700	3.66	15.08	250	202
Laser	S700	3.33	14.42	274	254
Waterjet	S700	4.26	17.30	328	310
Plasma	S960	5.57	20.03	291	264
Laser	S960	5.20	19.34	323	289

Fatigue test results of S700 specimens from Stenberg et al. (2016) study are presented in figure 24. Oxygen cut edges had the best fatigue life on failure test while waterjet cutting had the highest run out –level. High run out -level of waterjet cutting could be explained with no heat input in cutting and with compressive residual stresses. Without heat input in cutting also no softened zone was formed to specimens.

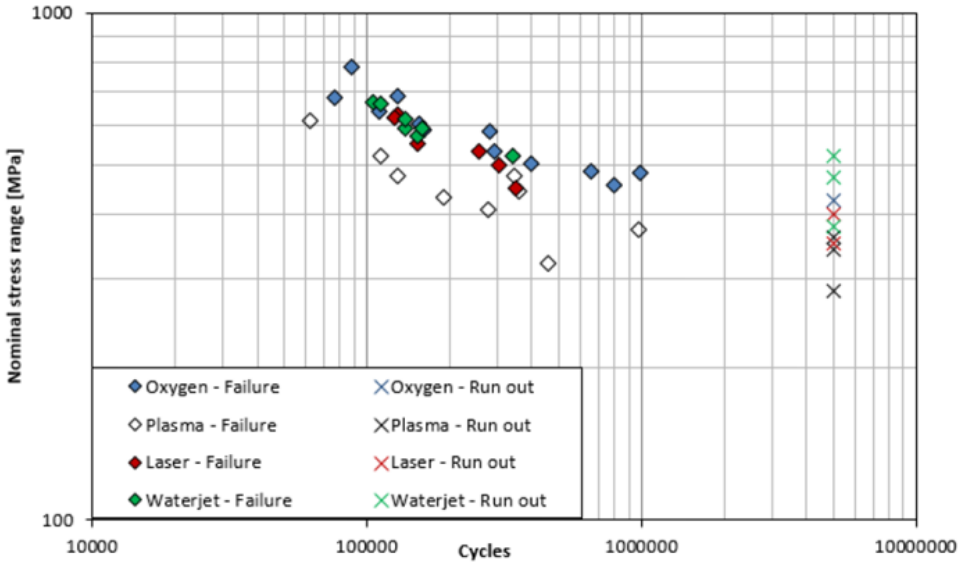

Figure 21. Fatigue test results of S700 (Stenberg et al. 2017).

Fatigue test results of S960 specimens from Stenberg et al. research are presented in figure 25. Plasma cutting had the worst fatigue performance in both S700 and S960 specimens. Fatigue performance of both materials were almost equal.

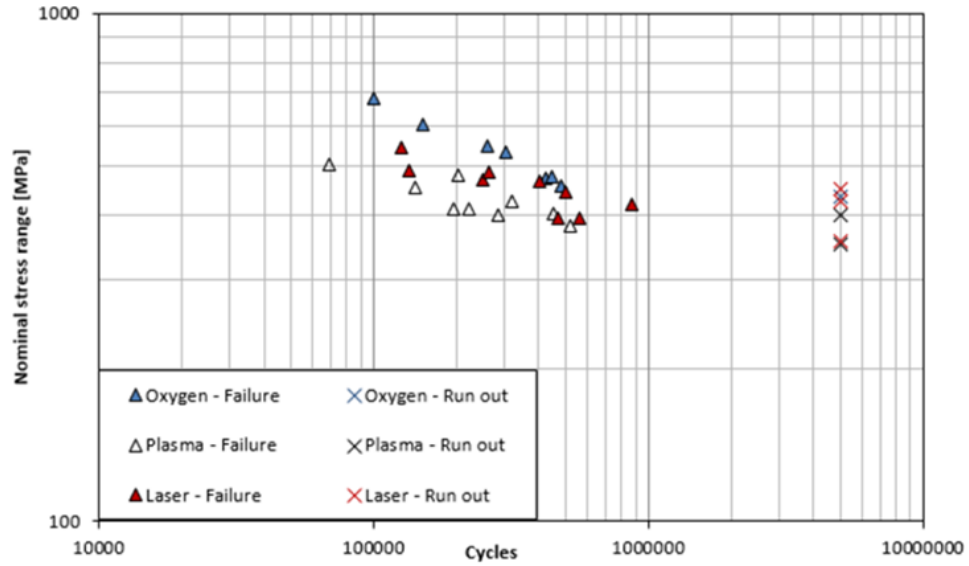

Figure 22. Fatigue test results of S960 (Stenberg et al. 2017).

Duplex steels were researched by Salo (2016). Tested 2507 Duplex steel had yield strength, $R_{p0.2}$ = 550MPa and thickness of 5 mm. Waterjet cutting was found to have similar cut edge fatigue performance than plasma cutting although it had higher R_z of 24.9 µm value than

plasma cut edges with 8.3 µm. Four tests were performed with R = 0.1 and four with R = 0.5. Mean FAT value of all eight tests were 278 MPa and FAT_{char} 198 MPa with m = 5 value. Test specimens with stress ratio of 0.5 had lower fatigue strength than with stress ratio 0.1.

Mattila (2016) researched duplex steel grade 2205 which had $R_{p0.2}$ = 625 MPa and thickness of 5 mm. Welded specimens where crack initiated to ground edge base material were included for comparison. Welding on test specimen affected significantly fatigue of ground edges by reducing it. Grinding improved laser cut edge fatigue and one crack even nucleated from center of the base material, not from cut edge on laser cut and ground specimen.

Results of Mattila and Salo studies are summarized in figure 26. In the results also welded specimens failing from base material near weld or away from weld are presented. Results show that R = 0.5 test resulted shorter fatigue life. On welded specimens, where fatigue crack occurred far from weld the fatigue capacity was the worst. In welded specimens, there was bending stress that may affect the results. There was small amount of test with high number of combinations and SN-curves could not be drawn. FAT 160 fatigue class with m = 3 and FAT 280 with m = 5 were added to relation of fatigue testing. The FAT 280 represents results better due to less steep slope.

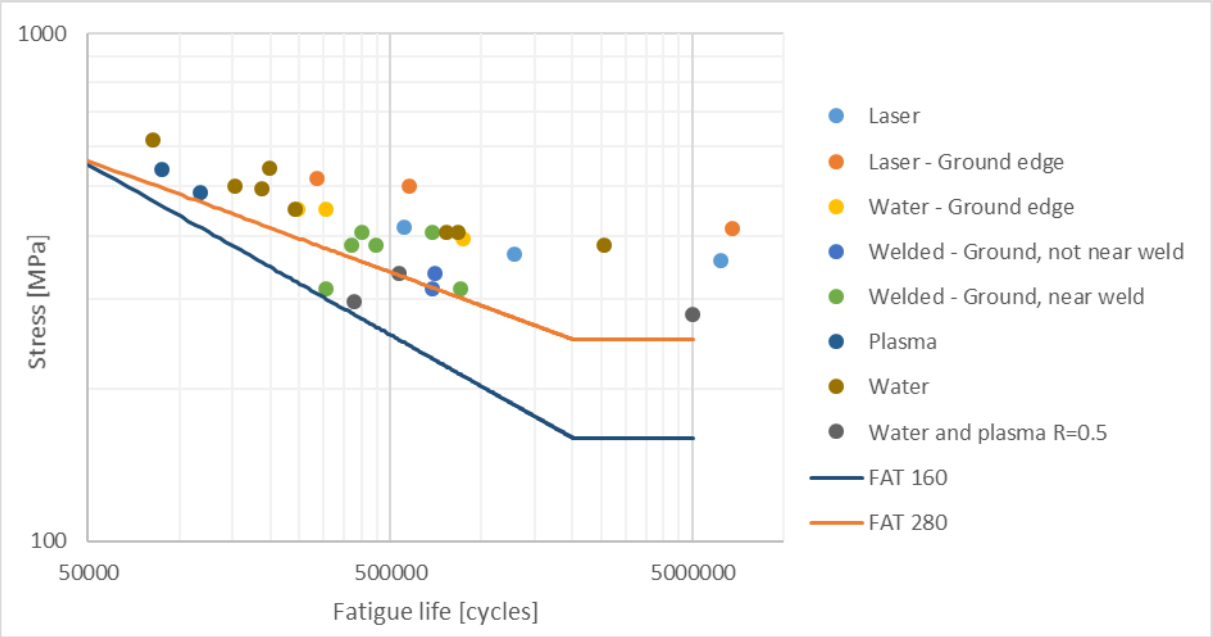

Figure 23. Salo and Mattila results combined and presented with FAT 160 and FAT 280.

Riski (2017) researched S960 steel LCF and also cut edges were studied. Laser, waterjet cut and machined edges were also tested. For machined edges 0.2 mm material was removed from laser cut sheet and removed material was less than HAZ of laser cutting. Only seven specimens were made and tested with cut edges.

Machined specimen failure from ground section as the second waterjet cut and two laser cut specimens. Two welded specimens failed from base material, one near weld and the other from machined section halfway weld and ground section. Welded specimens failure from base material were MAG and laser welded butt welds with HFMI treating. FAT 280 with *m* = 5 was added to figure 27 and all fatigue test exceeded the FAT 280 class even tough failure occurred to ground section in some cases.

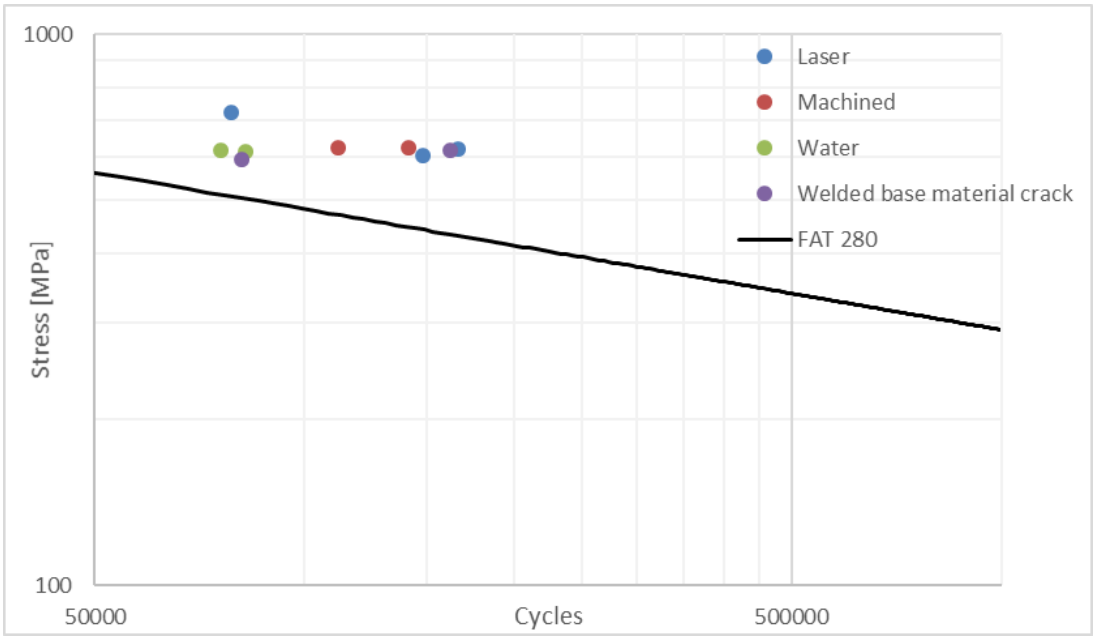

Figure 24. LCF of S960 cut edge (Riski 2017).

Diekhoff et al. (2019) researched oxygen, plasma and laser cut edges on 8─20 mm thick plates. Plasma cut edges were tested with 8 mm and 20 mm thick and laser cut with 8 mm S355 and S690 specimens. Laser cut edge of S690 had lower fatigue strength than S355 while plasma cut edge results were opposite. Cut of limit for laser cut S690 edge were 288 MPa and for S355 360 MPa. Cut of limits for plasma cut edge was 300─320 MPa. For thickness of *t* = 20 mm the cut of limit was 270─300 MPa. The results of Diekhoff's plasma and laser cut edges are presented in figures 28 and 29. As it can be seen, IIW FAT classes

125 MPa and 140 MPa with m = 3 were conservative at the high-cycle regime, after 10^6 cycles.

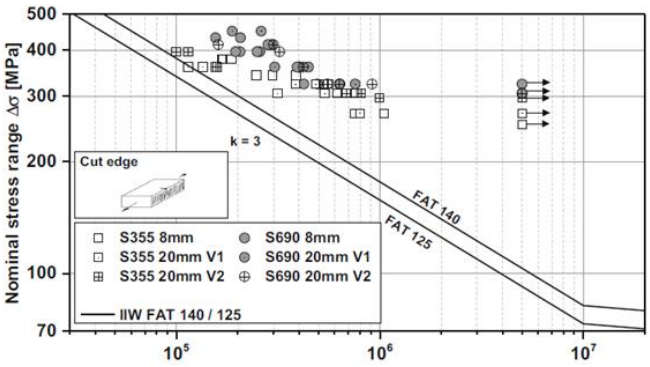

Figure 25. Plasma cut Diekhof et al. (2019)

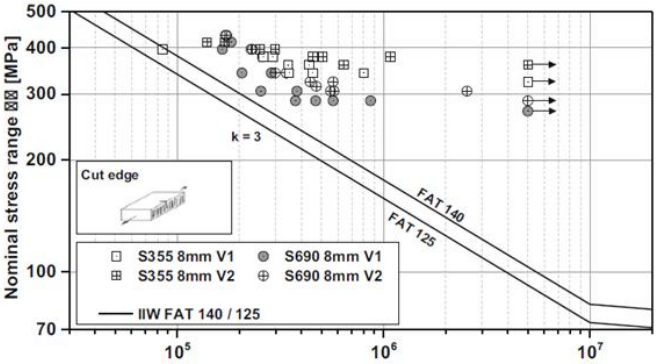

Figure 26. Laser cut Diekhoff et al. (2019).

Peippo (2015) researched fatigue of thermally cut corner. Results of fatigue testing are presented in figure 30 with calculated notch factor induced by the stress concentration. Fitted curves were characteristic with m = 3 and with free slope. The HAZ depth at the critical corner variated from 0.2 mm in the laser cut edges to 0.5 mm in the plasma cut edge. All failure and run out specimens were loaded with over 350 MPa stress corresponding to critical distance method on cut edge.

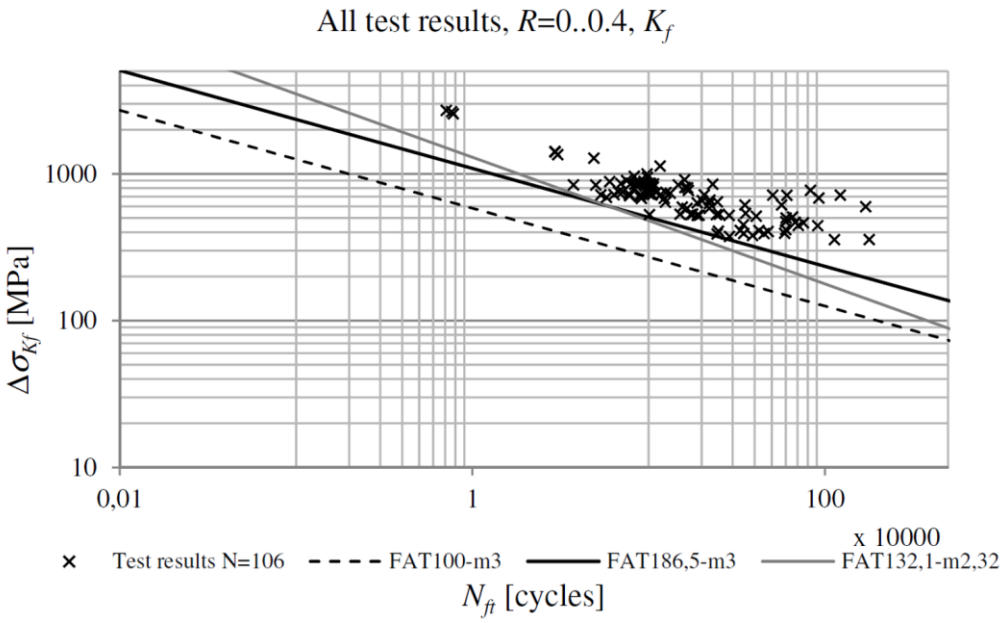

Figure 27. Notch stress corrected fatigue test results. (Peippo 2015 p. 186)

You et al. (2017) studied the effect of shot blasting on laser cut hole fatigue. Shot blasting improved fatigue life of thermally cut hole by increasing hardness and inducing compressive residual stresses near thermally cut edge. Fatigue life increased around 30% when the shot blasting treatment was conducted after laser cutting even tough shot blasting made rolled surface defects bigger. Fatigue cracks initiated to shot blasting defect instead of laser cut edge striation.

University of Oulu (2015) studied fatigue of CO2 laser and plasma cut edges at LCF regime with S690QL steel with R = -0.5. Cutting speed and surface quality of specimens is presented in table 6. In this study, every specimen failed from the curved area or in the vicinity of curved area where stress concentration exists. Crack nucleation point on specimen is shown in figure 31. Curved section was not ground.

Figure 28. The specimen and crack nucleation point on curved section.

Table 6. Cutting speed and surface quality (University of Oulu 2015).

Cutting method	Cutting speed [mm/min]	R_z [µm]
CO_2 laser	1600	30.1
Plasma	2230	18.3

FEA correction for the results is presented in figure 32. FEA model was made using measured dimensions of specimen and utilizing symmetry constraints. The notch factor from geometry to local failure point was 1.27. All cracks have been initiated at this stress concentration area on fatigue testing.

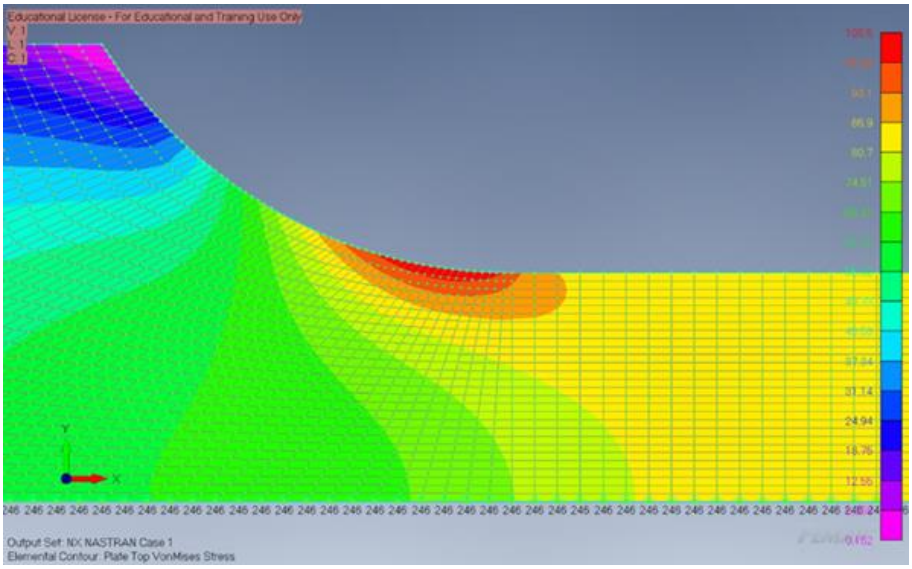

Figure 29. FEA correction for University of Oulu (2015) results.

Used stress amplitudes in fatigue testing were 493 MPa and 518 MPa. Trend lines of average lifetime between two stress amplitudes are presented in figure 33. For the presented results the FEA correction was added and only tensile stress was considered with reduction of the result to $R = 0$. The slope of laser cut test was $m = 13.5$ while plasma cut had slope of $m = 24.4$. The stress amplitudes were too close each other to determine slope of SN-curve reliable. Slope of SN-curve indicates LCF area before actual fatigue curve. On low cycle fatigue area when failure point was on geometrical notch factor area the laser and plasma cut edges had almost similar fatigue performance.

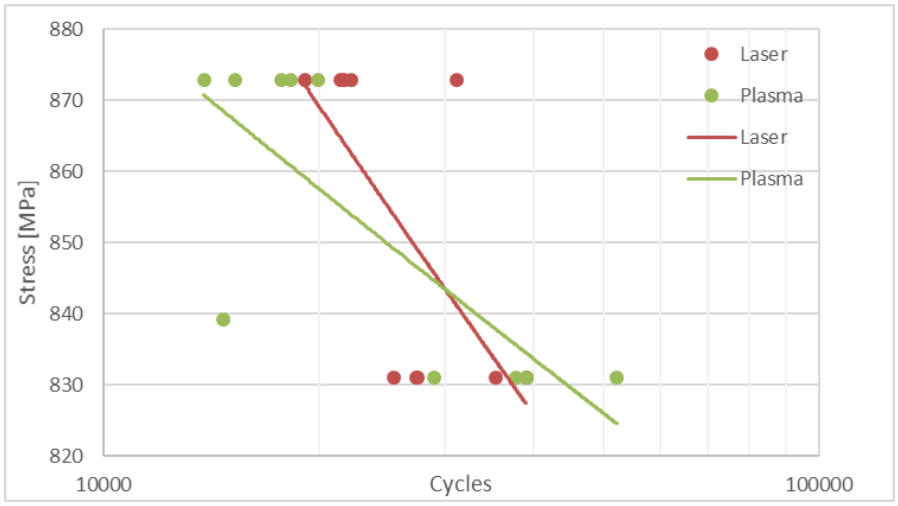

Figure 30. Laser and plasma cut fatigue life with local tensile stress. (University of Oulu 2015)

In the CO_2 laser cut specimen, two fatigue crack origins were found. Fracture had initiated from both cut edge and shot blasted surface while top corner of cut edge was between these two fracture origins. This second fatigue crack origin located outside HAZ. Microstructure examination was not done for these specimens but fracture origin 0.4 mm way from cut edge indicates possible softened zone or base material hardness on this area. For 0.4 mm away from cut edge the notch factor from global geometry had reduced from 1.27 to 1.2 and stress affecting crack initiation point was 828 MPa.

Simultaneous fracture origins presented in figure 34 are explained by very local notch stress and intersecting fatigue capacities of two different materials in their relative location to surface. The fracture origin from shot blasted edge located 0.4 mm from cut edge being on area of high residual stresses although residual stress effect should be low on LCF-area.

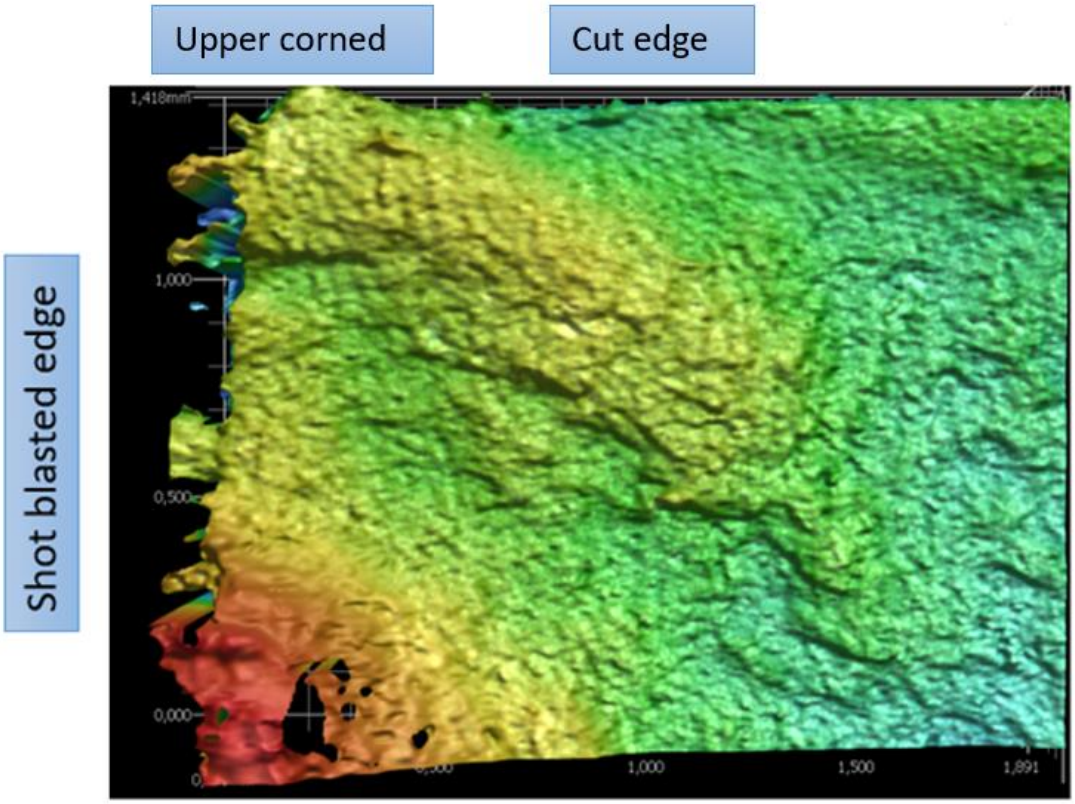

Figure 31. Fracture surface of CO_2 laser cut edge stresses with nominal yield strength.

The 4R method has close estimation to these results when FEA correction from geometry was used and 1.2 notch factor was used to simulate surface quality. Other parameters used for 4R method were *Rm* 1240 MPa with no residual stresses. Residual stresses have small effect on LCF and they are low on laser cut surface. Residual stresses were not measured from these specimens before loading. Based on fracture surface analysis 4R method could be used with base material properties together with high residual stresses taking account reduced notch factor and shot blasted surface reducing effect on fatigue strength. Fatigue assessment with parameters R_m 780 MPa and 700 MPa tensile residual stress had even better fatigue estimation than surface material properties and applied stresses.

3 SCOPE OF THE RESEARCH

Based on literature review the scope of research was selected. To find the most suitable engineering way to select parameters for 4R method the properties for local material behavior was done in literature review. Material properties were investigated, and measurements repeated when possible. If measurements could have not been repeated the results from literature findings were exploited.

3.1 Locality of fatigue failure

Fatigue of thermally cut edges is highly local phenome. On the basis of the literature review, several findings on possible fatigue failures at softened zone were found. To understand the phenomenon, and to utilize 4R method, the local material properties and loading conditions should be found. After crack nucleation the LEFM-theory can be used. If crack like flaws from thermal cutting are exceeding the threshold value of stress intensity with applied load, they have no nucleation period the specimen may the crack has only propagation phase.

3.2 Tensile strength

With certain limits tensile strength is linearly correlated with hardness and for 4R method critical point hardness should be used to determine local tensile strength. High tensile strength material has higher notch sensitivity compared to lower tensile strength material. If selecting too high R_m parameter the 4R method estimates conservative fatigue life when compressive residual stress is not present.

3.3 Hardness profile

Hardness has distinct correlation to local fatigue limit together with defect size. Based on these hardness measurements thermally cut edge have five hardness zones:

1) Very high hardness on cut edge
2) Hard layer after cut surface
3) HAZ with typically measured hardness
4) Possible softened zone by cutting method and material properties
5) Base material hardness

Local hardness distribution of cut edge should be considered when defining stress for fatigue estimations. For 4R method the hardness should be considered as generalized zones to obtain notch stress that is truly affecting structure.

3.4 Residual stress

In plasma and laser cut edges next to HAZ, to base material direction, there is high peak of tensile residual stress parallel to loading direction. Residual stress peak is relative to yield strength with factor of 0.8─1. Residual stress on cut surface is low or compressive depending of cutting method and treatments.

3.5 Notch stress

In single inward facing notch the notch effect is fully effective. Effectivity of notch stress decreases by regular notch pattern by 10%. Outward facing edges of notch decreases effectivity of notch effect on both single and regular notch cases based on FEA from scanned cut edges. For regular thermally cut edge pattern 5─15% decrease from notch stress should be done when notch is modeled as a single notch in FEA. Schematic outward facing notch at cut surface is presented in figure 35. Burr can also form outward facing notch but the stress from burr is difficult to estimate.

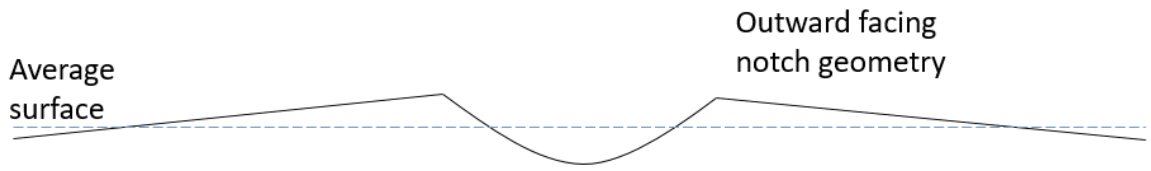

Figure 32. Partially outward facing notch geometry.

Global notch stress from detail geometry should be added to stress on thermally cut edge. Depending of approach adding is done with factor together with local notch stress or if local notch stress is considered as a defect size the global notch stress is the only stress affecting thermally cut edge.

Notch stress and material properties are changing when distance from cut edge increases. Hardness zones have different fatigue capacity. Softened zone failure may happen if harder layers have more capacity than layer specific stress is acting.

3.6 Fatigue limit approach

From literature review of previous fatigue testing the cut of limit of thermally cut specimens variated between 220 MPa and 520 MPa. On previous researches variating cutting method, cut quality and base material strength, base material delivery condition and rolled surface quality were tested. On previous researches all of these factors were not reported.

If fatigue limit on cut edge was close to material yield strength the slope of SN-curve was low. Based on literature review the fatigue limit exists locally on thermally cut edges on uniform cut edges. The weakest point of specimen determines tested fatigue limit. On many cases rolled surface with low hardness was the critical zone for fatigue limit. Also higher fatigue limit of harder base material indicated this approach. If base material or softened zone is not restrictive the cut surface becomes critical. On fiber laser cut edges where pores or burr on cut surface exists the behavior is closer to LEFM than fatigue limit approach.

4 EXPERIMENTAL TESTS

Experimental testing was done in LUT University by Laboratory of Steel Structures. Metallurgy examination of test specimens was done in LUT University laboratory of welding metallurgy. HBM 3/120LY11 strain gauge with 3 mm grid length and 120 Ω nominal resistance was used to measure strain on specimens. The strain gauge was glued at the middle of the specimen. Mathcad 15 was used to solve 4R method equations numerically. Siemens Femap 12.0 was used for finite element modeling of notch stress. Hexagon Romer Absolute Arm was used for 3D-scanning of specimens and Polyworks Viewer was used to evaluate and measure 3D-scanned cut edges. Keyence VR-3200 profilometer was used for surface profile examination and to obtain notch dimensions.

4.1 Material properties

Material properties of researched steel grades are presented in tables 7 and 8. Measured yield strength $Rp_{0.2}$ for S1100 Plus was 1160 MPa and tensile strength R_m 1190 MPa according to the material certificate. These values were used for the linear correlation of hardness and tensile strength for 4R method.

Table 7. Material properties of S690QL and S1100 Plus from SSAB.

Material	Yield strength [MPa]	Tensile strength [MPa]	Elongation [%]
S690QL Nominal	690	770─940	14
S1100 Plus Nominal	1100	1130─1350	10
S1100 Plus Typical	>1100	1170─1210	11─12

Table 8. Nominal chemical composition of S1100 Plus.

Material	C max[%]	Si max[%]	Mn max[%]	P max[%]	S max[%]	Al max[%]
S1100Plus	0.20	0.50	1.80	0.020	0.005	0.015
S690QL	0.20	0.60	1.6	0.020	0.010	-

4.2 Specimens

Dog bone test specimen was used for two different material. S690QL specimens were 12 mm thick and S1100 Plus specimens 8 mm thick because of S1100 Plus was not available on thicker sheets. The used laser cutting assist gas is shown in table 10 with specimen

identification. Fatigue crack is wanted to the gage length area of specimen with length of 170 mm. The curved section was Baud curve to minimize the stress concentration, and to avoid failures at the curved area. To reduce stress concentration and possibility of fatigue cracks on curved sections, the curved sections were ground. Specimens were cut in plate rolling direction. The width of specimen at the center was 52.05 mm in drawing and 51.65 mm at the end of straight section.

Table 9. Test specimen identification and user laser cutting assist gas.

Parameter	CO_2 laser	Fiber laser S690	Plasma	Fiber laser S1100
Specimen ID	LC	LF	PB	LF11
Laser assist gas	Oxygen	Nitrogen	-	Nitrogen

Complete test program is presented in table 10. Specimens were cut with Plasma, CO_2 laser and fiber laser and total number of 42 S690QL were cut and 30 of them were fatigue tested according to original test program. In addition, four extra tests were performed after finishing the test program. Stress ratio 0.5 was changed after one test to 0.4 because fatigue performance exceeded material yield strength in CO_2 laser cut edge.

Fiber laser cut specimen LF5-5 were tested with the forces similar to the LF1-1 specimen, after removing the burr by chisel and grinding sharp edge. The CO_2 laser cut specimen LC5-5 was re-tested with LC5-1C values to eliminate and measure residual stress relaxation affect from run out -tested specimen. A static test was performed for the LCS-1. The HAZ of plasma cut specimen was machined and specimen fatigue tested. Ten S1100 Plus specimens were fiber laser cut and fatigue tested with stress ratios of 0.1 and 0.5.

Table 10. Complete test program.

Name	Cutting method	Stress ratio	Material
LC1-1…6	CO_2 laser	R = 0.1	S690QL
LC5-1…5	CO_2 laser	R = 0.4─0.5	S690QL
LF1-1…6	Fiber laser	R = 0.1	S690QL
LF5-1…4	Fiber laser	R = 0.4	S690QL
PB1-1…6	Plasma	R = 0.1	S690QL
PB5-1…4	Plasma	R = 0.4	S690QL
LF11-1…5	Fiber Laser	R = 0.1	S1100 Plus
LF11-6…10	Fiber Laser	R = 0.5	S1100 Plus
LF5-5	Fiber Laser + burr grinding	R = 0.4	S690QL
PB5-5	Plasma + 1 mm machining	R = 0.4	S690QL
LCS-1	CO_2 laser	Static test	S690QL

Specimens were 2D-laser scanned before fatigue testing. Relative deflection of typical specimens are presented in figure 36. Typical deflection of specimen was 1 mm although 0.5 mm variation existed. The dimension on figure are shown in millimeters and are relative to measuring height. Strain gauges were glued to center of the specimen before fatigue testing. Strain gauges were reset after attachment to measuring system while specimen was free. Strain was measured after specimen was attached to test rig. The bending stress from rig attachment variated between 2 and 20 MPa on two different LUT test rigs.

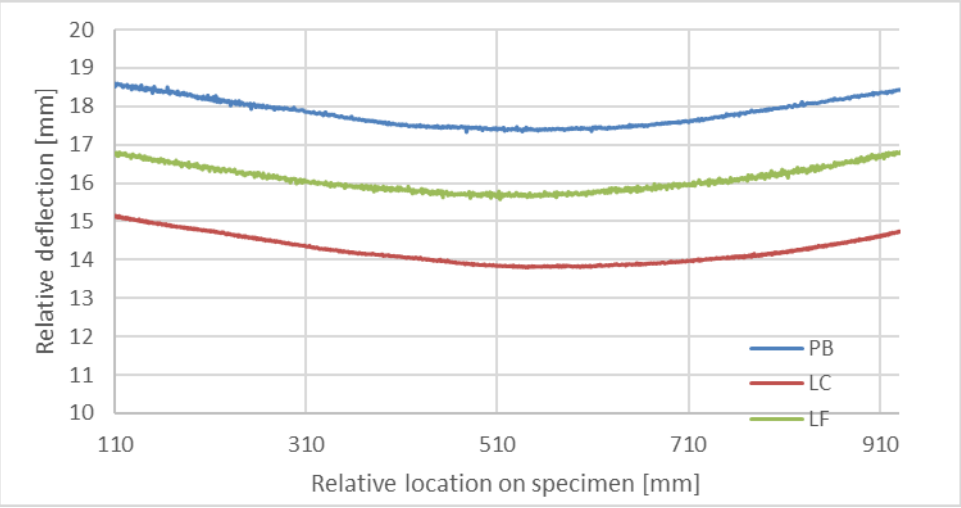

Figure 33. Deflection of S690QL specimens by cutting methods.

4.3 Surface quality and microstructure

Surface quality was measured with Mitutoyo Surftest SJ 201P by Khan (2018). Two specimens from each type were measured from twelve different points. The results are shown in table 11. Bevel angle of plasma cut edge was clearly visible and a 0.3 mm bevel was measured from the top of the cut with round cut edge. Also straight cut edges were found with more visible bevel. On plasma cut edge there was also more global wavy shape in bottom of the cut edge besides surface quality. The fiber laser cut edge was the straightest and most perpendicular to rolled surface. On CO_2 laser cut edge there were visible striations in about one third length of the plate thickness measured from plate surface to jetting direction.

Table 11. Surface quality of test specimens. (Khan 2018)

	CO_2 S690	Fiber S690	Plasma S690	S1100 Fiber
R_a	6.8	8.7	3.0	6.6
R_z *Avg*	37.9	50.8	15.9	37.4
R_z *Max*	55.7	73.5	25.1	57.8

Surface quality of cut specimens is presented in figure 37. From left there is CO_2 laser, fiber laser and plasma cut S690QL with 12 mm thickness and on the right S1100 Plus with fiber laser cut edge and 8 mm thickness. Fiber laser and plasma cut S690QL specimens had dross attachment at bottom of cut edge while other specimens were visually dross free.

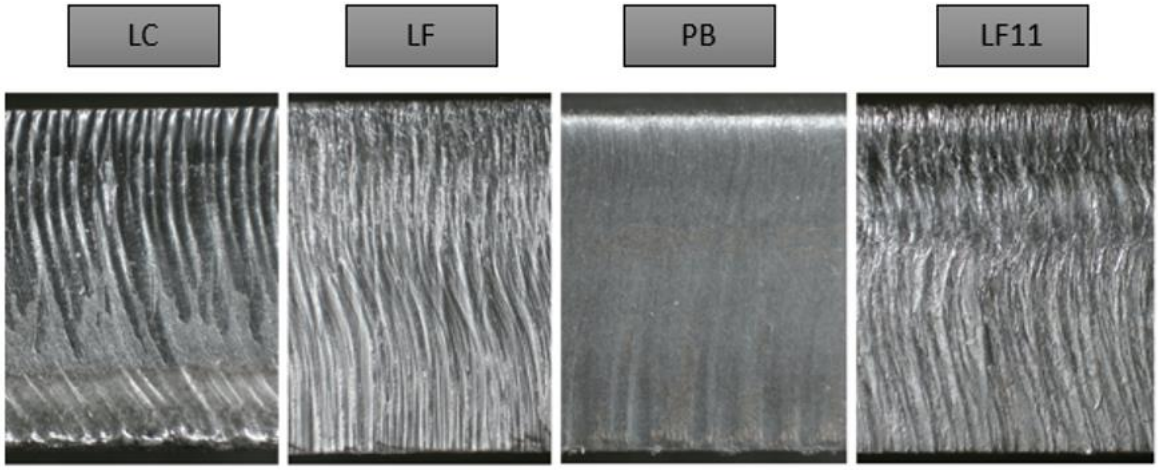

Figure 34. The surface quality of cut edges.

Keyence VR-3200 3D-profilometer was used to evaluate surface quality of specimens. Surface quality was inspected with line measurement and $R_{z,max}$ values were obtained from

measurement lines. The most notable defects were examined by notch stress. Selecting the most significant notch stress was made by visual inspection and it was not unambiguous in all cases. Overall surface quality with the traditional surface quality meter was compared to the surface quality from profilometer with worst case line of all specimens. The results are presented in table 12 as an indicative because measuring length was not selected but depth of striations were evaluated individually. The $R_{z,max}$ values were significantly higher measured by profilometer than ordinary surface quality inspection.

Table 12. $R_{z,max}$ *values obtained from profilometer from worst case line on cut surface.*

CO_2 S690	Fiber S690	Plasma S690	S1100 Fiber
100 µm	90 µm	30 µm	70 µm

A sample surface profile of the CO_2 laser cut edge is presented in figure 38 where millimeter was used as unit. The most significant notch effect was on notch where two striations were together at top of the cut before separation. The notch from this striation had 100 µm depth and was 400 µm wide. This kind of striation has probability-based formation instead of regular pattern. There was low number of the significant striations, but the fatigue failure would initiate in these striations.

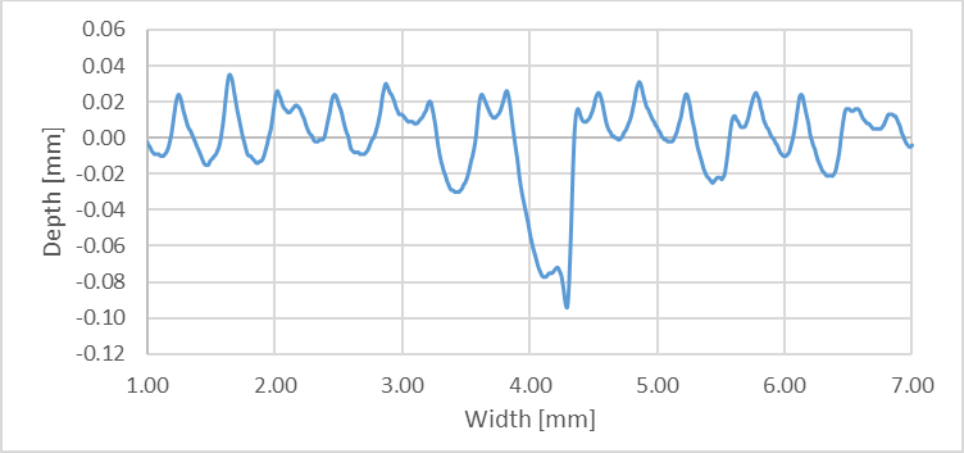

Figure 35. CO_2 laser cut surface profile, note the different scale of axis.

Profilometer obtained surface quality data from rolled and shot blasted PB-specimen is presented in figure 39. Height difference was 60 µm between lowest and highest point in measurement. Circular defects from blasting can be seen and these defects are identified as

a starting point of fatigue failure. Fatigue failure from blasted surface was assumed because of lower quality than cut edge. Failure at shot blasted edge would explain the low variation on plasma cut edges fatigue test results. Corrosion noticed on plasma cut specimens could have been influenced surface profile results.

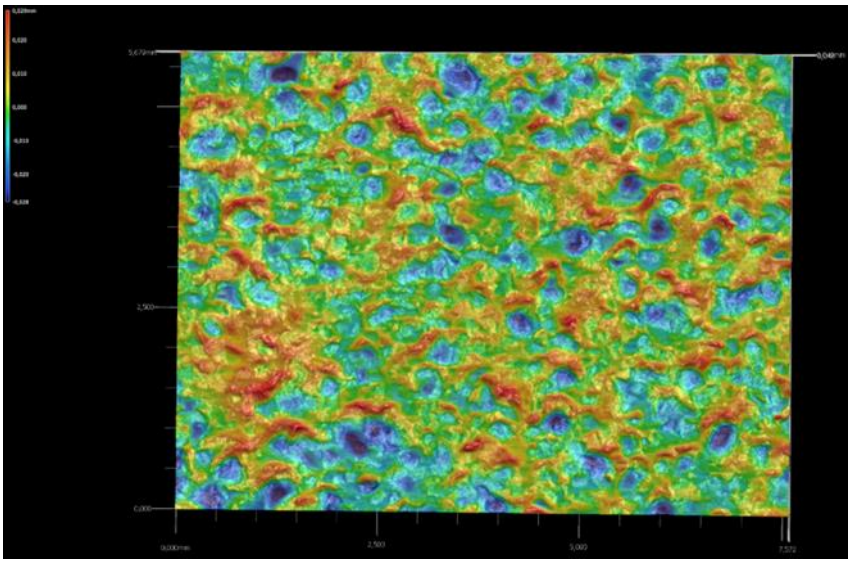

Figure 36. Rolled and shot blasted surface of PB-specimen.

Rolled surface of S1100 Plus was measured and defects on sheet top and bottom sides were minor compared to shot blasted surface. The measurement result is presented in figure 40 where total scale for defect depth was 12 µm with 2.5 mm measuring length. The good quality rolled surface in reference had better surface quality than best measured cut quality, however material properties on these areas are different.

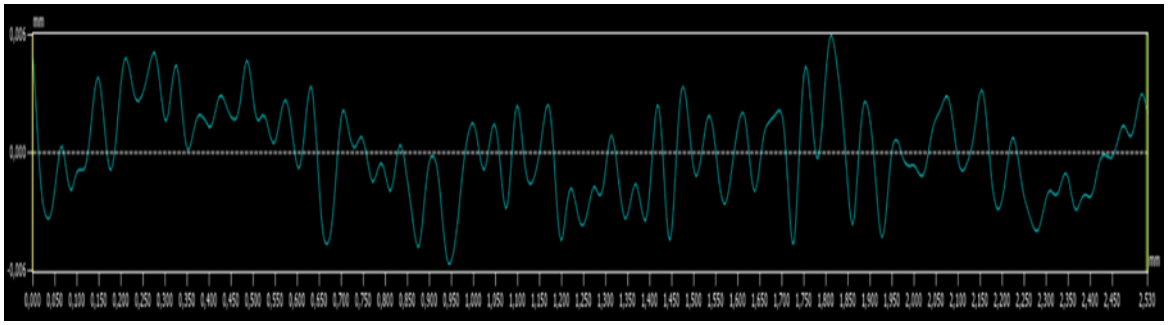

Figure 37. S1100 Plus rolled surface quality.

Microstructure and hardness were researched from the specimens. For microstructure examination the samples were ground and polished. After polishing, samples were etched with Nital which contains 4% nitric acid and methanol. Macrographs from a S690 QL t = 12 mm cut surface are presented in figure 41. The cut surface from left to right are from CO_2 laser, fiber laser and plasma cutting. The difference between HAZ, produced by the different cutting methods is seen from figures. In plasma cut edge the HAZ is equal on top and the bottom of the cut edge. In CO_2 laser cut specimen the HAZ was smallest where striations were biggest. These micrographs represent the other cut edge of hardness measurement samples. HAZ of the thermally cut edge is only 0.1─0.5 mm wide and hardness measurement with HV10 measurement according to standard is difficult because of narrow measuring areas. On plasma cut sample eight measurement point were at various distances from edge on HAZ.

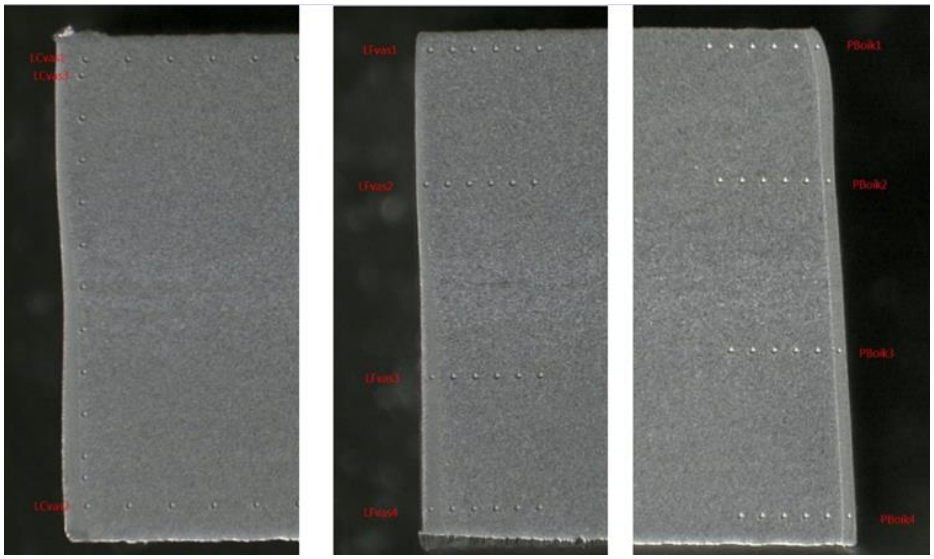

Figure 38. The cut surface from left to right CO_2 Laser, fiber laser and plasma

Figure 42 shows the HAZ of S1100 Plus cut edge. The specimen top side is in left and the figure is constructed from three macro images. The hardness measurement of HAZ may have given too low hardness values due to softening because of measurement point were difficult to get inside the HAZ. All hardness measurement point located on HAZ but not close to cut surface.

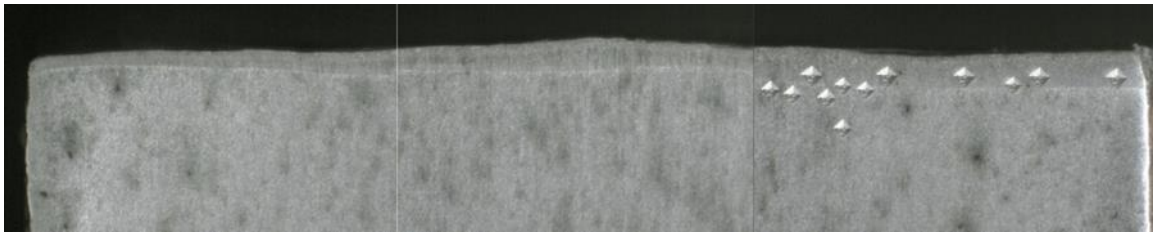

Figure 39. S1100 Plus cut edge HAZ.

Vickers hardness with 3 kg (HV3) and 5 kg (HV5) mass was measured. Hardness measurement results are shown in figure 43. No softened zones could be found from hardness measurements on S690QL steels. From S1100 Plus the minor softened zone were found with HV3 measurements. The minimum measured hardness was 368 HV while base material hardness was 370─390 HV HAZ. Hardness drop of 10─20 HV after HAZ was published in research by Pirinen (2019) dealing with laser butt-welded specimens. Micro hardness measuring equipment would have been needed for better investigations of local hardness.

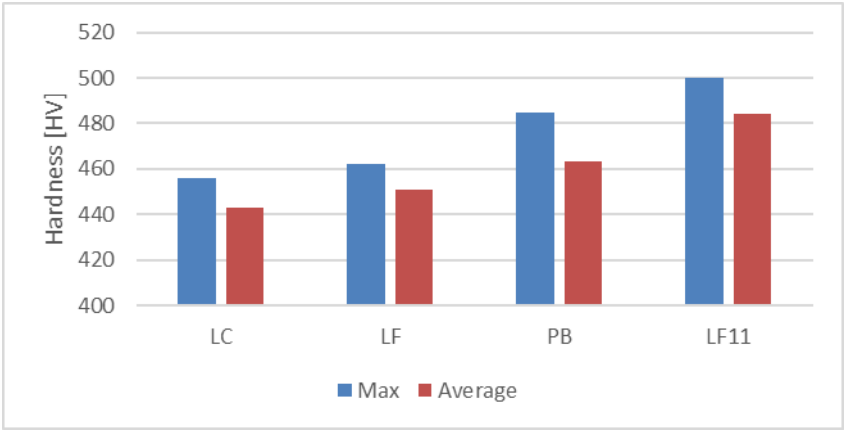

Figure 40. Hardness measurement inside HAZ.

Hardness on base material was 60% on value of HAZ in S690QL specimens and 80% on S1100Plus specimens. On S690QL specimen's soft zone was not found and on S1100Plus specimen the material softening was not significant.

Hardness from plasma cut surface was evaluated by a non-standard method. Hardness measurement point with HV10 measurements were pressed to cut edge and diagonals were measured with microscope after polishing with aluminum oxide with 1 µm gain size. Diagonals between 172 µm and 177 µm were obtained and are presented in figure 44. Even

smaller diagonals with HV10 measurement were obtained but due to reliability they were not reported. These smaller diagonals corresponded to hardnesses between 650 and 800 HV.

Although hardness test of surface was done with experimental method the results are similar to the HIPERCUT (2016) results with nano hardness testing. With HV10 measurement the 170 µm diagonal corresponds around 6 GPa hardness measured to 20─40 µm depth from cut edge HIPERCUT project. Vickers hardness measurement tip has 22 degree angle so measurement depth was 35 µm. Hardness testing was repeated after first tests from polished surface. After grinding no increased hardness values were measured compared to measurements on HAZ.

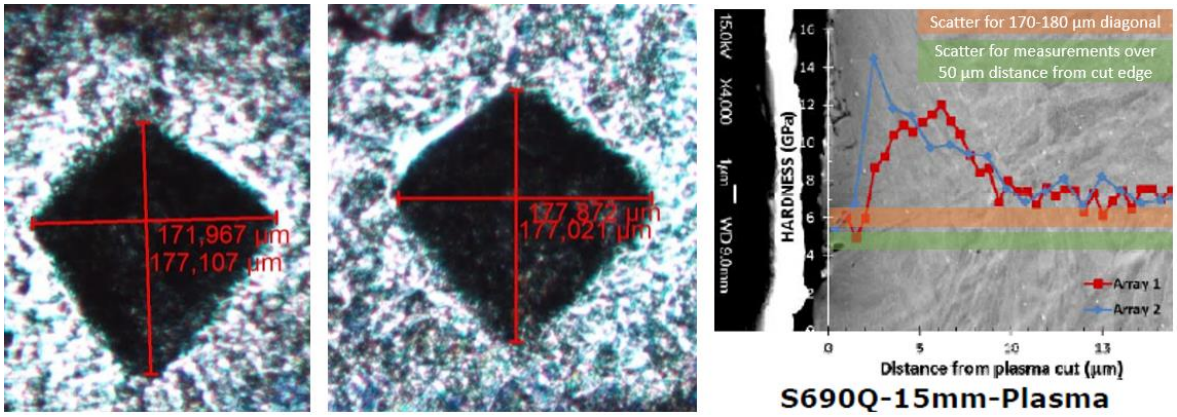

Figure 41. HV10 measurement points with diagonal dimensions and HIPERCUT (2016) plasma cut edge nano hardness result with LUT measured scatter.

Reduced notch effect at the transition zone between HAZ and base material where high residual stress concentration locates. A HAZ and a microstructure from the top of the CO_2 laser cut edge is presented in figure 45. The HAZ had constant depth of 100─120 µm and adapted to striation. Grinding, polishing and etching reduced notch depth compared to profilometer obtained results by material removal.

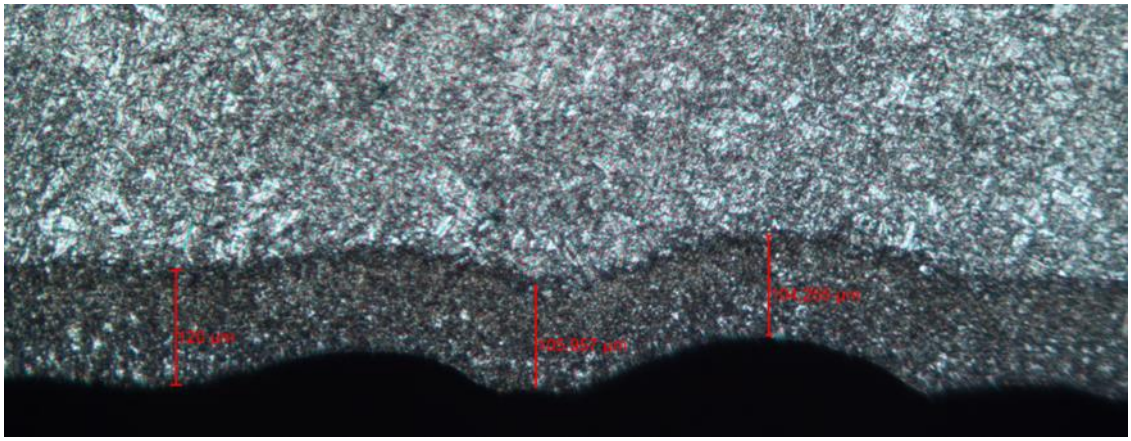

Figure 42. Microstructure image for top corner of CO_2 laser cut edge of S690QL.

4.4 Residual stresses

Residual stresses were measured by X-ray diffraction using Stresstech Xstress 3000 G3. Exposure time on residual stress measurements was 42 s, measurement head was tilted four times to left and right to 40° angle. Residual stresses were measured before the fatigue testing. Measuring area in X-ray diffraction equipment was 1 mm^2. The residual stress state was estimated to change on 1 mm distance when measured from rolled surface. In residual stress measurements the variation on thermally cut edges was very high compared to ordinary measurements due to hard surface layer.

Residual stresses from cut surface were tensile except acid treated S1100 Plus. Fiber laser cut S1100 have smallest tensile stress value at the cut surface. Four fiber laser cut S1100 Plus specimens were cleaned with citric acid and six specimens was measured without treatment. Treated and as cut measured averages are separated in figure 46. S690QL specimens were measured without citric acid treatment. Measurements from middle of the cut surface had big deviation. Average deviation in single measurement variated from 21 to 46 MPa from cut surface and CO_2 laser cut specimens had biggest deviation. Standard deviation from measurement results variated between 97 MPa (CO_2) and 17 MPa (Acid treated S1100 Plus). Residual stress measurements could have been disturbed at the cut edge because of changes in crystal structure especially when oxygen was presented at CO_2 laser and plasma cutting.

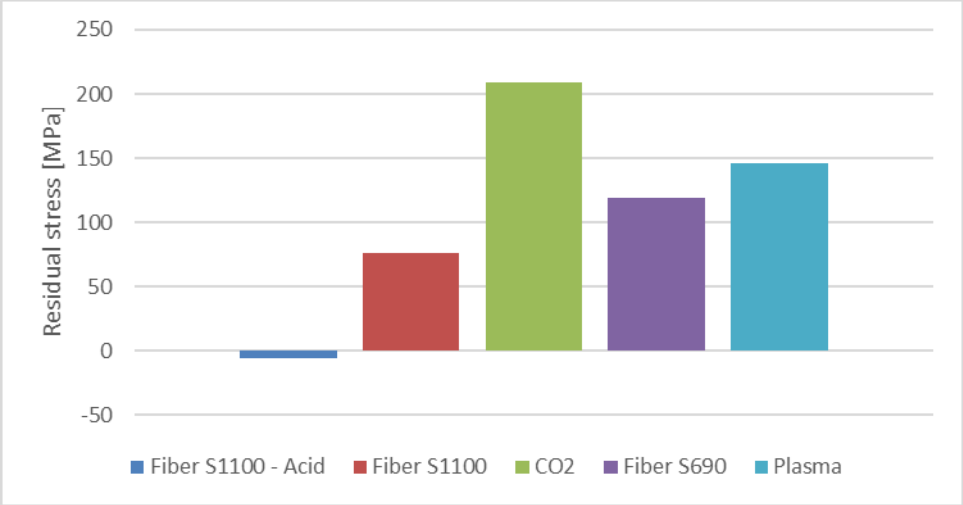

Figure 43. Residual stress from the cut surface.

Residual stresses measured from top and bottom of the specimens near cut edge. This measurement procedure was not used for every specimen and two different methods were used with 14 or 6 measurement point per specimen. Residual stress measurement from bottom of the S690QL with fiber laser cut specimen was distracted because of dross attachment on the edge and measurements point being further from the edge than in other measurements. For S1100 Plus acid cleaned specimens were measured from top and bottom sides. Because of limited measurement data and variated methods only minimum and maximum values are shown in table 13. Shading of the most tensile and compressive values was done for easier evaluation of table. Variation of measurement results can be seen when min and max values are compared.

Table 13. Maximum and minimum values of residual stresses from top and bottom sides and cut edges. Results are presented as [MPa]

Specimen	Top edge max	Top edge min	Bottom edge max	Bottom edge min	Cut edge max	Cut edge min
LC	176	-114	195	30	451	117
LF	-35	-120	-66	-177	252	-28
PB	185	83	88	-105	342	76
LF11	-116	-352	-66	-259	181	-32

Residual stress from LC5-1 specimen was measured from three points, middle of cut surface and top and bottom sides as close the edge as possible after fatigue testing. Before fatigue testing, 176 and 213 MPa residual stresses were measured from cut edges on from test specimen. After fatigue testing performed with stress ranges of 330 MPa and 397 MPa with $R = 0.5$ and $R = 0.4$ values, 78 MPa with 20 MPa variation was measured from cut edge. The measurements were done from top and bottom points also corresponding previous before testing points. From top and bottom sides, near cut edge, 13 MPa compressive residual stress was measured with 13 MPa variation while from bottom 20 MPa tensile stress was measured with 5 MPa variation. Based on this measurement the high hardness edge has more stable residual stresses than base material and HAZ that were measured from top and bottom directions.

4.5 Fatigue tests

Fatigue testing was done at LUT University by using the 750 kN and 1200 kN hydraulic test rigs with MOOG servo-control system. Four specimens were tested at Jyväskylä University of Applied Sciences (JAMK) laboratory with 600 kN test rig. The test setup is presented in figure 47. Constant amplitude loading was used with stress ratios of $R = 0.1$ and $R = 0.4$─0.5. For the S690QL specimens the maximum force was limited to 95% of yield strength. The maximum used force was 410 kN. In $R = 0.5$ test, the run out -levels were experienced with this maximum force and the stress ratio was set to 0.4 for further testing. Loading frequencies between 1 Hz and 3 Hz were used. The frequency was set according to test rig capacity. Run out level was expected after $2 \cdot 10^6$ cycles. If specimen reached run out -level and no crack initiation was evaluated the loading was started again with higher force and these re-tested specimens were included to test results.

Figure 44. Test setup in 1200 kN test rig.

Unexpected stress concentrations affected specimen. There was eccentricity on specimen and variable thickness of gage length area. FE-analysis was done for specimen with straight attachment on rig which resulted worst case scenario and attachment 1.25 mm offset loading corresponding specimen attachment position on fatigue testing. The stress concentrations affected crack initiation location on specimen. The worst case stress concentration factor in FEA was 1.06 and on the fatigue test rig simulated case 1.03 which is shown in figure 48. The stress was higher on ground edge than on straight cut section.

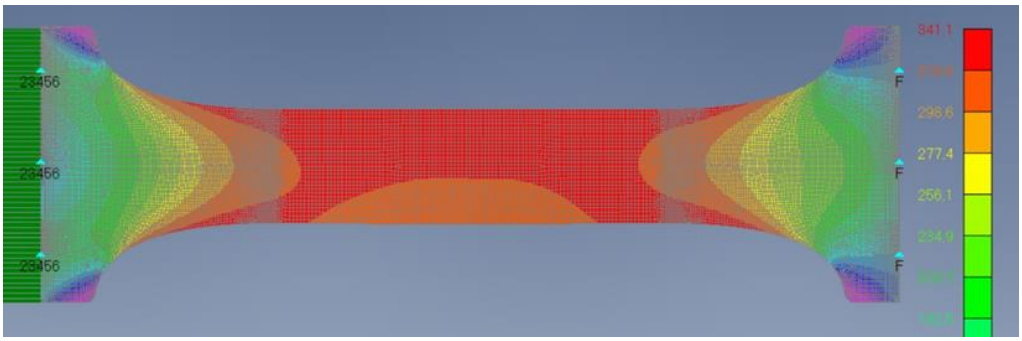

Figure 45. The specimen stress concentrations with eccentric loading.

Strain gauges were attached to assumed stress concentration areas to verify the FEA results. Strain gauges measured strain from notched side as close as possible cut edge on centerline and on beginning of researched section after ground section on moving end of specimen. Position of strain gauges is presented in figure 49. The crack initiated to notch on ground edge is shown and highlighted.

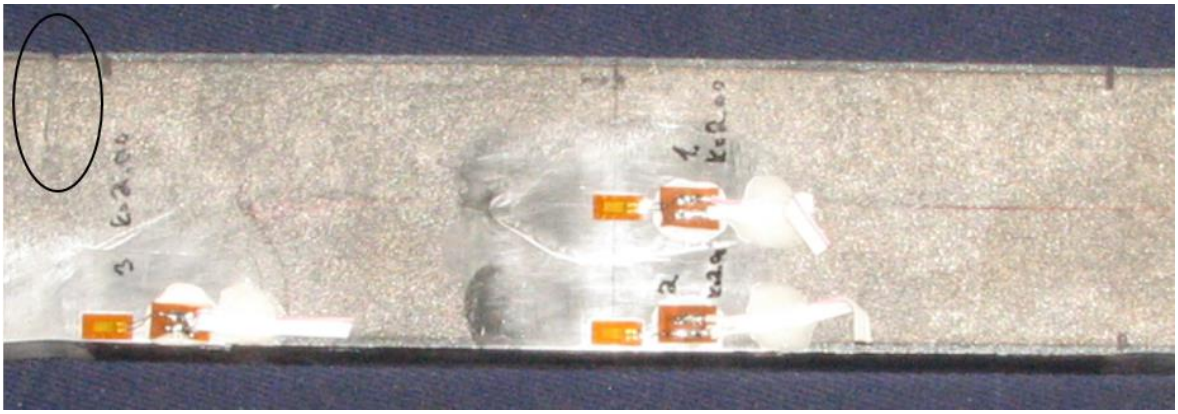

Figure 46. LC5-4 specimen with three strain gauges attached and crack on ground edge.

Static test for LC5-4 specimen was made with two different methods. The first test was done with specimen attached on straight position to the rig. Strain gauges were reset and static test to 350 kN loading was done. For the second static test the specimen was attached with 0.25° tilt angle. On straight attached specimen there was 2% extra stress on strain gauge on middle of specimen at the edge and by tilting the specimen 3 %-unit extra stress was applied in the middle of specimen. At beginning of ground and curved section tilting increased extra stress to 6% that FEA estimated. These extra factors were not included to fatigue test results but were calculated to evaluate total fatigue capacity of cut edges. The nominal stress from center of specimen strain gauge remained same in both straight and tilted cases.

4.6 SEM examination

Scanning electron microscope (SEM) was used to evaluate microstructure and fracture surface of specimens. SEM was used with SE (Secondary Electrons) and BSE (Backscattered Electrons) detectors. SE-detector was used to evaluate surface geometry and BSE-detector to evaluate impurities of surfaces. EDS-analyzer (Energy Dispersive Spectrometer) was used for elemental analysis for cut surface. EDS-method is based on X-rays. Atom emits X-ray when electron is replaced from outer orbital. EDS-detector measures energy of emitted X-rays and detects atom by emitted energy. Carbon content analysis of sample is not accurate with EDS because of contamination on sample surface.

4.6.1 Microstructure

Microstructure evaluation of CO_2 laser cut edge was performed with optical microscope and SEM. With optical microscope was it was not possible to classify microstructure zones and edge was curved in the preparation of polished section. Because of ground edge the actual edge was always out of focus with optical microscope. Microstructure image from BSE detector is presented in figure 50. At the cut edge, no grain boundaries were visible. Coarse grain zone followed the surface layer. The coarse grain zone turned into fine grain zone after transition zone.

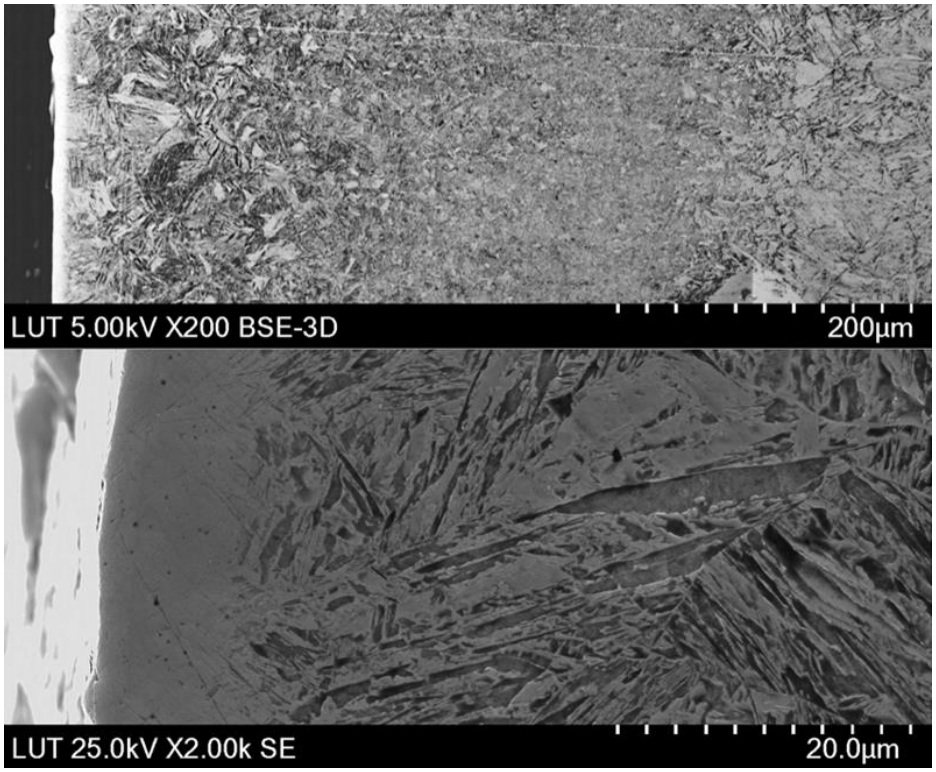

Figure 47. Microstructure of CO_2 laser cut edge with two different scaling.

Microstructure of fiber laser cut edge is distinguishing the CO_2 laser cut edge. Smooth layer on cut edge was not found. Discontinuity point was seen at boundary layer separation where defects had sharp edges. Three similar defects were found close together at laminar to turbulent gas flow transition zone. Microstructure of fiber laser cut S690QL edge with defect is presented in figure 51.

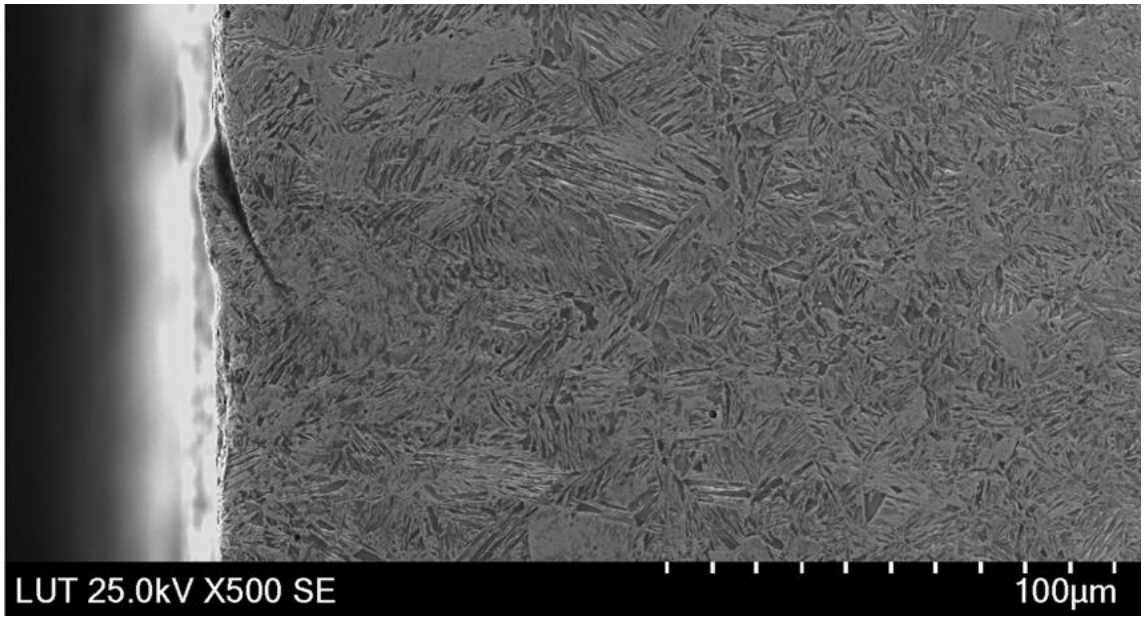

Figure 48. Microstructure and defect of fiber laser cut edge from S690QL specimen.

Pore like defects were found from fiber laser cut edge at 40─60 µm depth from cut edge from both SE and BSE detectors. Pore like defects on fiber laser cut edge are presented in figure 52. There was no certainty weather these defects were present after cutting or were they formed in grinding. Also smaller pore like defects closer to edge were found but with visual inspection was impossible to identify them as real defects in material instead of surface contamination.

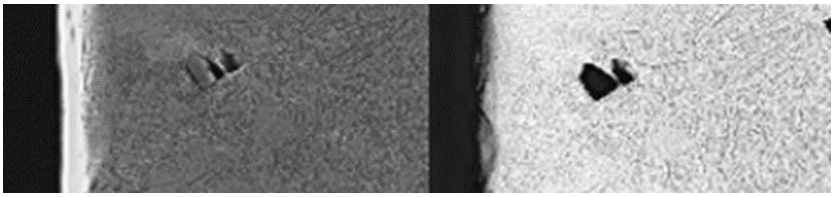

Figure 49. Pore-like defect on fiber laser cut edge.

4.6.2 Elemental analysis

Elemental analyses was made with SEM EDS-detector with 20 kV voltage and measuring spot size of 2 μm^2. 20 µm steps were used to evaluate element distribution from cut edge to the base material direction. Carbon was excluded from the analyses because of possible contamination and inaccuracy on metallic materials although it is shown in spectrum presented in figure 53. The spectrum has different spikes for elements because of different

energy of electron shells. If oxygen was present at high percentage, it would have been visible at the beginning of the spectrum but low amount of oxygen cannot be detected because of secondary spikes of other elements. For more accurate oxygen detection lower voltage would have been suitable but other elements would not have been visible with lower voltage.

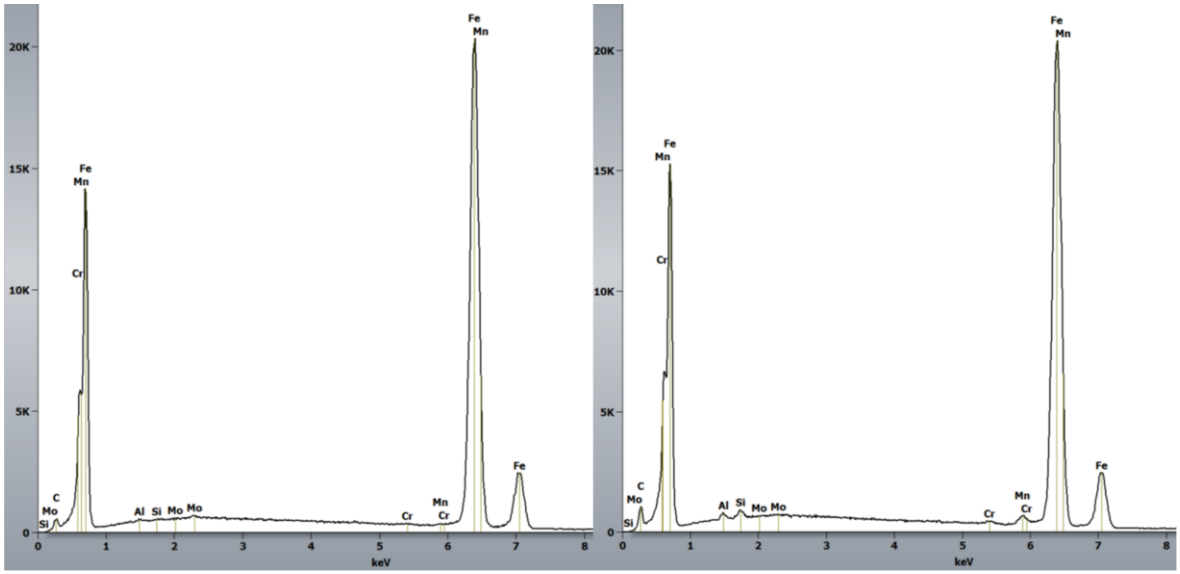

Figure 50. Spectrum from elemental analysis at CO_2 laser cut edge (left) and 0.1 mm from away edge (right).

Elemental analysis as a weight percentage was calculated from the spectrums without carbon are presented in table 14. Element change close to cut edge and full elemental mapping was made for specimens 20 µm steps from cut edge with EDS. In the S1100 Plus analysis was found that aluminum would possibly react with nitrogen forming aluminum nitride close to cut edge but further from cut edge chemical composition remains the same.

Table 14. Elemental analysis of S690QL with CO_2 and fiber laser cutting.

Element / electron shell	CO2 laser		Fiber laser	
	edge [m-%]	0.1 mm from edge [m-%]	edge [m-%]	0.1 mm from edge [m-%]
Al / K	0.2	0.4	0.3	0.3
Si / K	0.1	0.5	0.4	0.5
Cr / K	0	0.2	0.2	0.3
Mn / K	0.25	1.2	1.1	1
Fe / K	99.25	97.6	98	97.9
Mo / L	0.2	0.1	-	-

Based on the elemental analyses on small single spot the CO_2 laser cut edge was chosen for a detailed analysis. Mapping resolution of 256 by 192 was used with 5 by 5 pixel results averaging to reduce noise because of small amounts of elements. Elemental percentage was formed by X-rays emitted by the inner K shell of atom. Results of elemental mapping by pixel method is shown in figure 54 with the original SE-detector image. No sharp edge was found but elemental distribution followed area where grain boundaries were not visible. The change on elemental distribution was not restricted to edge but percentage of alloying elements continued increasing to 50 µm distance from edge.

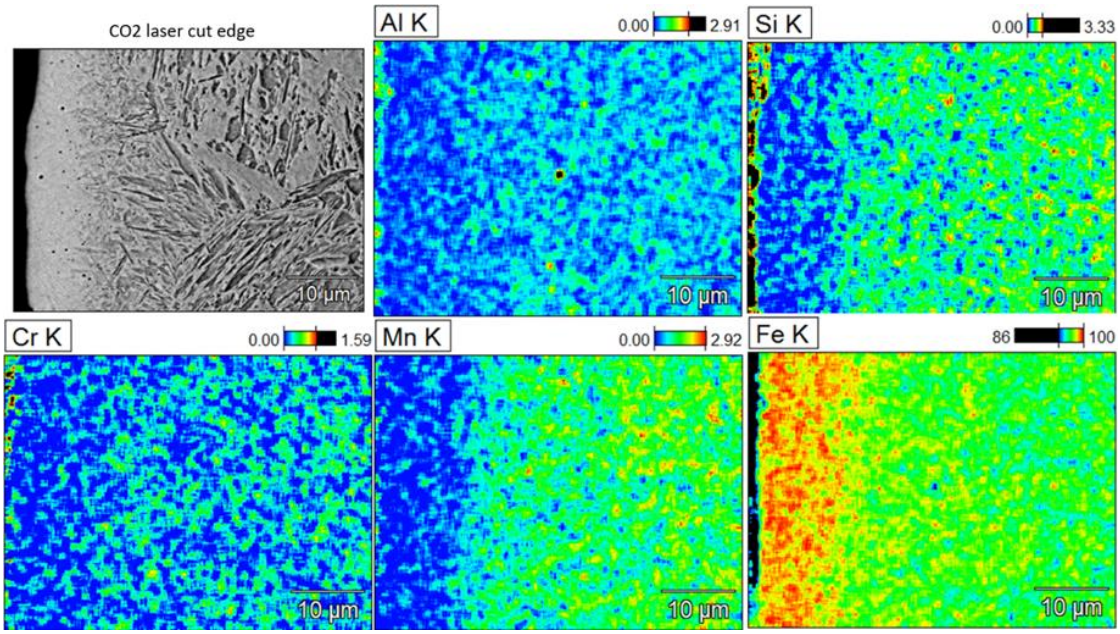

Figure 51. Elemental analysis by averaged pixel information.

Alloying elements react with oxygen forming oxides. Decrease in alloying elements could be explained by chemical reactions and because alloying elements are more reactive than iron, their relative share decreases close to cut edge. Carbon is more reactive element with oxygen than iron and even tough carbon content could not have been measured reliably can be assumed that carbon content has decreased with the other elements. In the spectrum there is a higher peak at 0.3 keV 0.1 mm way from cut edge than close to cut edge. If the contamination level was identical there was reduced amount of carbon at the cut edge.

Oxide layer was removed with grinding and etching but minor concentrations of aluminum, silicon and chrome were visible at the cut edge. This can be explained by measuring error or enrichment of element content due to oxidizing.

5 RESULTS

Fatigue testing was made for 40 specimens according to the test program and 3 extra specimens were fatigue tested. Specimen was re-tested with higher stress range if runout level was achieved and these continued tests were included for analysis. Run outs are included to results but not taken into account when calculating the slope of SN-curve. On welded specimens recommended practice is to include specimens broken before 2 million cycles to calculation of SN-curve. Only one specimen failed between million cycles and run out level.

5.1 Static test

Static test was performed for CO_2 laser cut S690QL specimen named to LCS-1. Specimen was not ground from the curved section. Test speed was 0.03 m/s and test was performed displacement controlled. Force was measured from test rig and displacement with Kyowa extensometer with 80 mm gage length. Maximum force in test was 505.8 kN and measured cross section area was 618.5 mm^2. Engineering tensile strength of specimen was 818 MPa while material nominal tensile strength was 780 MPa. Yielding started with 465 kN loading corresponding 760 MPa stress. Stress and strain values are presented in figure 55.

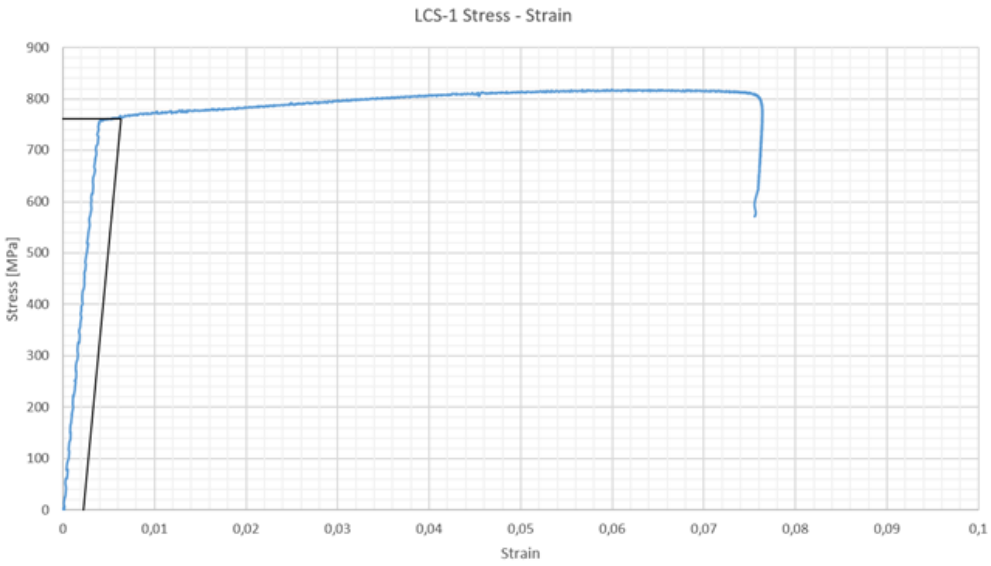

Figure 52. Stress and strain values from static test measured from extensometer.

Final failure location of specimen was outside extensometer but yield strength could still be obtained. The yield strength of specimen was 760 MPa while nominal yield strength was

700 MPa. Displacement of 26 mm was measured from failed test piece and from test rig displacement. For divided by straight section the elongation would have been 15% but also curved section had displacement.

After the static test the surface dimensions were 42 mm width, 9.5─10 mm near cut edges and 6.5 mm at the centerline of specimen. Calculated cross section area of the ruptured surface (Fig. 54) was 350 mm^2, around 60% from original cross section area. Elongation was different on edges than on specimen centerline due to changed material properties. Final rupture the thickness was reduction was smaller on edges than on center of specimen. Thermal cutting influence could be seen from different textures on fracture surface. In the HAZ, material behaved differently than on rest fracture surface and 45° angle between HAZ and smooth fracture surface was visible like cup and cone –type fracture. After HAZ there was 1─3 mm wide smooth zone followed by 0─3 mm parabolic rough surface which had straight edge 5 mm from cut edge. Parabolic fracture surface could be explained by cooling rate of material which is fastest at the center of specimen and slowest at rolled surfaces.

At the center of specimen there was most significant necking in both width and through-thickness directions In the middle of the through-thickness direction, also lamellar tearing occurred. The fracture had two similarly angled surfaces. After static test the specimen had lost 2 mm from its original width and yielded equally over the specimen. Gap visible on fracture surface was 5 mm wide while highest force on test was used at 16 mm displacement, 10 mm displacement before final failure. After failure at center of fracture surface the specimen had yielded 5 mm globally based on fracture surface measurements. Extensometer with 80 mm measuring distance was attached at the center of specimen and it measured 6.1 mm displacement measuring area being partly on necked area. At the moment of ultimate tensile strength 5.4 mm displacement was measured from extensometer. In figure 56, the final rupture is presented.

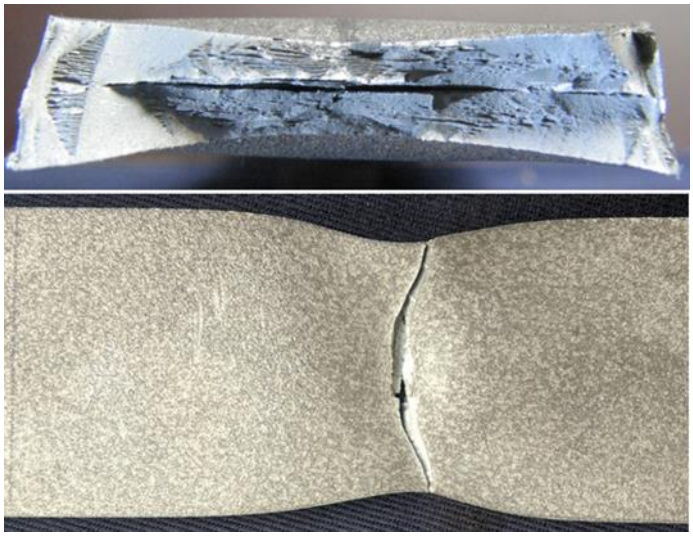

Figure 53. Fracture surface of static test specimen LCS-1.

Based on the measured data and fracture surface analysis, the stages of static test were analyzed. Displacement difference between center and edge of specimen was 5 mm. Total deformation of specimen was 26 mm. Center fracture at 21 mm displacement was estimated. Digital image correction technology (DIC) would have been provided more information about static test.

5.2 Fatigue tests

Fatigue test results are shown with the fitted SN-curved. Nominal stress was calculated with 51.65 mm width and nominal thickness of specimen, 8 or 12 mm. The results may be conservative due to bending stress and variable width of specimen. The extra stress applied to specimens from these factors was between 0% and 5 % of nominal stress depending on the specimen attachment to the test rig and crack initiation location. Minimum square sum of perpendicular distances (MSSPD) curve fitting was used instead of the standard regression analysis proposed in the IIW recommendations because of better R^2 value of MSSPD curve fitting. The specimens, failed outside the cut edge, were not included in the analyses. Effect of residual stress relaxation and fatigue limit was researched and, in some figures, multiple SN-curves were fitted. All results are presented with nominal stress range [MPa]

5.2.1 Test results

The fatigue tests are performed with stress ratios of 0.1 and 0.4─0.5. Collected test data is presented in figure 57 with specimens classified to test data used in fatigue analysis, run out results and failed test where crack initiated at the ground section. As can be seen the failed test had poor fatigue performance and are shown as an example of importance considering grinding in both design and manufacturing phases. In some cases grinding can decrease fatigue strength. The slope of SN-curve was 4.10 and the mean FAT-class was 234 MPa, calculated from test data.

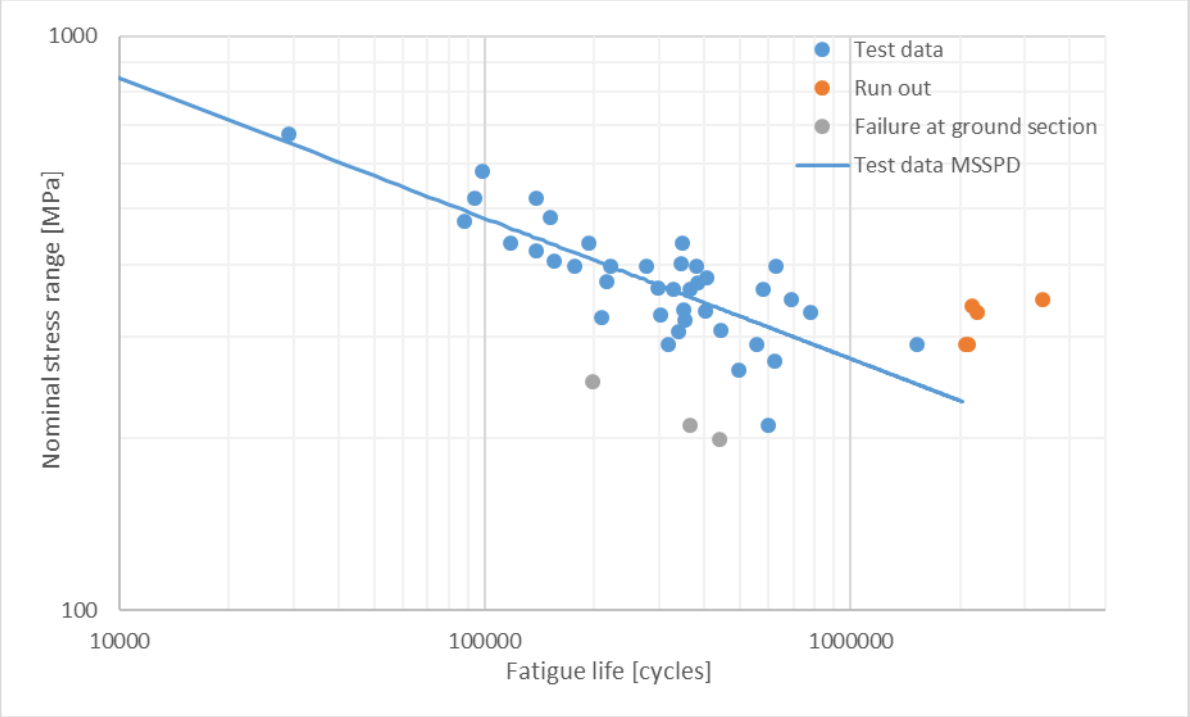

Figure 57. Results of all fatigue test.

Fatigue test results are presented individually for each test series to highlight the characteristics of different cutting methods and materials. Fatigue test results of fiber laser cut S1100 Plus are presented in figure 58. The slope of combined curve from both stress ratios R = 0.1 and 0.5 was 4.15 and calculated FAT class 235 MPa. Two stress ratios were combined in the same analysis because of low number of tests. The fatigue strength was slightly higher on lower mean stress test. From results should be noted that the knee point of the SN-curve was at $4 \cdot 10^5$ cycles and run out testing was done twice with 340 MPa nominal stress range.

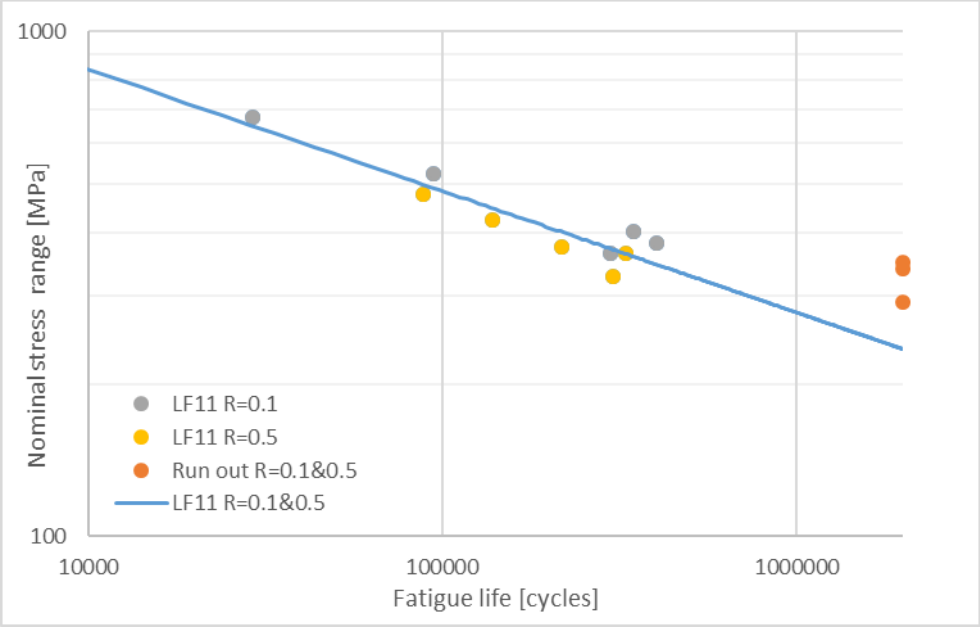

Figure 58. S1100Plus fatigue test results.

Fatigue test results of Plasma cut S690QL are presented in figure 59. With plasma cut, fatigue test the only failure occurred between million and decided run out level of 2 million cycles. Test were performed with R = 0.1 and R = 0.4. In the higher mean stress test, the fitted curve was had perfect fitting to the four test points while in the R = 0.1 test higher scatter in the test results was found due to long lifetime specimen better performance.

The SN-curves were fitted to all five R = 0.1 test results with R^2 coefficient of 0.91 and without the test result at the HCF regime, R^2 coefficient was 0.975. In testing below 10^6 cycles the R = 0.1 and R = 0.4 had almost identical slope R = 0.1 series had slightly better fatigue capacity. FAT values in plasma cut test were 252 MPa with m = 3.94 on PB R = 0.1 and with alternative fitting excluding HCF test 194 MPa with m = 2.79. FAT value calculated from R = 0.4 tests was 180 MPa with m = 2.80.

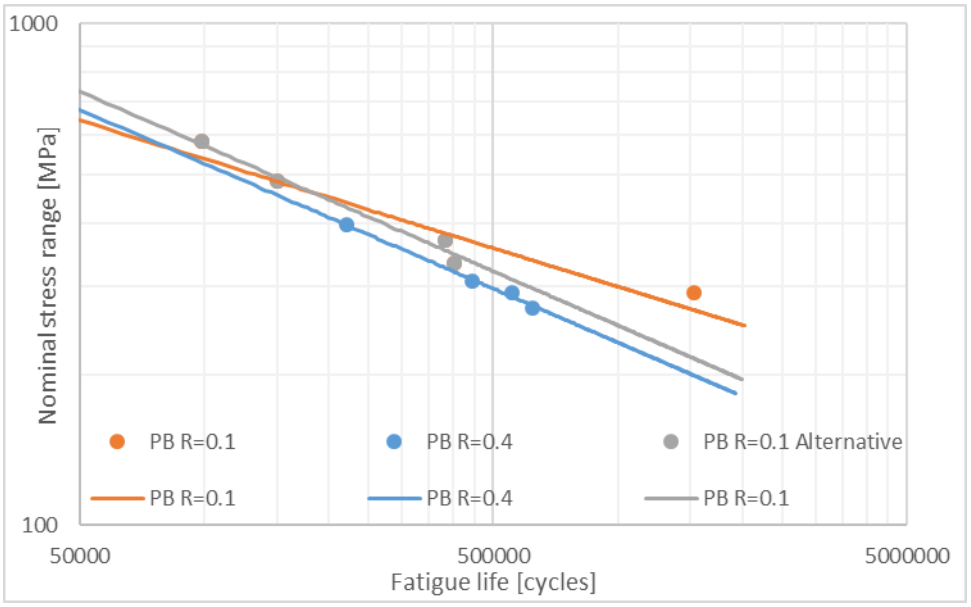

Figure 59. Fatigue test results plasma cut S690QL.

Fatigue test results of fiber laser cut S690QL test is shown in figure 60. Fiber laser cut t = 12 mm specimens were tested without removing the burr, and for one test (blue marker in figure 59), the burr was removed and the sharp edge was ground before testing. Slope of fitted curves was steeper with higher mean stress but the test results between $1 \cdot 10^5$–$2 \cdot 10^5$ cycles were almost converged. FAT value with R = 0.1 was 173 MPa with slope of m = 2.99 and with R = 0.4 FAT value was 118 MPa with m = 2.09.

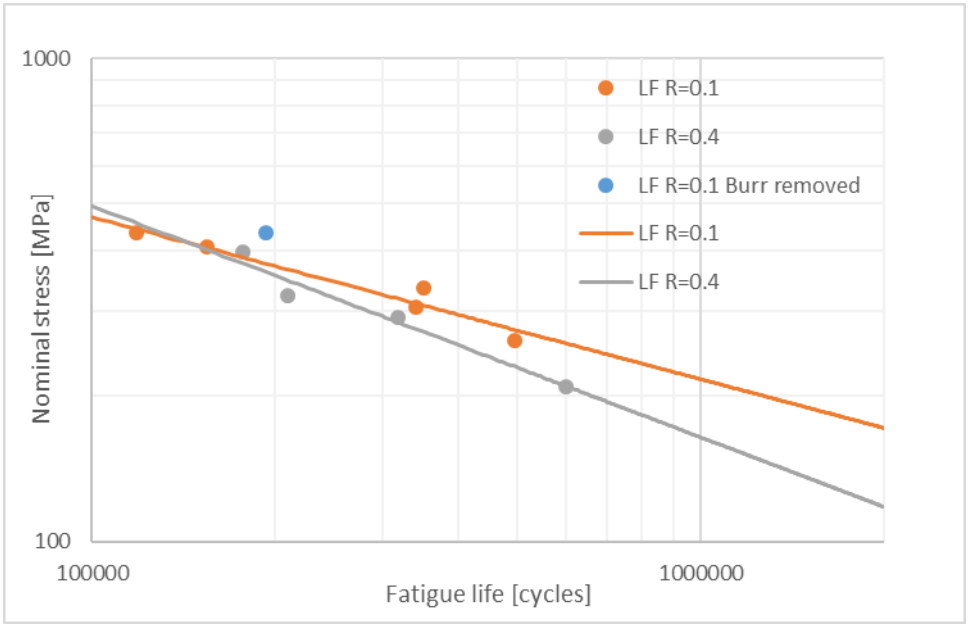

Figure 60. Fiber laser cut S690QL fatigue results.

Results of CO_2 Laser cut S690QL are presented in figure 61. SN-curves of LC1 and LC5-strest series intersected at $7 \cdot 10^5$ and run out -level was higher with R = 0.5 stress ratio. The slopes of fitted SN-curves were 3.77 and 6.99 with 264 MPa and 300 MPa corresponding FAT values.

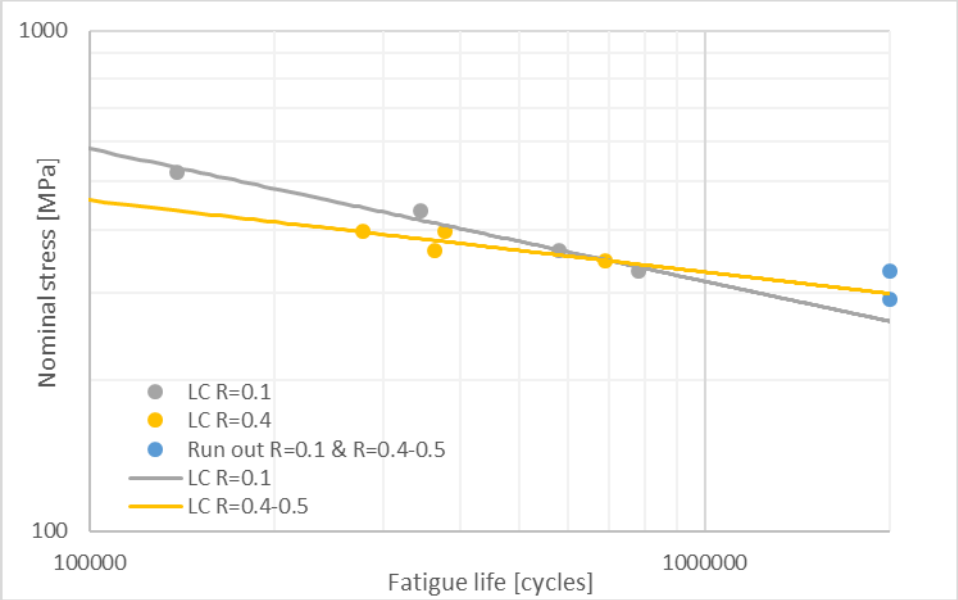

Figure 61. CO_2 Laser cut S690QL test results.

Milled specimen was tested as a reference for thermally cut edges. Crack initiated to ground section at 629379 cycles with 410 MPa stress range at R = 0.4 stress ratio. Visible crack was not found from milled specimen after fatigue testing. Milled specimen had significantly higher fatigue strength than any thermally cut edge.

5.2.2 Crack nucleation

The crack was nucleated from edge between rolled surface and cut edge from cutting direction. Crack growth in the S1100Plus was different than in S690QL steel. On fatigue testing of the S690QL, total rupture were not found while several S1100Plus specimens were broken to two pieces. The displacement limits for the test was set to 2.7 mm. Test was not continued to final rupture of the specimen because of lateral forces may harm the fatigue test rig. The displacement increased 0.1─0.2 mm on S1100Plus specimens after initial crack while on S690QL specimen where long crack was initiated the displacement increase was 0.3─0.5 mm measured from test rig with test force still applied. After displacement had

exceeded the limits, test was aborted. Crack nucleation of S1100Plus is shown in figure 62. Crack initiation from bottom corner was due to burr attachment at bottom of the cut. The burr act as an initial defect for crack growth.

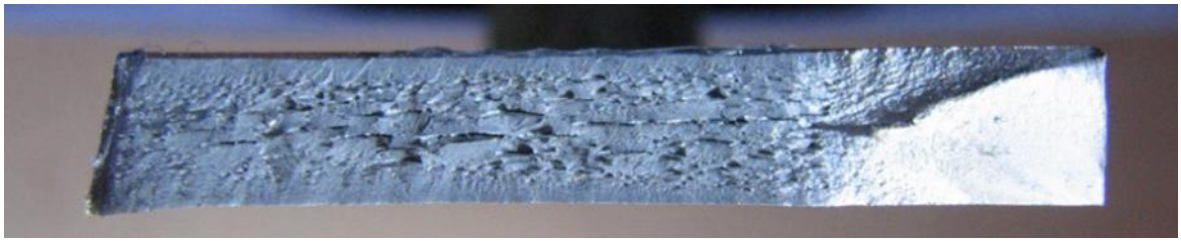

Figure 62. Fracture surface of the fiber laser cut of S1100 Plus.

From the CO_2 laser cut S690QL specimens various crack locations were found. The crack was initiated from top and bottom sides of the plate depending of specimen and loading. On top of the cut the HAZ was narrow but the notch effect was present and on bottom of the cut, there was wide HAZ but the notch effect from cut edge was smaller. Rolled surface was shot blasted on both top and bottom forming same stress concentration to both sides. Bottom initiated cracks were found only from specimens loaded in high cycle regime. From crack nucleation location the effect of residual stresses could be estimated. Residual stress was estimated bigger at bottom of the cut while it was significant factor on top of the cut also.

The LC5-5 –specimen was extra specimen in which relaxation of residual stresses were studied with comparison to run out -tested specimen. Failure occurred from ground section and cut edge was inspected carefully for cracks in propagation phase. In figure 63, the found crack is presented on the rolled surface (left figure) and on the cut edge (right). Scaling in both direction was same and length of the crack was 2 mm to both directions. The crack had initiated to location where two striation were on top each other total length of striation being 0.5 mm with 100 μm depth. On out of the focus on left macro image smaller 50 μm deep striation can be seen. These smaller striations are measured in standard surface quality measurements where 50 μm $R_{z,max}$ value was measured.

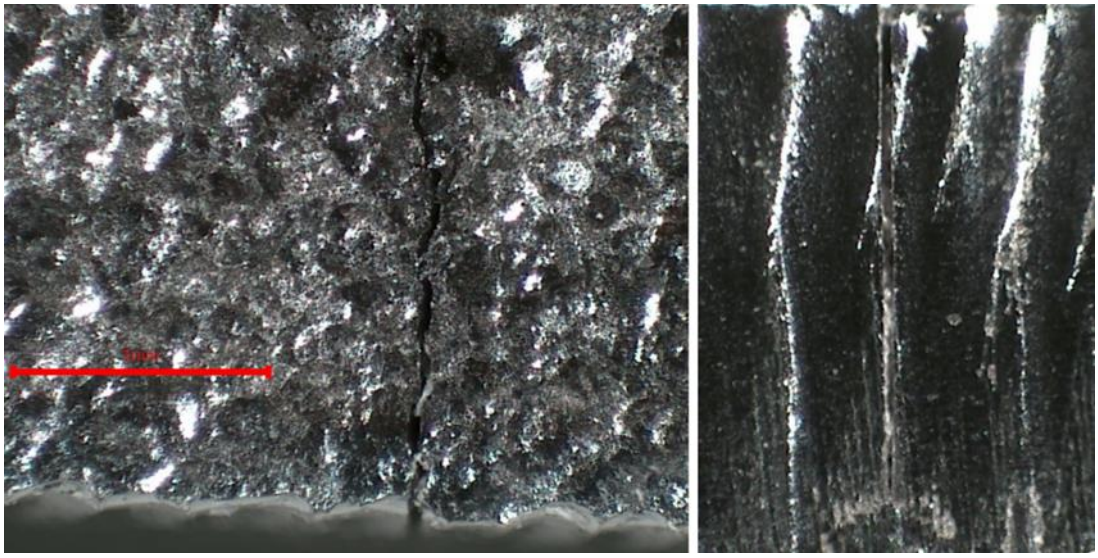

Figure 63. Fatigue crack on LC5-5 specimen.

Figure 64 shows the second failure mode of S1100 Plus specimen LF11-1-6 that was run out -tested before increasing load. Also small plasticity can be seen on rolled surface. This failure mode differed from other LF11-specimens where crack initiated from bottom corner of the cut. Crack initiation was similar to LF5-5 specimen with ground burr. Finding this kind of crack from LF11-series also indicates that there would have not been extra fatigue capacity if burr would have been ground from the LF11-specimen. Fracture was at the section where the turbulent assistant gas flow is present. In the LF5-5 –specimen in which the burr was removed, crack initiation was similarly at turbulent gas flow transition zone. For this kind of crack initiation the high pressure flow could turn inside the material and form defect to molten material acting as initial defect similarly as the burr.

Figure 64. Fracture on cut surface on LF11-1-6 specimen.

Fracture surfaces were analyzed from specimens with SEM. In figure 65, the top corner of fracture surface from LC1-2 specimen that was tested to run out at first test and then loaded

with loading of 360 to 36 kN obtaining 520 MPa stress range. Tested fatigue life of the specimen was 138998 cycles. The crack has initiated from the top corner of cut edge and with high stress range the area of fatigue fracture was small and the area of fast fracture was large. Crack had propagated at the top surface inside the specimen and smooth dark area could be seen 500 µm below cut edge.

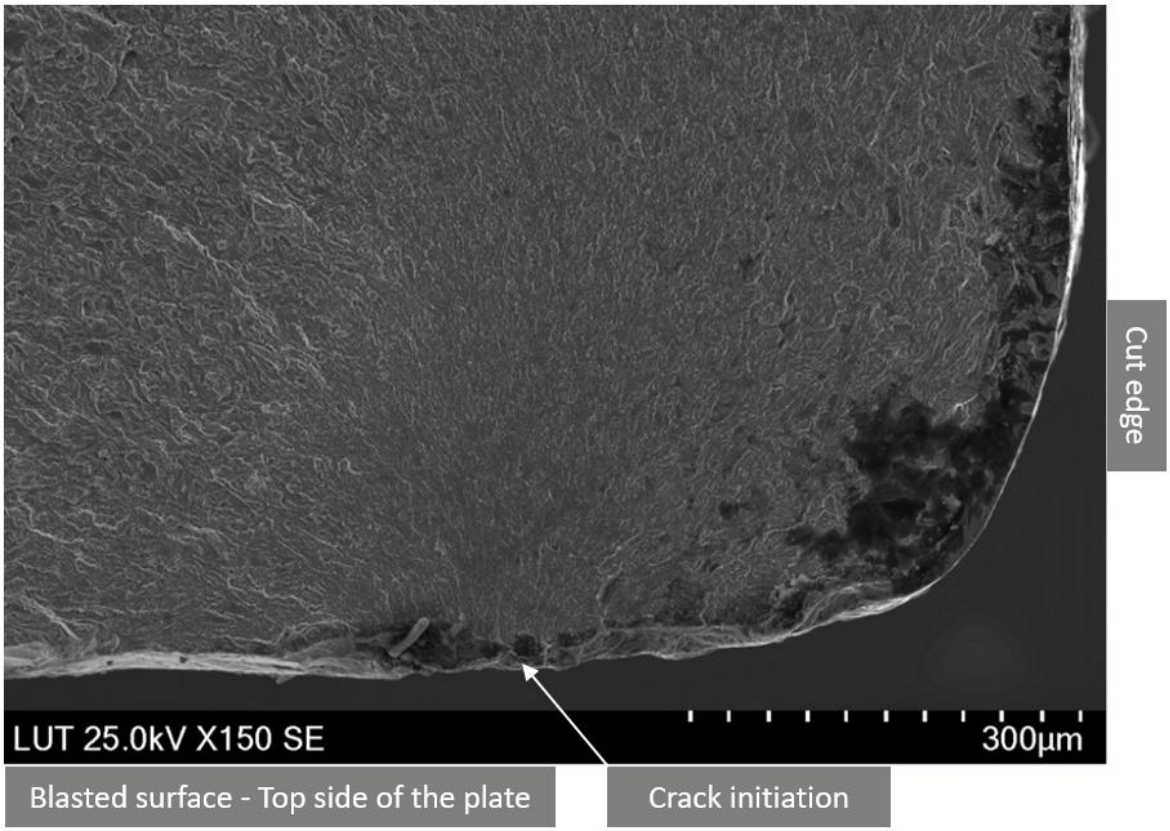

Figure 65. Top corner of fracture surface from LC1-2 specimen.

Defects from shot blasting are visible in figure 66. Notch from blasting may be reason for crack initiation from bottom of the cut. When fatigue crack was initiated from bottom side of CO_2 laser cut specimen, it indicates fatigue limit on striation area because this failure mode happened only with low loading cases. On fatigue testing CO_2 laser cut specimen the fracture initiation point was dependent on tested stress range. With high loading crack initiated to top side of specimen while on low loading crack initiated to bottom side of specimen.

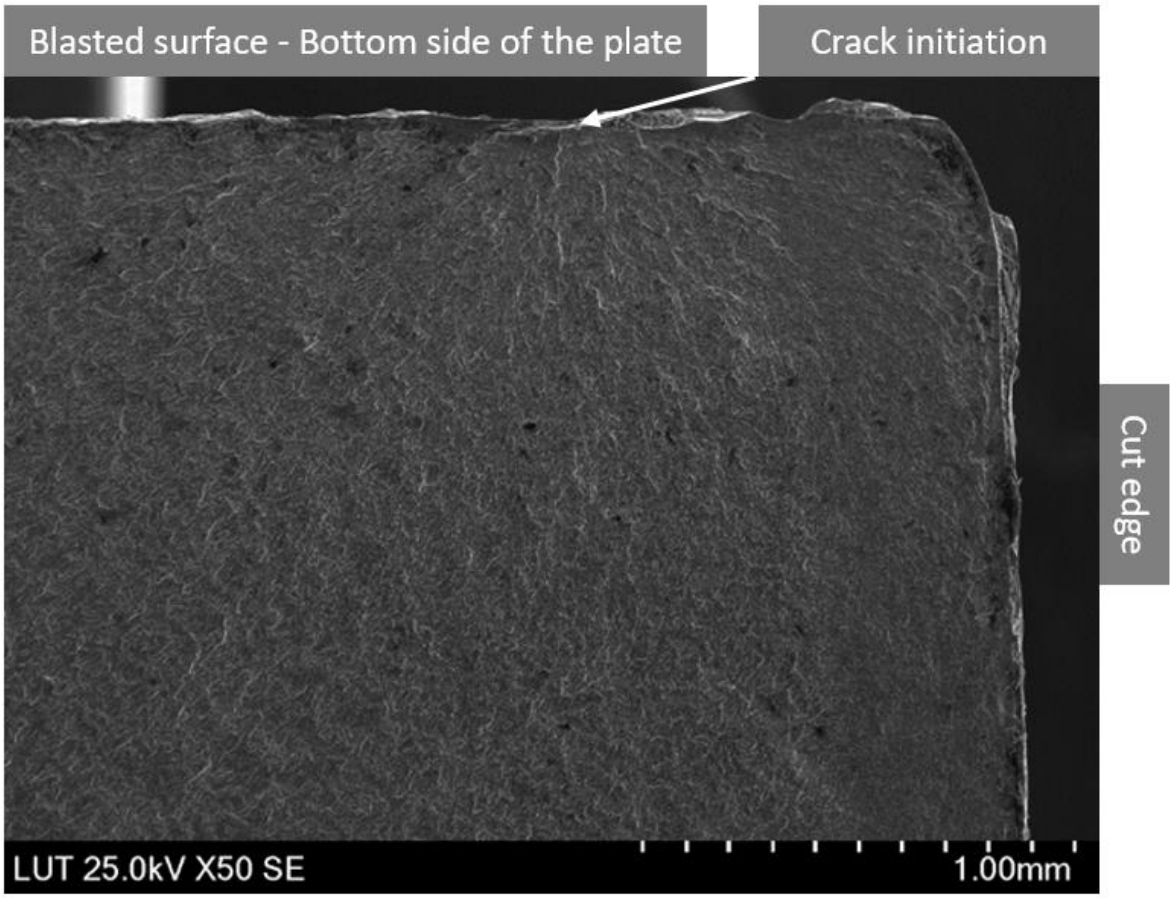

Figure 66. Bottom corner of fracture surface from LC1-5 specimen with low stress range.

The fiber laser cut LF1-4 specimen fracture surface is presented in figure 67 where crack initiation location is marked. In this specimen, the lines to fracture origin can be clearly found. In LF1-4 specimen there was dross attachment on bottom of the cut surface and fracture line can be found on HAZ pointing to bottom corner of the cut. There are also lines next to HAZ. On fiber laser cut S690QL specimens small cracks around the bottom corner and when burr was removed the crack were found. This type of crack propagation differs from CO_2 laser cut edges where crack initiated to rolled surface on base material hardness zone and eventually penetrated the cut surface.

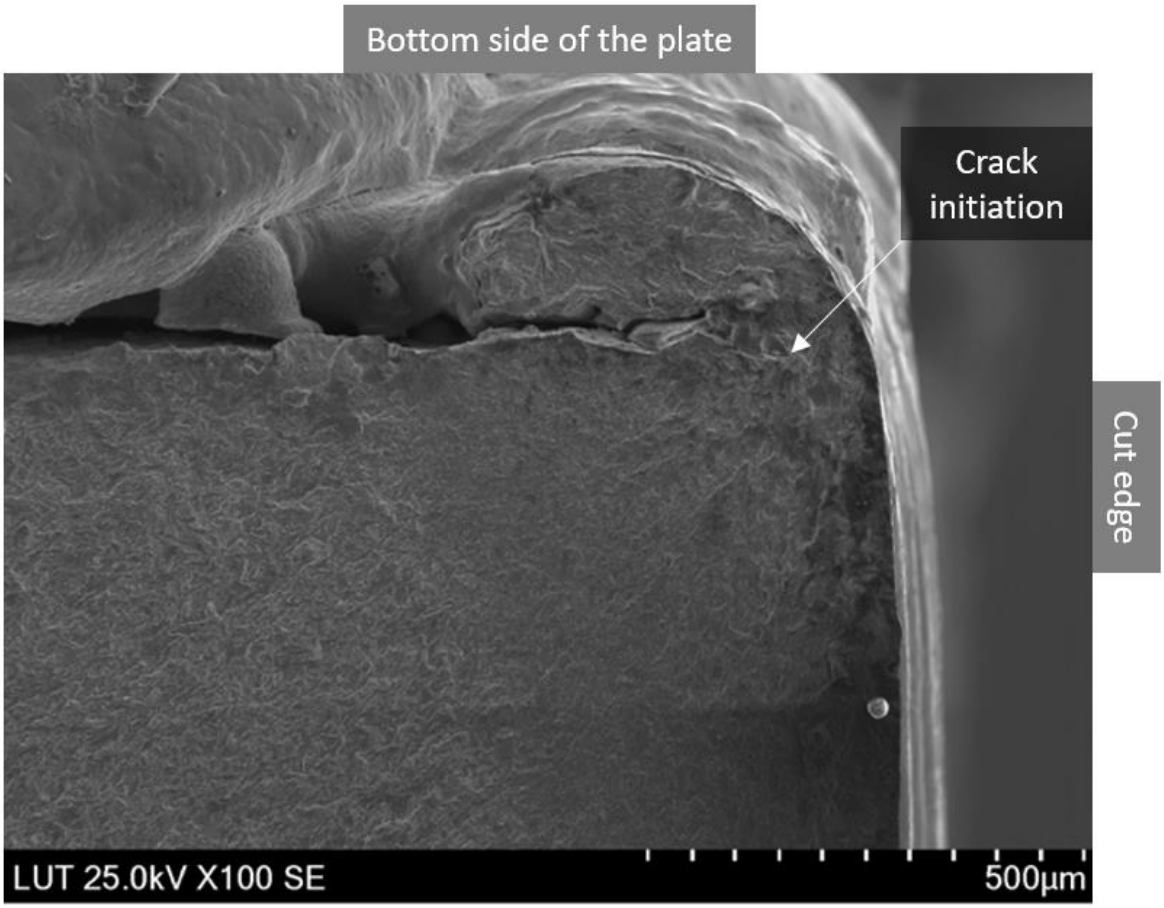

Figure 67. LF1-4 Fracture origin at burr.

Plasma cut specimen fracture surface is shown in figure 68. The HAZ of plasma cut specimen was straight and 300 µm wide. The smooth gray area extends to base material shot where blasted surface had notch in profilometer examination. On SEM-image small notch at the burr is visible. The defects locate on different material properties area. Cutting defect locate at hard surface with low residual stresses while blasted defects were on base material with high residual stresses. Combined notch factors from burr attachment and shot blasted surface affected fatigue performance of plasma cut specimens.

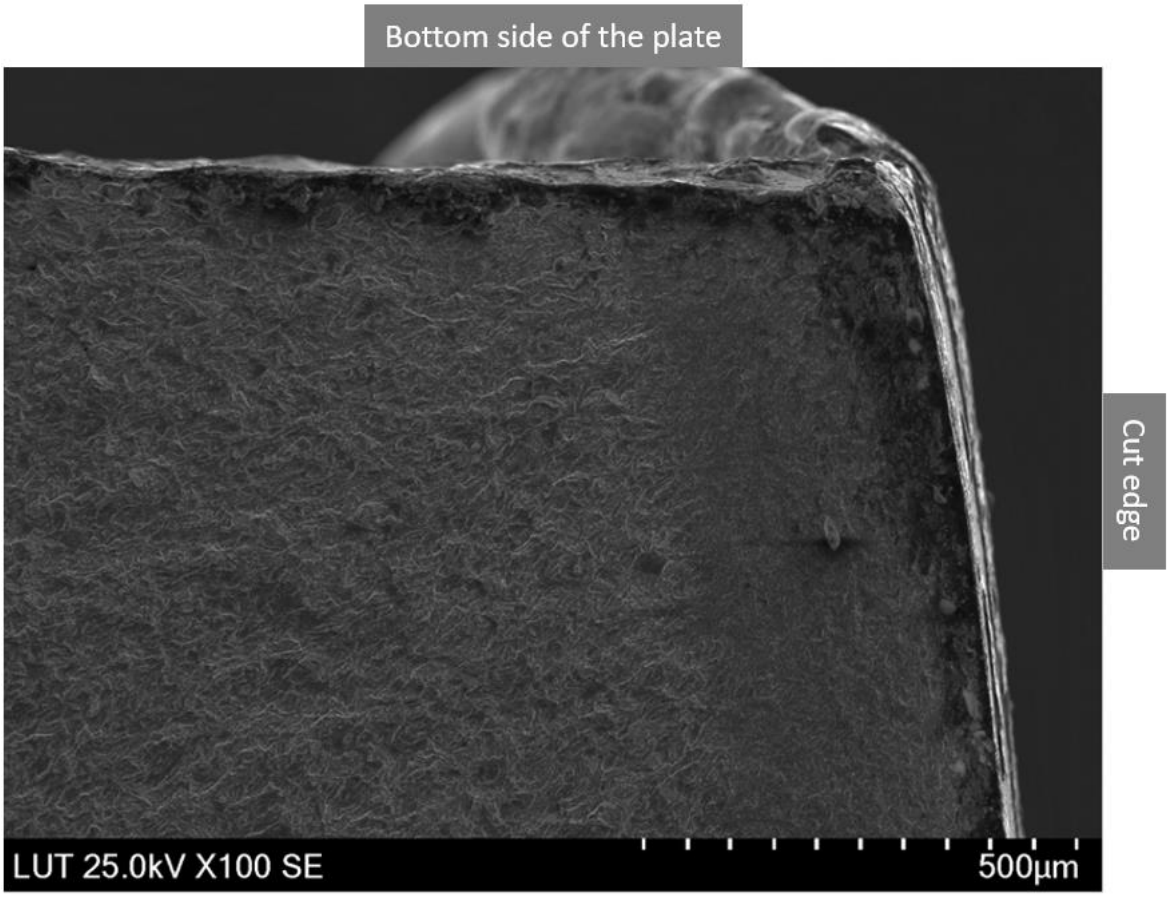

Figure 68. Plasma cut fracture surface.

The S1100 Plus specimens behaved differently than S690QL. In S1100 Plus specimens, there was small but sharp burr on bottom of the cut. The burr was almost invisible for eye but was felt by hand clearly as a sharp edge. For the S1100 Plus steel, more accurate hardness measurements were not available in literature but hard surface layer is visible in figure 69. Fatigue propagation marks are visible after 50 µm very high hardness zone that has different surface texture. For hardness measurement in this area very small measurement tip should be used. For the 4R method the ordinary HAZ measurements can be used because of crack nucleation from ordinary HAZ with measured hardness of 480─500 HV. The HAZ can be seen in figure 69 as a straight gray area 300 µm width from cut edge. The smooth crack propagation, dark grey area extends 30 µm to base material before crack propagation becomes faster. Shades visible at the corner in the figure were formed in crack propagation because contamination or different elements were not visible at BSE-detector.

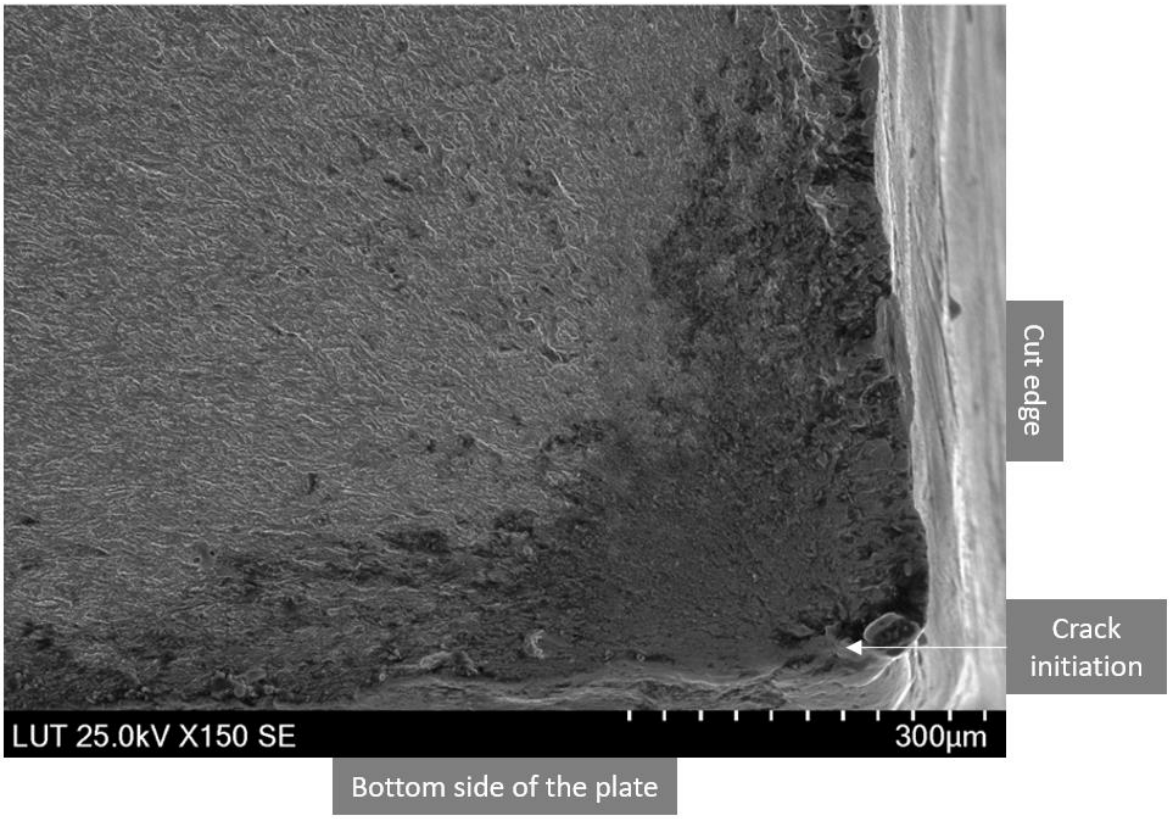

Figure 69. Fracture surface of LF11-1-3 specimen from burr at the bottom corner of the cut.

The effect of burr attachment was hard to research because It was difficult to estimate reliably the burr shape. In general outward facing notches do not form stress concentration because force is not transmitted through them. Burr acts as discontinuity point and in the PB, LF and LF11 –specimens crack initiation marks were found on burr area. The burr attachment might affect the cooling time locally and influence material properties like residual stress, hardness, microstructure and strength. LF-specimens had the most significant burr and one re-test was made with burr removed and sharp edge ground. Re-testing was done with F_{max} 300 kN and F_{min} 30 kN. In test series the LF1-1 had fatigue life of 118241 cycles while burr removed and edge ground extra specimen LF5-5 had fatigue life of 193234 which was clearly shorter than LC1-1 specimen 344487 cycles with same forces and no burr attached at cutting. When surface striations were modeled in FEM, the LC-specimen had higher obtained notch stress from biggest striation than LF-specimen.

In thermally cut edges, the burr may be attached to bottom of the edge and form stress concentration. The burr of fiber laser cut S1100 Plus specimen is presented in figure 70 with

detail image superimposed to figure. Optical microscope image of the burr demonstrates problem with cut edge imaging with optical microscope. On figure 70 the exact edge is not visible but fading of cross section to out of focus and darkness. In fatigue testing the burr behaved as an initial crack. In literature review, was found that removing this kind of burr would improve fatigue life by 33%.

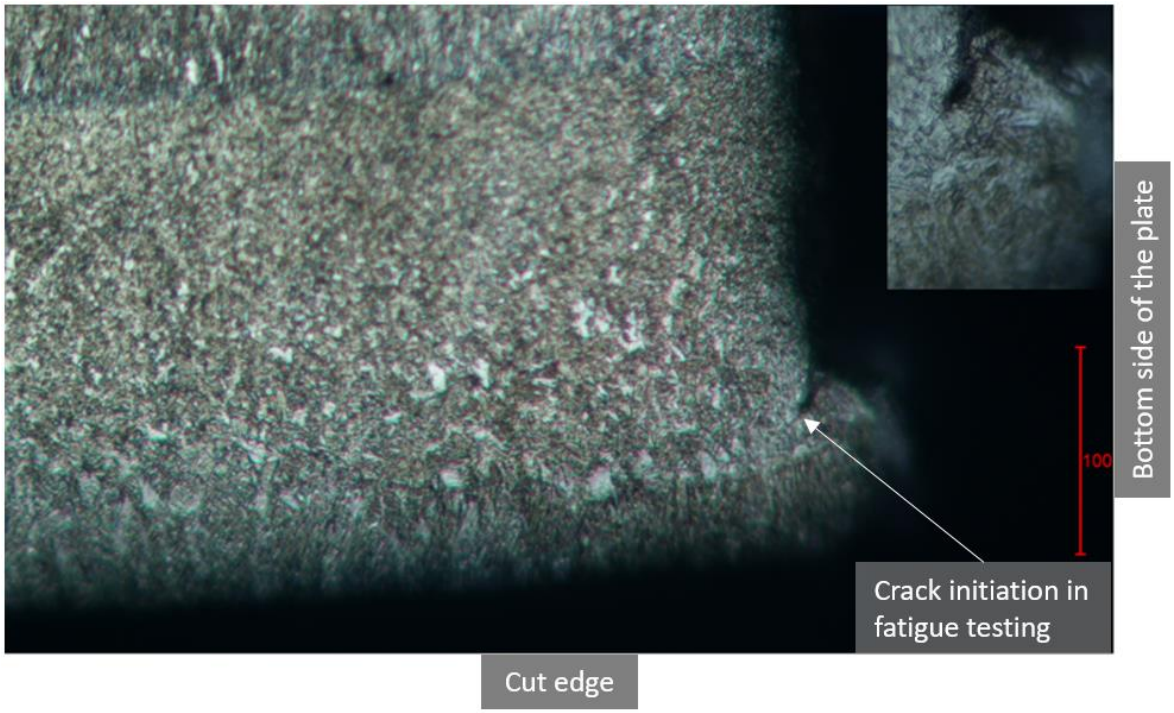

Figure 70. Burr in a S1100 Plus specimen. Scaling in [µm].

When S1100 Plus specimens were fatigue tested, there was tearing at the center of the plate. The tearing did not influence the fatigue performance of the cut edge specimens while it was significant factor affecting on final fracture. Also high number of cracks in base material were found from opposite side to crack nucleation with increased stress by reduced cross section area.

One fiber laser cut specimen was tested burr ground. Crack initiation location moved towards centerline of cut edge to point where striation pattern changes. The LF5-5 specimen was interesting because it could be compared to CO_2 laser and plasma cutting because burr was removed and ground. Fatigue performance was still worse than other cutting methods. SEM-images were taken from crack initiation point and fracture surface is presented in figure 71 with detail from fracture origin. Reason for fracture initiation was not visible but

inward facing defect was considered. The higher magnification detail location is marked with an arrow.

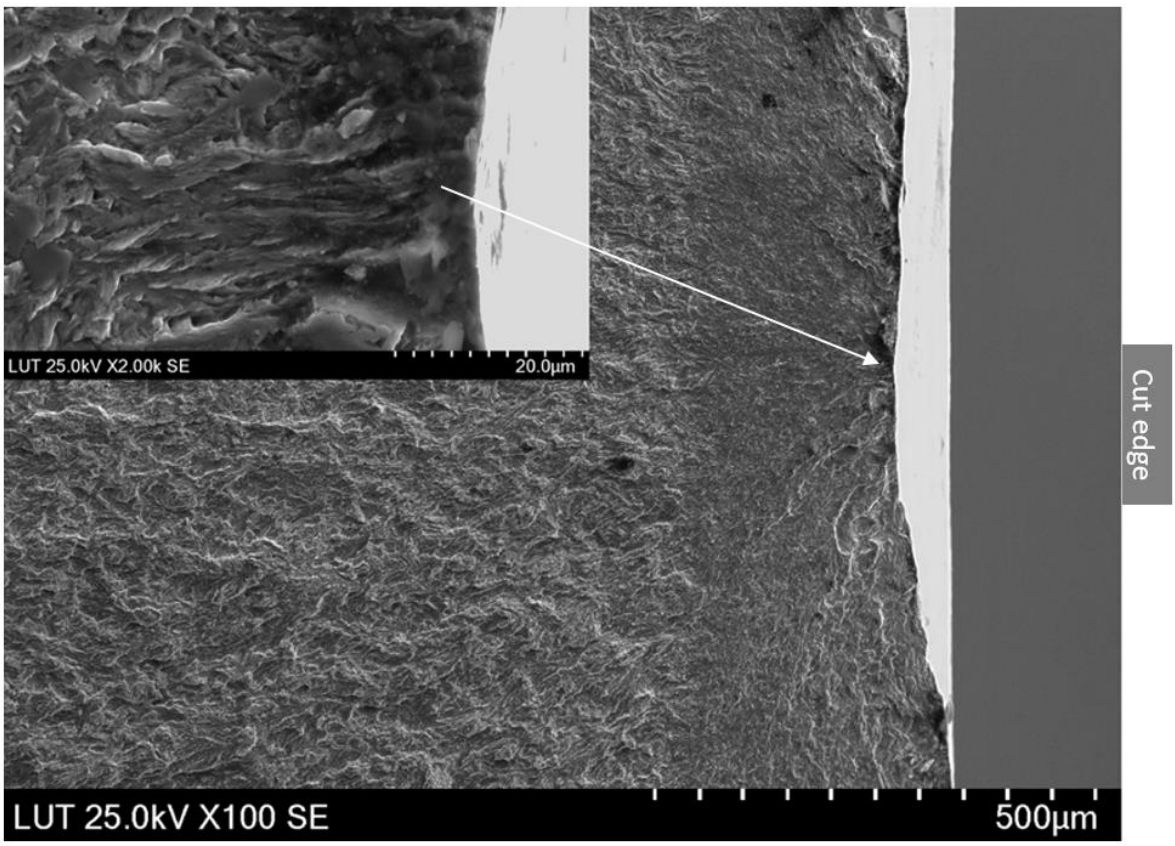

Figure 71. Fracture origin on burr ground LF specimen.

Failures from ground section occurred several times on S690QL specimens. Fatigue performance of these specimens were poor except specimen milled after plasma cutting. Crack initiated from rolled edge instead of cut edge. Defects from shot blasting were initial defects that restricted fatigue performance. Grinding of curved section increased stress on critical section and led to poor fatigue life. Crack propagation from shot blasted surface at ground section is presented in figure 72 with SEM-image from BSE-detector.

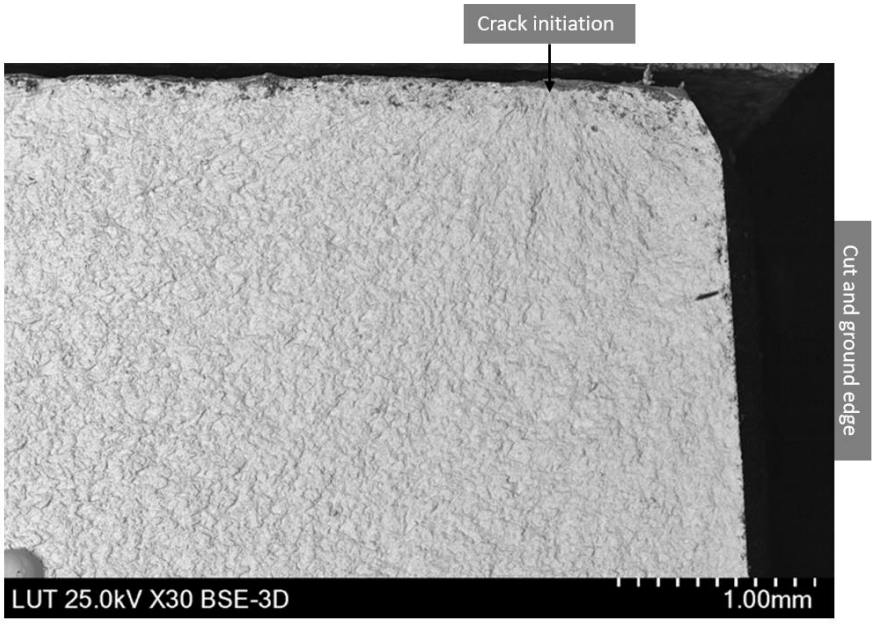

Figure 72. Fracture surface of LC5-5 –specimen failure from ground section.

Crack initiated close to strain gauge in two specimens, PB1-3 and LF11-1-2. Figure 73 shows the crack location and direction related to strain gauge. Maximum micro strain value from measurement period of these specimens are presented on figures 74 and 75. Run out - test were evaluated and micro strain remained steady during test and increase in micro strain can be assumed to cause by crack growth. Based on these measurements the crack nucleation time was 15% of total lifetime on S690QL specimen and 25% on S1100 Plus specimen although the stress variation of specimens differed and the crack was not exactly on the centerline. The steady crack growth for S690QL and S1100 Plus specimens was around 60─65%. The rest lifetime with steady force still applied was 25% for S690QL and 15% for S1100 Plus specimens.

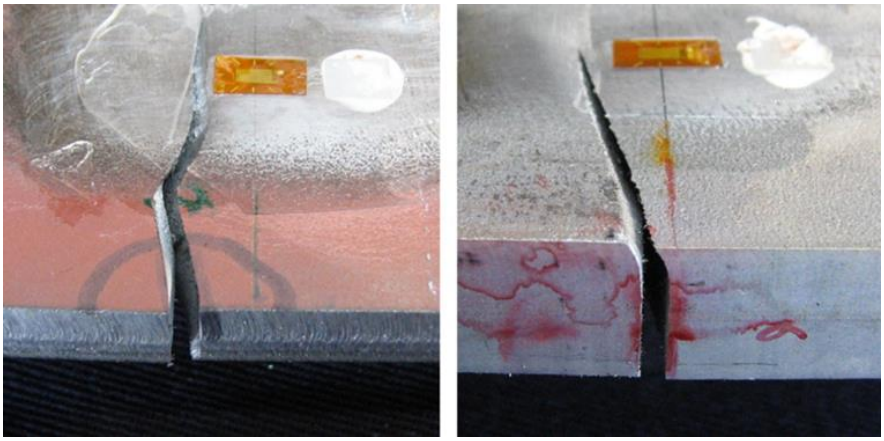

Figure 73. The crack relative location to strain gauge on micro strain specimens.

In PB1-3 specimen the crack initiated on strain gauge area. Strain gauge obtained micro strain is presented in figure 74. The micro strain was steady at the beginning of the fatigue test and then it started to grow without changes in forces. The crack nucleation can be seen as increase in micro strain. Steady increase in PB1-3 specimen micro strain indicates area reduction of 15–20 mm^2 or 2–3% in cross section.

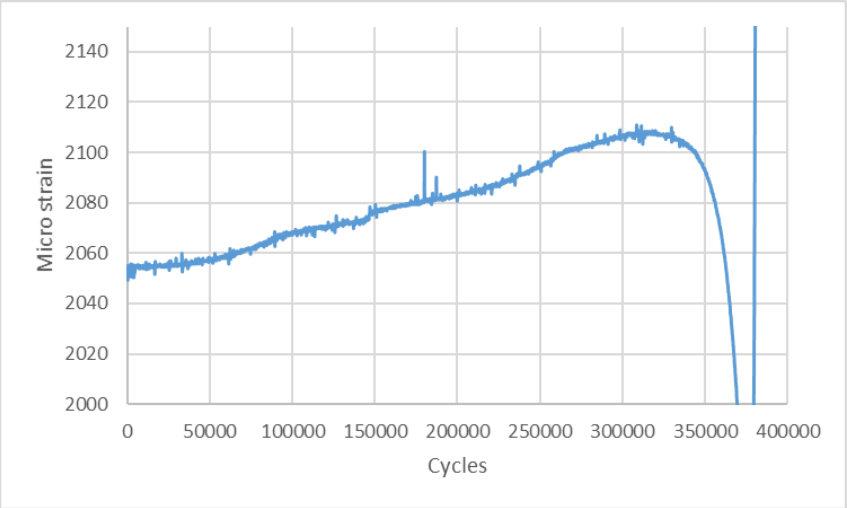

Figure 74. PB1-3 specimen micro strain.

Figure 75 shows corresponding micro strain and force diagram of S1100 Plus specimen. The micro strain was steady to 25000 cycles and then it started to grow linearly to 80000 cycles. After linear increase the micro strain began to grow exponentially and at 94207 cycles thee specimen failures.

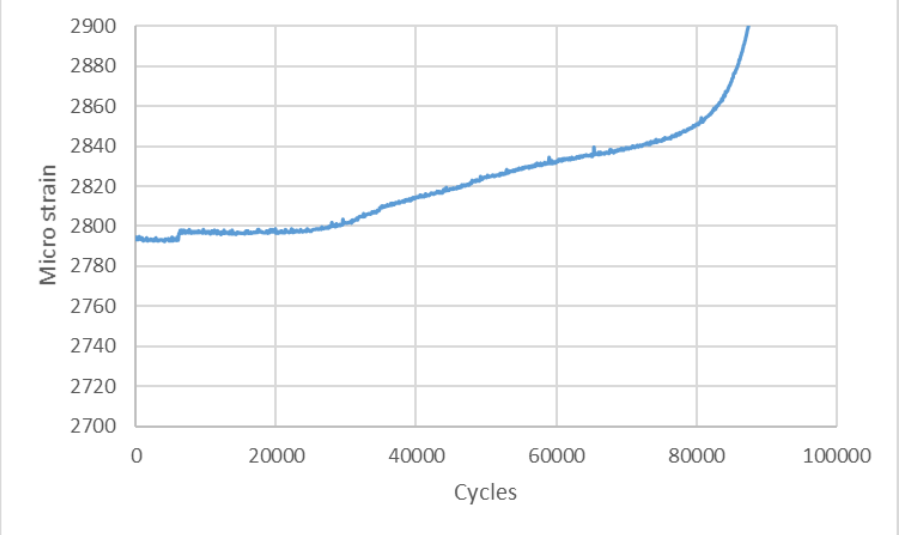

Figure 75. LF11-1-2 specimen micro strain.

5.2.3 Notch effect

Pessoa et al. (2017) researched fatigue of laser cut edges and found that hard layer with fine grain microstructure on cut edge could protect cut edge against the notch effect. The most significant notch effects were evaluated from burr and pores on or under hard surface layer. Research in this thesis support the theory. Notch effects are presented at bottom of the notch. Also burr and pore influence was noticed on fatigue testing over notch effect from striations.

Notch effect of striation was evaluated from microscopic images and 3D-scanned specimens and utilizing FEA. The notch effect evaluated with width and depth parameters and adapting notch radius for these parameters. This ideal notch is close to existing notch but small differences due to shape can be estimated. The biggest notch effect was evaluated from CO_2 laser cut specimen with factor of 2.0 and smallest from plasma and 8 mm sheet fiber laser cutting with factor of 1.25─1.35. Fiber laser cut quality decreased on thicker sheet and notch factor of 1.5─1.6 was evaluated for 12 mm sheet. Profilometer obtained notch FEA results for notch effect on CO_2 laser cut edge is presented in figure 76 which represent the short notch (table 16) with 50 µm depth and 250 µm width with notch factor of 2. Notch stress was highest on CO_2 laser cut specimens while fatigue strength was still best on LC series compared to other tested series.

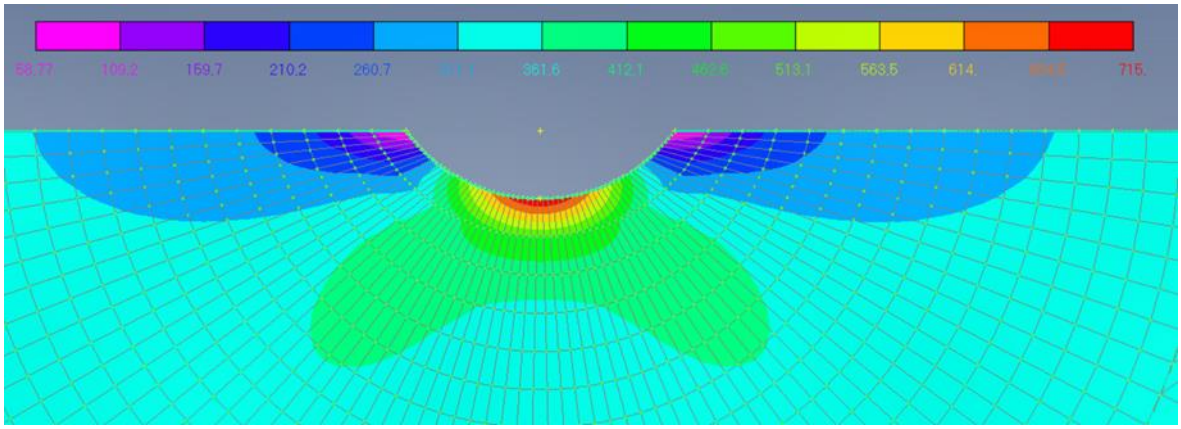

Figure 76. Notch effect on CO2 laser cut edge.

Profilometer obtained notch dimensions were gathered to table 15. Notch effect is results of notch width and depth. Notch dimensions are usually expressed with depth parameter only but also the width parameter is important when notch stress is considered.

Table 15. The estimated notch dimensions from striations from different cutting methods.

Specimen	Location	Width [mm]	Depth [μm]
LF	Bottom	0.5	50
LF burr ground	Middle	0.8	70
LF11	Middle/Bottom	0.5	50
LC short notch	Top	0.25	50
LC long notch	Top	0.4	100
PB	Bottom	0.3	20

5.3 4R method

4R method is originally developed for welding and the master curve from 4R method is obtained from fatigue test results of welded specimens. Mechanized thermal cutting is more stable process than welding and characteristic master curve of 4R is conservative for thermally cut specimens. Further research would be needed for determining the characteristic master curve for thermally cut edges. The 4R method mean curve seems suitable for thermally cut edges but the crack initiation point variates. Crack may propagate from cut surface due to stress concentrations or from the softened zone due to high residual stress and lowered fatigue limit of base material.

In 4R method, the material ultimate tensile strength can be obtained from local hardness based on equation.

$$R_{m,HAZ/soft} = \frac{H_{HAZ/soft}}{H_{bm}} \cdot R_{m,bm} \tag{16}$$

Where

$R_{m,HAZ/soft}$	local tensile strength	[MPa]
$H_{HAZ/soft}$	local hardness	[HV]
H_{bm}	base material hardness	[HV]
$R_{m,bm}$	base material tensile strength	[MPa]

For cut edges the hardness properties have been defined in the EN-1090 standard. For 4R method, hardness-related tensile strength correction maximum hardness defined in EN-1090 standard can be used. For S355 steel, the maximum permitted hardness is 380 HV and for higher yield strength steel grades 450 HV. Tensile strength of HAZ can be derived from maximum permitted hardness divided by base material hardness and multiplied with original tensile strength. In other researches S355 have had similar fatigue strength at run out -level than on higher strength steels (Diekhoff 2019). By hardness correlation the R_m of mild steel in is close to HSS in 4R method and similar or even better fatigue strength can be estimated depending on residual stresses that are lower on base material with mild steel than HSS. Tensile strengths calculated by equation 16 are shown in table 16.

Table 16. Hardness related ultimate tensile strength.

Material	Base material hardness [HV]	Soft zone hardness [HV]	HAZ hardness [HV]	Soft Zone Tensile strength [MPa]	Surface tensile strength [MPa]
S690QL	280	270	450	725	1250
S1100Plus	380	360	480	1070	1500

Table 17 presents the 4R method parameters for notch factor and residual stresses compared to yield strength. Residual stress profile was not available for this thesis so residual stress equaling $+f_y$ was used for the CO_2 laser cut specimens. The notch effect obtained from the blasted surface was 1.3. In the CO_2 laser cut specimen, the heat was found to have effect to rolled surface also and clear step was measured with profilometer at rolled surface. Novel calibration of these parameters was done based on fatigue test results, fracture surface analysis and material property zones. The parameters relation to each other should be researched when residual stress distribution is available. Presented values were used for 4R method fatigue assessment with relative accurate results although method for obtaining parameter need more fatigue tested samples

Table 17. Used values for 4R method fatigue estimation.

Cutting method	Notch factor	Residual stress [MPa]	R_m [MPa]
Fiber laser S690	Burr 1.5 No burr 1.3	$0.165 \cdot f_y$	1250
Fiber laser S1100	1.3	0	1500
CO_2 laser	1.15	$1 \cdot f_y$	780
Plasma	1.3	$0.20 \cdot f_y$	1250

In this research, only four different types of specimens were tested. 4R method should be still suitable for general material properties and cutting methods with parameter modification. For 4R method simple parameters for evaluation of fatigue life can be estimated for simple method with normal engineering practice or by more accurate method that may include residual stress distribution and hardness measurements, inspecting surface quality by 3D scanning, metallurgy examination and possibly calibration by fatigue testing depending on accuracy level of parameters.

4R method fatigue estimation for fiber laser cut S690QL specimen was done with previously presented parameters with default that fatigue crack initiated to cut surface. Both stress ratios 0.1 and 0.4 were combined to figure 77 and also extra test with ground bottom corner was included to results. On tested range of cycles 4R method have very good prediction of fatigue life with surface measured residual stresses, estimated tensile strength on HAZ and scanned & microscopic examined surface quality.

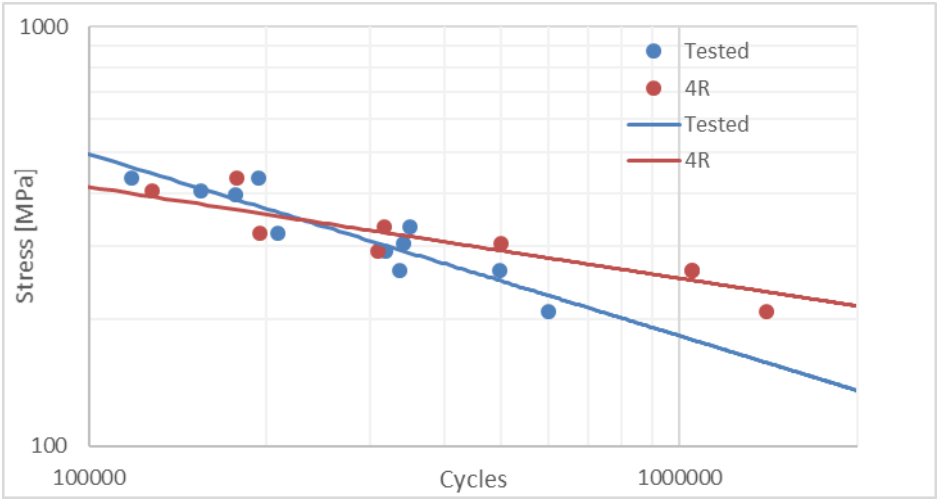

Figure 77. Test results and corresponding 4R predictions for fiber laser cut S690QL.

Plasma cut series had very small deviation and good test coverage on whole test range from low to high cycle counts. Plasma cutting 4R-parameter were close to fiber laser cut parameters but with smaller notch factor for loading. For plasma cut edges 4R method had very good fatigue prediction which was valid through entire tested range. Test and 4R-results are shown in figure 78.

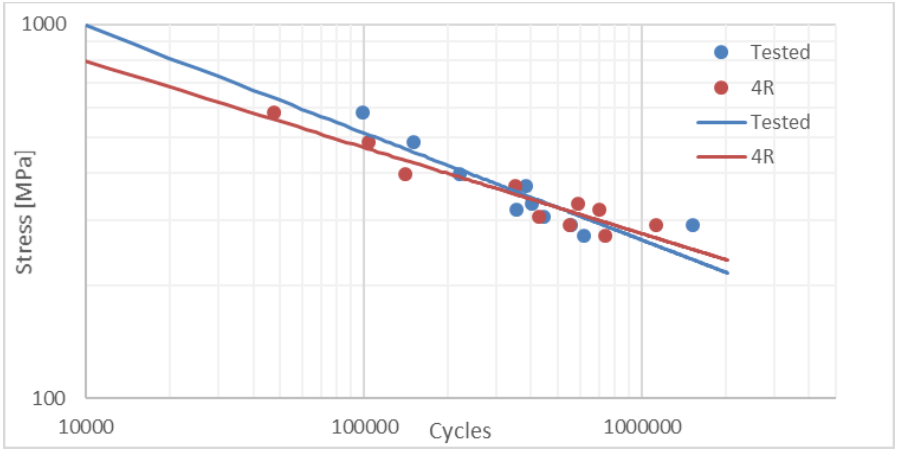

Figure 78. Test results and corresponding 4R predictions for plasma cut S690QL.

Failure mode of CO_2 laser cut specimens was different than all other specimens. The crack initiation point was clearly inside the specimen and cut edge had high resistance against fatigue. Different parameters were used at 4R method for CO_2 laser cut edges than other specimens. Residual stresses equal to yield strength was used while notch stress from blasted surface was used. The method estimated fatigue lifetime with good accuracy at $R = 0.1$ stress but with $R = 0.4$─0.5 the estimation becomes highly conservative on high cycle counts. Test and 4R-results are shown in figure 79.

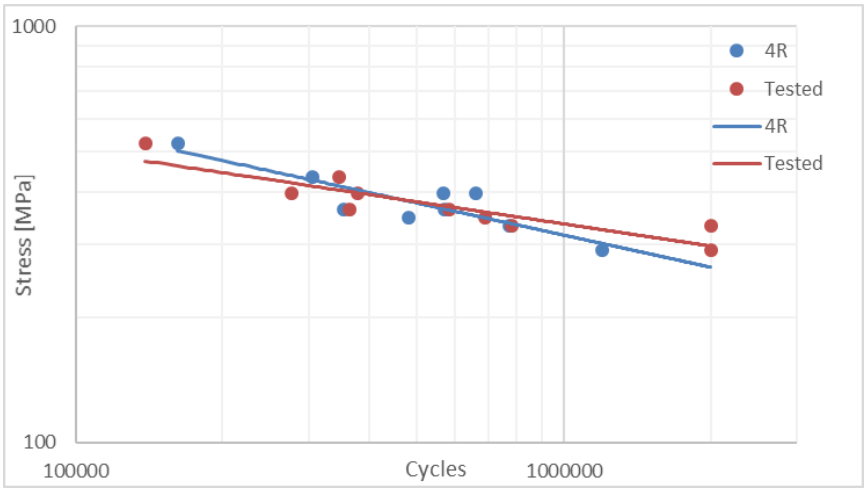

Figure 79. Test results and corresponding 4R predictions for CO_2 laser cut S690QL

4R method was tested also for S1100 Plus fiber laser cut edges. Fatigue estimation was relatively accurate with obtained parameters although notch stress was estimated by novel method when other parameters were known because notch effect was formed by burr attachment. Calibrating 4R method to estimate low- and high cycle fatigue was challenging but curve fitting was done with relatively good accuracy. Results of 4R fatigue assessment are presented in figure 80.

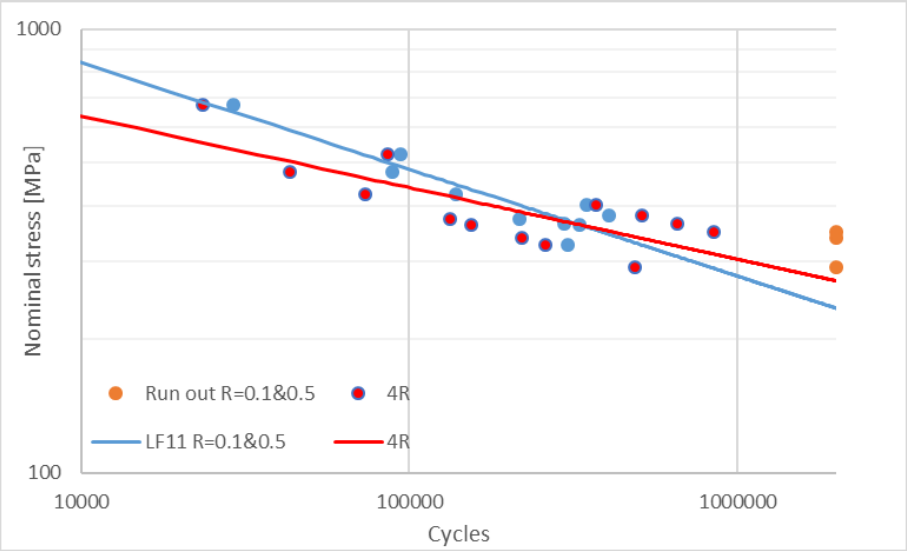

Figure 80. Test results and corresponding 4R predictions for fiber laser cut S1100Plus.

Milled edge specimen was also considered with 4R method. Tensile residual stress parallel to loading was measured from milled edge with 214 MPa value. The tensile strength used was 780 MPa because hardened surface was removed by machining. 4R method estimates 782 700 cycles lifetime with these parameters when no notch effect was assumed while in tested specimen crack initiated to ground section and test ended at 629379 cycles. Accurate estimation to milled edge and 4R method could have not been done because of ground section failure but 4R method estimated results seem reasonable. Calculated 4R curves and fatigue test results are presented in figure 81 with estimated fatigue limit for shot blasted surface.

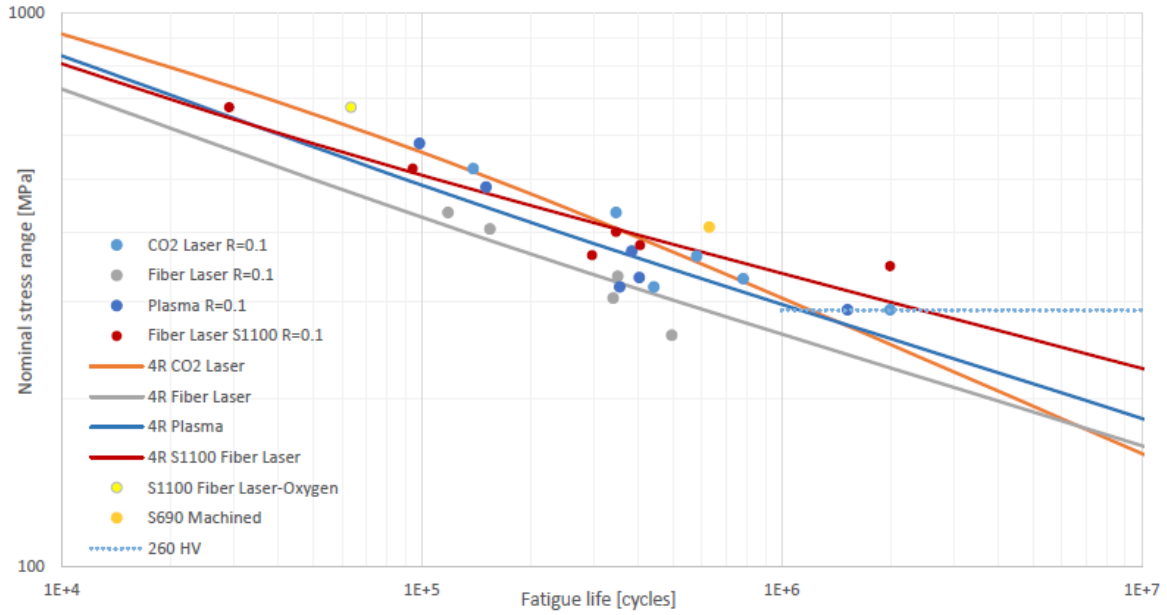

Figure 81. Calculated 4R curves and fatigue test results with R = 0.1 stress ratio

Effect of hardness corrected tensile strength is presented in figure 82. Nominal stress of 333 MPa with 1.3 notch factor, stress ratios of 0.1 and 0.4, from loading. Analysis was performed without residual stresses. Fatigue performance decreases when R_m value is increased. For thermally cut edges this behavior matches fatigue test results if crack initiation point is close to cut surface. If increased tensile strength is used on HAZ, the fatigue estimation may become conservative. This phenome have not been concerned on welded structures because experience had shown the most probable failure mode without considering other possible failure options.

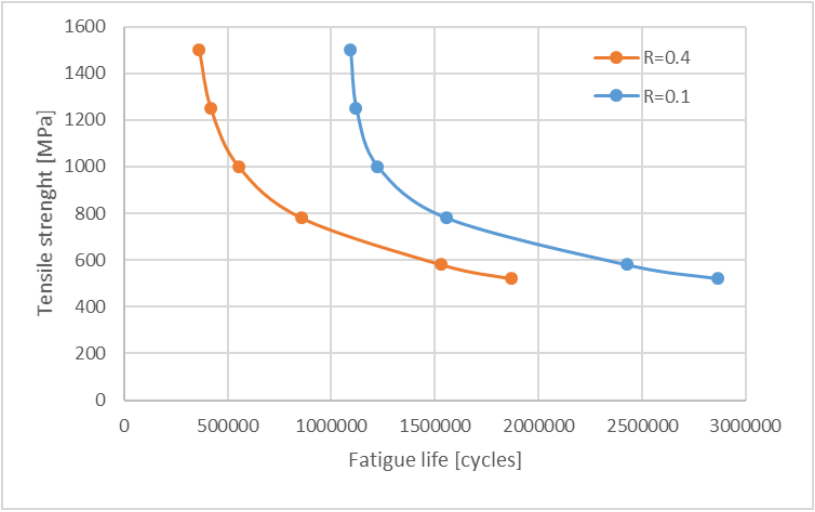

Figure 81. Tensile strength effect on fatigue life on 4R method.

Residual stress is another parameter considered in 4R method that has great influence on fatigue estimation. Residual stress effect was calculated with R_m = 780 MPa, nominal stress range of 333 MPa with notch factor of 1.3 and stress ratio R = 0.1. On compressive residual stress the effect on fatigue strength is more significant than on high tensile residual stresses. Residual stress effect on fatigue life on 4R method is presented on figure 83.

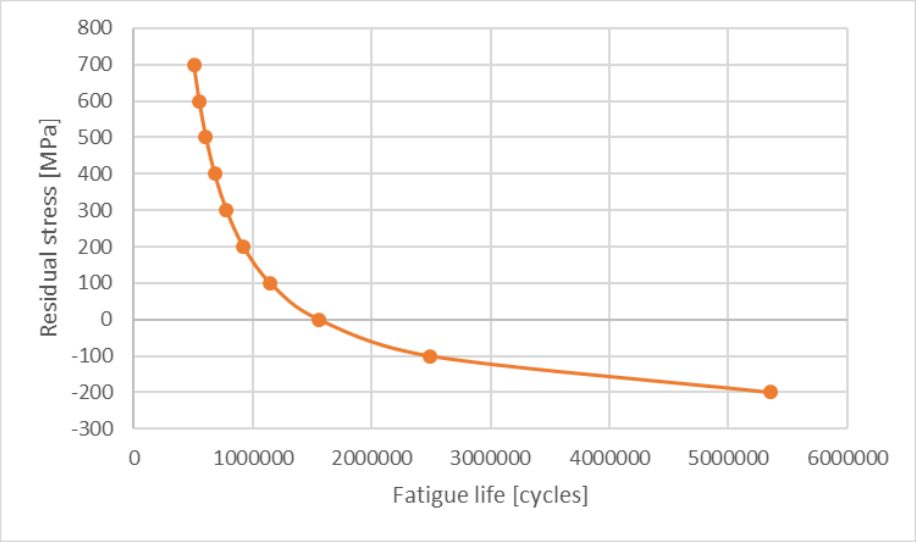

Figure 83. Residual stress effect on fatigue life on 4R method.

Fatigue assessment by 4R method is adaptive to usable resources and demands. Using the method, it is possible to estimate fatigue life by simple parameters but estimation should be conservative by simple parameters. More accuracy can be gained with refined parameters and calibration by fatigue testing. The fatigue testing calibration can be compared to strain-life –method where parameters are obtained by fatigue testing to evaluate low cycle fatigue life. For fatigue test calibration of 4R method only relative low cycle count of 100 000─300 000 cycles should be sufficient. The parameters obtained with low cycle count are scalable to high cycle count but may be more conservative than parameters for high cycle and mean stress fatigue testing. Novel 4R-parameters for design phase are shown in table 18.

Table 18. Generalized values for 4R method depending on engineering practice obtained parameters

Cutting method	Notch factor	Residual stress [MPa]	Tensile strength [MPa]
All, general estimation	1.3-1.5 by visual inspection; - 1.3 Smooth or good quality - 1.5 Harsh striations or defects	Surface measured	Linear hardness correlation by HAZ hardness applied to nominal R_m
All, detailed estimation	Scanned surface with FEM-correction or microscopic image evaluation by most sharp defect	Residual stress distribution measurement	Selecting R_m by cutting method and local material properties on crack initiation point

A flowchart for the 4R method was created as a guideline and conclusion of work in this thesis. The 4R method adaption to cut edges was kept as close as original 4R method for welded structures as possible. Flowchart for 4R method is presented in figure 84. Uniform cut quality means that there is no burr or any crack-like defects at the cut edge. Further development of 4R method for thermally cut edges is still needed to justify 4R method usage for thermally cut edges.

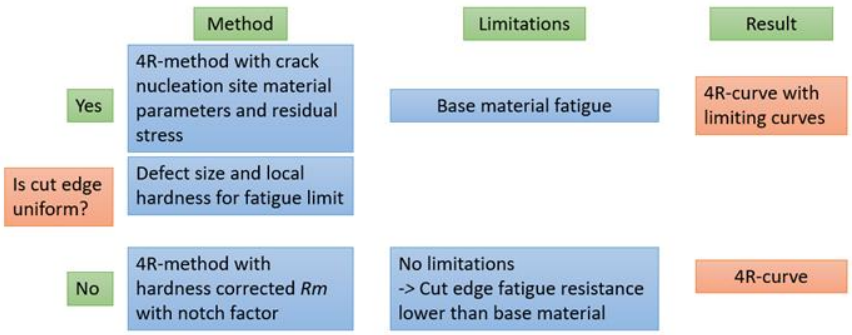

Figure 84. Flowchart for modified 4R method.

5.4 Combination of tested and literature results

Results of LUT University, Peippo (2015) and Diekhoff (2019) were gathered and are presented in figure 85. Materials used in tests were structural steels from S235 to S1100. Critical distance approach stress was used for comparing thermally cut corner results of Peippo. Results are combined to compare stress influencing thermally cut edge without surface quality effect. The results are not directly comparable but from results the effect of geometrical stress to fatigue assessment can be estimated.

Thermally cut corner seems having better fatigue capacity than straight cut edges if critical distance method obtained stress was used. Delivery condition of the tested sheet metals were not reported but according to this thesis, the delivery and tested condition has significant effect on fatigue performance.

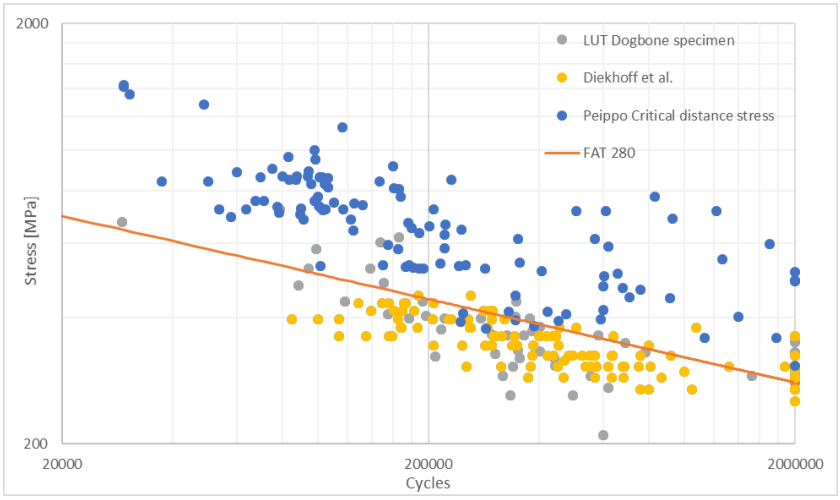

Figure 85. Fatigue test results from materials S235-S1100 from LUT, Peippo (2015) and Diekhoff et al. (2019) compared to FAT 280.

Thermally cut edges have usually stress concentration caused by various details, such as holes, openings and curved shapes. The method to consider the effect of these stress concentrations, obtained e.g. by FEA, in the fatigue strength assessment need further development. The ideal notch stress on mild steel is significantly higher (10%) than critical distance stress and on UHSS the difference is smaller (5%). The critical distance method used by Peippo was first proposal for obtaining stress for the 4R fatigue assessment. Because the results presented with critical distance method were better than straight cut edges results, the method for obtaining stress should be developed.

Within this thesis and 4R method application development, the stress obtained from ideal shape notch and the most significant concentration at 0.5 mm perpendicular distance from laser and plasma cut edge was found to match test results of dog bone -specimens on both University of Oulu (2015) with geometrical shape and Peippo (2015) cut corner with small radius.

6 ANALYSIS OF RESULTS

The results were analyzed mainly by MSSPD-curve fitting but also IIW-method was considered. The FAT classes and slopes were calculated for individual test series and for all specimens tested for this thesis. Mean FAT class of 234 MPa was calculated from all test results. Every run out -tested specimen performed significantly better than calculated mean FAT class.

The failure mode of test series was strongly correlated to the fatigue test results. Discontinuity points on specimens were correlated to fatigue test results and run out –level. Based on this thesis the rule of small defect size of welded structures is relevant also for cut edges. If cut edge is not uniform the finishing of cut edge is needed for fatigue critical applications.

6.1 Cutting methods

Based on this research, thermal cutting methods can be divided to two categories. On first category no initial crack is present from cutting and on second category crack is formed by recast layer on surface or from burr attachment at bottom of the cut. CO_2 laser cutting had the highest fatigue capacity among the test series while the most significant striations and notch effect was evaluated from CO_2 laser cut edge.

Fatigue tests were analyzed to tables 19 and 20 with MSSPD curve fitting. The results from both stress ratios are highlighted in tables. In curve fitting, failure points from successful test were used without run out-test. Curve fitting with free slope is not usually done with small test series but the slope of cut edges variated by cutting method significantly and curves had high correlation. The best fatigue capacity was achieved by CO_2 laser cutting with total FAT of 260 MPa. Fiber laser cut edges had the lowest FAT of 143 MPa. The plasma cut edges had lowest deviation of cut methods and FAT of 219 MPa. The S1100 Plus specimens were cut with same fiber laser than S690QL specimens but they had better cut quality due to lower sheet thickness.

Table 19. Mean FAT-values calculated with MSSPD slopes with S690QL.

Cutting method	Stress ratio	Slope	FAT [MPa]	Highest run out [MPa]
CO_2 laser	0.1	3.77	264	290
CO_2 laser	0.4-0.5	7.19	298	331
CO_2 laser	All	4.12	265	331
Fiber laser	0.1	2.99	173	-
Fiber laser	0.4	2.09	118	-
Fiber laser	All	2.49	143	-
Plasma	0.1	3.94	252	290, failure at $1.5 \cdot 10^6$ cycles
Plasma	0.4	2.80	180	-
Plasma	All	3.50	219	290, failure at $1.5 \cdot 10^6$ cycles

Table 20. Mean FAT-values calculated with MSSPD slopes with S1100 Plus.

Cutting method	Stress ratio	Slope	FAT [MPa]	Highest run out [MPa]
Fiber laser	0.1	4.37	255	348
Fiber laser	0.5	3.97	215	339
Fiber laser	All	4.15	235	348

Calculated FAT values with free slope are difficult to compare. The FAT classes are presented graphically in figure 86 with the *FAT 160 m = 3* curve as a comparison.

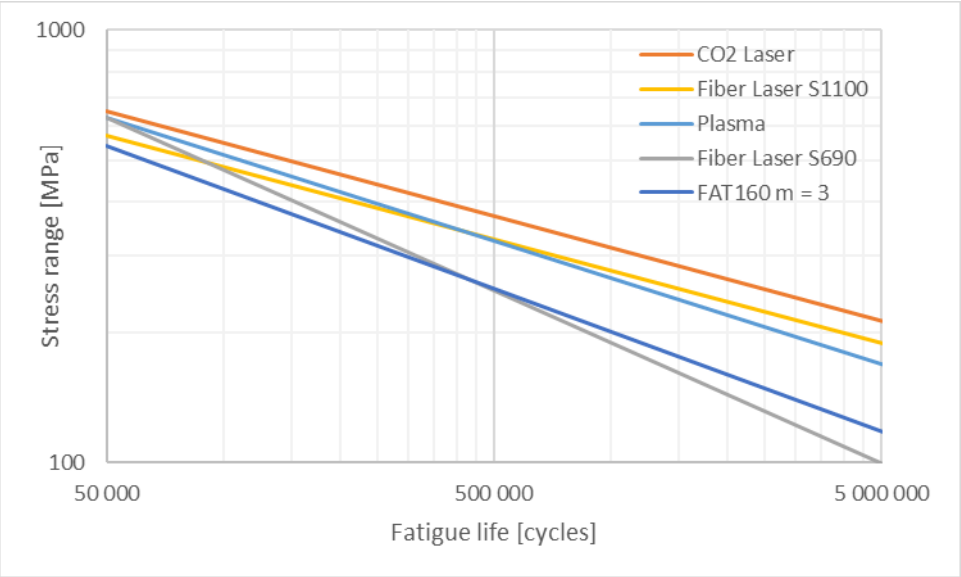

Figure 86. Calculated mean FAT curves compared to FAT160 curve

Both the IIW and MSSPD curve fitting was used to obtain mean FAT-values. Test data was highly scattered because of low fatigue performance of fiber laser cut S690QL specimens. Although R^2 coefficients of curve fittings were close together MSSPD giving slightly better factor the MSSPD fitted curve has better estimation of fatigue life. Values without fiber laser cut S690QL specimens were also calculated with both curve fitting methods. Removing LF-test series data increased R^2 coefficient on both curve fitting methods but more on MSSPD curve fitting. After excluding LF-series, FAT values could be compared to tested run out levels. Run out were experienced with both S690QL and S1100 Plus materials and lowest run out -value was 290 MPa highest value being 348 MPa. High run out -values exceeded mean FAT value by IIW safety margin for characteristic FAT value. On high cycles the traditional design code approach is very conservative. Results are presented in table 21.

Table 21. Mean FAT-value with IIW and MSSPD curve fitting and slope of all tests.

Curve fitting	Slope	FAT [MPa]	R^2 coefficient
MSSPD	4.10	234	0.63
IIW	2.57	175	0.59
MSSPD – No LF	4.35	248	0.75
IIW- No LF	3.28	217	0.64

6.2 Effect of material strength to fatigue strength

Two different steel grades were tested but no specific comparison could be made because of different sheet thickness. At the LCF regime, higher tensile strength offered more capacity because of potential of base material against plasticity. Tested steel grades had different delivery conditions, S690QL was shot blasted while S1100 Plus had smooth rolled surface.

Burr attachment from fiber laser cutting changed the characteristic of t = 8 mm and t = 12 mm comparison. S1100 Plus performed better than S690QL on same forces despite higher stress variation. Based on this thesis yield strength influence fatigue performance at improved cut quality due to thinner sheet is needed for same application. Cut quality is related to material thickness but not to material yield strength.

6.3 Surface quality

Specimens with four different surface qualities and characteristics. Surface quality was measured with traditional method according to standard and evaluated from both 3D-scanned model and microscopic images. When surface quality and striation dimensions were compared there was no correlation between surface quality by R_z value to notch effect which would have affected fatigue test results. However tested specimens limited fatigue capacity with shot blasted surface instead of pure surface quality testing on CO_2 laser cut specimens. Instead of surface quality the shape and location of notches have major effect to fatigue life.

Standard R_z value combined with the width of striation had significant correlation to fatigue life when FEA for fitted arc was done and also rolled surface was considered. The crack initiation location was considered in FEA because notch effect was smaller on crack initiation location than on cut edge. In thermally cut edges, surface quality also surface quality of rolled surface should be measured.

6.4 Residual stresses

Cut methods had different crack nucleation stage. On CO_2 laser cut edges the effect of residual stresses was the most significant due to good fatigue capacity and possibility for residual stress relaxation. Surprisingly the high mean stress fatigue testing estimated better FAT than ordinary fatigue testing, possible due to residual stress relaxation.

Fatigue strength of welded structures decrease when stress ratio increases. In thermally cut edges the crack initiation mechanism differs from welded details. Residual stresses have significant influence on crack initiation. The effect of overloading structures in residual stress relaxation have been researched and it is already included in 4R method guidelines. The residual stress relaxation under fatigue loading have not been researched widely on thermally cut edges measurement in thermally cut edges challenging from inside the material. Researches about residual stress relaxation on welded joints have been conducted and the results can be adapted to thermally cut edges.

From LUT fatigue testing with stress ratios of 0.1 and 0.4─0.5 the effect of residual stress relaxation is faster on higher stress ratio but notable also on low stress ratio. On low stress ratio the residual stress relaxation can be expected to influence fatigue test results after million cycles and on higher stress ratio after 500 000 cycles.

The effect of residual stress relaxation could have been seen on LC5-1 specimen. The specimen was first run out -tested with 331 MPa stress and R = 0.5 stress range. After run out -testing the specimen was tested again with high loading. On the second test the specimen performed clearly better than other specimens or its fatigue estimation. On LC-specimens fatigue failure location was bottom of the cut where no striations were visible. If crack initiation mechanism is influenced by high tensile residual stresses, described results seem reasonable.

The effect of residual stresses seems on fatigue strength to be dependent on the cut edge quality, dross attachment and changes in hardness. Based on literature review and laboratory measurements, the residual stresses are low or even compressive on cut surface and HAZ while between base material and HAZ they become very high. The location of high residual stresses makes the measurements challenging.
Residual stresses have different effect on straight and curved cut edges on thermally cutting methods. High residual stress concentration below surface has strong effect on fatigue life with certain conditions. Blasted or low quality rolled surface combined with high tensile residual stress concentration limits fatigue capacity of straight cut edge. When global notch factor from curved geometry is added the residual stress concentration away from the most significant global notch factor area has not influence on fatigue strength because cut edge itself is limitation of fatigue strength.

Reliable research of residual stresses is challenging and in the 4R method the value for residual stress should be decided reliably. In this thesis, residual stress state recommendations have been considered and residual stresses have been measured from surfaces before and after loading. If cut surface material parameter was selected, the residual stress should be kept low or zero but for base material parameter the residual stress should be high. Residual stress state changes during loading and 4R-master curve includes initial change at first cycles. Based on experiences in this research run out -level stress should be estimated with residual stress relaxation. Residual stress measurement from rolled surfaces support this approach with almost equal to zero measured values. Changes of microstructure at cut edge may have been affected residual stress measurement from cut edge.

6.5 Loading ratio and stress range

Effect of loading ratio was relative to crack nucleation. If crack nucleation occurred in high residual stress area, the $R = 0.4 \text{─} 0.5$ had better fatigue strenght but crack nucleation near cut surface the effect was opposite. On CO_2 laser cut test the higher mean stress increased the fatigue performance after 700 000 cycles but on other cutting methods the tested fatigue life was shorter and the slope of SN-curve steeper.

7 DISCUSSION

With basic parameters and linear behavior of hardness and tensile strength, the 4R method is valid to 10^6 cycles and it may estimate run out stress too low or high depending on application. By analyzing original 4R-master data with run out data, the method would be possible to modify to estimate run out level better with cut edges. For fatigue of thermally cut edges there appear to be multiple limiting curves for fatigue failures.

1) Global plasticity at high loading
2) High residual stress concentration at base material
3) Rolled surface quality
4) High tensile strength material behavior at cut edge with notch effect
5) HCF-properties and knee point of SN-curve

The 4R method applicability is presented in figure 87 schematically and limitations are presented for mild steel and UHSS. The limiting curve of mild steel proceed from master data of 4R method where materials from S235 to S1100 were researched. With low cycles the plasticity of low strength material limit performance even thermally cut edge would allow better fatigue life, estimated from 4R method. Also run out –level fatigue is not explained by 4R method and equations that considered fatigue limit should be embedded to 4R method. Other possibility for high cycles fatigue estimation with 4R method would be residual stress relaxation estimation.

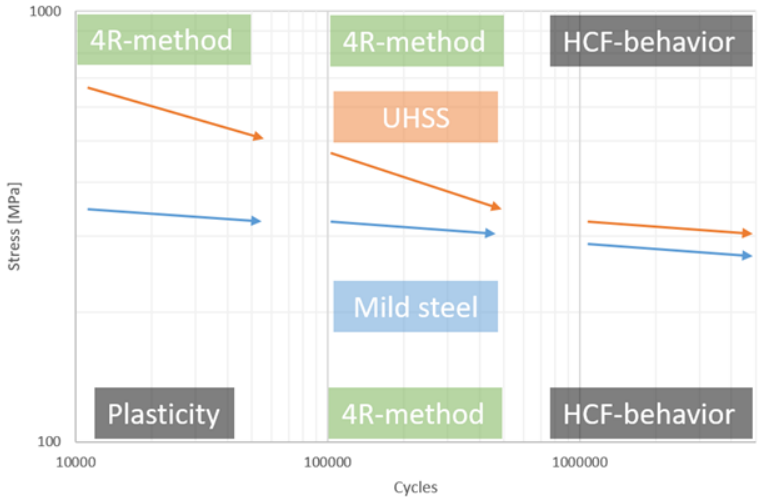

Figure 87. Schematic 4R method application range on UHSS and mild steel.

Based on this research, standard cut surface quality has insufficient relation to the fatigue performance of thermally cut edges. Traditional surface quality measurement does not consider the width of defect. The shape of defect affects stress concentration. For traditional measuring devices, accessibility is poor to the most significant defects and reliable measurement is challenging. Surface quality limits are still good practice to define general cutting quality but in fatigue analysis they should not be used. Default values by different qualities, like cutting method and burr attachment, offer better tool for estimating fatigue capacity if no advanced tools can be used. Default values can be validated or calibrated by fatigue testing if they are conflicting with current design codes. The FKM-guideline for notch factor by cut edge quality and steel grade was not found valid because it highlights overly the notch sensitivity of UHSSs and does not consider the shape of defects.

Residual stress relaxation on cut edges may differ from welded detail residual stresses because typically higher load levels are allowed in the structures with cut edge details than in the structures with welded details, at the same fatigue life. Residual stresses were tried to evaluate from previously researched HFMI-treated joint with strain gauge attached to $0.4 \cdot t$, at hotspot measurement location, from weld toe before HFMI-treatment with 10^6 cycles and high mean stress. Also strain gauge was attached to rolled surface close to laser cut edge but, on either method, no residual stress relaxation could be measured with strain gauge.

Cutting method have different characteristics compared to each other's. Plasma cutting has wider HAZ than laser cutting while surface quality is better than in laser cut edges according to this study. Residual stresses were researched in this thesis and plasma cutting caused tensile residual stresses while compressive residual stresses were measured in the laser cut specimens. Waterjet cutting was researched briefly in re-analysis of previous results. In waterjet cutting, relatively high compressive residual stresses are induced to cut surface while neither in HAZ nor inside the specimen residual stresses are highly tensile. Compressive residual stresses of waterjet cutting decrease effect of worse surface quality than thermal cutting when fatigue performance is concerned.

In this research, fiber laser cutting had lowest fatigue strength with respect to CO_2 laser and plasma cutting. Fiber laser cut edges from LUT University Laboratory of Production Engineering were measured for a reference. The reference fiber laser cut edges were cut

with low power fiber laser using oxygen to increase energy input. Typical parameters in LUT sheet metal workstation integrated 4 kW fiber laser cutting for 8 mm structural steel sheet were 1900 mm/min, 3 kW laser power, 0.5 bar oxygen pressure from 1.2 mm nozzle and beam focused to top of sheet with 0.3 mm beam radius. The productivity with these parameters is lower than on fatigue tested cutting parameters and oxide layer is formed to cut surface. Reference measurements for surface quality are presented in figure 88. Deepest notches of measured sections were 20 µm and 30 µm while 70 µm deep notches were measured from fatigue tested cut edges with same 8 mm material thickness. Cross section and metallurgy inspection for these reference fiber laser cut edges were not performed and information of initial defects in cut edge was not available.

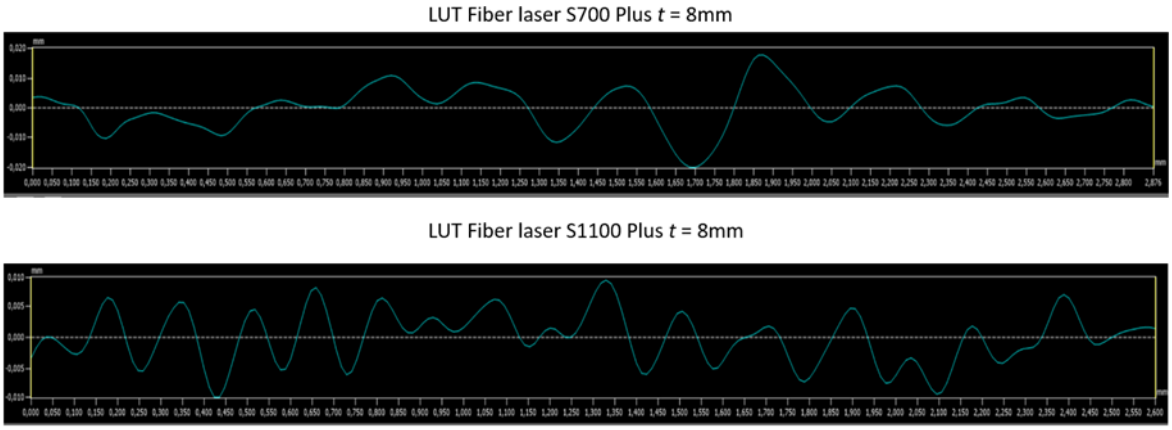

Figure 88. Surface quality at worst section on LUT fiber laser cut edge with oxygen cut.

Reference cut edge fatigue test with LUT University cut edges was significantly better than tested specimens. The specimen failure from ground section and no visible crack were found from cut section. The reference specimen had was tested with R = 0.1 stress ratio and 675 MPa stress variation. Fatigue life of 63599 cycles was achieved and FAT-value of 306 MPa was calculated with same slope than tested series. The reference FAT was 51 MPa higher than R = 0.1 tested LF11-series which means that reference specimen achieves twice more cycles at equal loading than tested series and with this fatigue performance increase the failure did not occur at laser cut edge. The real difference between these results is higher than tested result. Test matrix did not include fiber laser cutting with oxygen cut similarly than CO_2 laser cutting. The results from extra test indicates that fiber laser cut edge does not have worse fatigue performance than CO_2 laser cut edge. Within extra test was found that nitrogen cutting has worse fatigue performance than oxygen cutting.

Comparing oxygen and nitrogen as an assistant gas is difficult. Nitrogen consumption is higher than oxygen consumption and cost of nitrogen cutting per minute is higher. On nitrogen cutting the cutting speed, nozzle diameter and gas pressure should be balanced to achieve straight striations on cut edge with laminar gas flow. Oxygen cutting was also found to change elemental composition close to cut edge by decreasing alloying elements and increasing iron content. This phenomenon might be harmful in stainless steels in which the alloying component chrome protects the material from corrosion. Also cutting with nitrogen as an assistant gas is difficult and sensitive to correct parameters especially in thicker, $t > 6$ mm, sheets. Reference specimen with fiber laser cutting nitrogen as assistant gas with full laminar flow was not possible with available machinery.

Steel grades and sheets also have different properties on fatigue. In this research S690QL sheet was shot blasted before cutting and blasting itself with high residual stresses caused by thermal cutting limited fatigue performance of cut edges. In fact, the blasted surface had worse surface quality than plasma cut edge. Changing working order to, cutting and shot blasting after cutting would be beneficial because of induced compressive residual stresses from shot blasting. Shot blasting of plates is done because painting or coating of structure requires surface treatment.

The knee point of SN-curve $0.5 \cdot 10^6$─$1 \cdot 10^6$ cycles was noticed instead of two or five million cycles of welded structures, but the reason is not known yet. In low strength steel, found in the literature review, fatigue failure nominal stress variation were close to material nominal yield strength at HCF-regime in laser and plasma cut edges. In mild steel there are two different fatigue mechanisms due to low yield strength. Local cut edge fatigue phenomenon is similar to HSS cut edge fatigue with hardness correlated material properties, but fatigue performance is restricted from base material fatigue.

7.1 Design codes and 4R method suitability for thermally cut edges

Based on this research, design codes are unambiguous for the fatigue strength assessment of thermally cut edges. With fiber laser cutting t = 12 mm sheet, only 149 MPa FAT was achieved in this study with m = 2.5 slope and design guides recommend 125─140 MPa FAT classes at the lowest, with m = 3 and high safety factor. Fatigue capacity of edges is often more critical than welded details because stress from global geometry is often influencing

edges more than welds. Secondly, almost 300 MPa FAT was achieved with CO_2 laser cut edges with free slope. In literature review, the run out stresses were notable higher than FAT-calculated by curve fitting. For high quality cut edges million cycles as a knee point of SN-curve could be considered to remove double safety factor from characteristic curve and assumed knee point at 2 million cycles.

Standard FAT classes do not suit well for thermally cut edges. Generally, thermally cut edges have better fatigue capacity than IIW FAT classes estimate and such steep slope is not suitable for thermally cut edges. EN13001-standard gives a slope of $m = 5$ and it is better applicable to thermally cut edges. On cut edges FAT 180 is the maximum allowable fatigue strength according to the EN13001 standard for thermally cut S690 edge with normal production quality and FAT 280 can be achieved with UHSSs and EN ISO 9013 class 1 surface quality which is difficult to achieve with thermal cutting. Nominal FAT-classes may estimate too high fatigue strength for the cut details with stress concentration and FE-model should be still used for cut edges with stress concentrations from geometry.

Edge hardening in cutting seems to be harmful if a discontinuity exists on cut edge. In the case of burr, pores or other crack-like defects, the harder surface reduces fatigue life. If surface has good integrity and above described defects are not present, the surface hardening should not be harmful although EN1090-standard restricts surface hardness. The standard should be extended for UHSS and maximal edge hardness should be increased because only steel grades up to 700 MPa yield strengths are included.

Fatigue testing of the milled and CO_2 laser cut –specimens gave comparison to strain life –method that was estimated by Potiris & Mettänen (2018). Fatigue testing milled specimen had approximately two times higher fatigue life with respect to laser cut specimen although milled specimen failure from notch on ground section. Strain life –method may offer good estimation for thermally cut and milled or mechanized grinding without crack like defects or notch effect. Residual stresses should be noted on grinding and milling of thermally cut edge.

The 4R method seems to be suitable for ground and milled edges but further research should be done with known factors for stress because ground section research was not made by

purpose in this research and no 3D-scanned data was available from shape of ground sections to obtain stresses for 4R method. No residual stress measurements were performed for ground edges.

The 4R method was highly accurate below 10^6 cycles and development and the use of the 4R method may decrease the need of fatigue testing or unexpected failures when parameters of the 4R method are calibrated by fatigue testing and microscopic images by crack nucleation position. Also the notch effect should be known or estimated. Estimated notch effect should be more conservative than from surface scan obtained notch effect.

7.2 Improving fatigue life of thermally cut edges

Material removal from kerf is crucial for achieving good fatigue performance of cut edges. CO_2 laser cut edges had very good fatigue life in this research compared to literature findings. The use of HSSs makes material removal easier on laser cutting because of thinner sheet is needed for same capacity at tensile loading. Especially with fiber laser cutting with nitrogen as an assist gas it is important to be aware of possible reduction in fatigue performance. With nitrogen cutting the fatigue performance is better at thinner sheets and use of UHSSs improve the fatigue strength if thinner sheet can be used.

Laser cut parts may not be always used without further processing. Processing should be done with a high precision because ground notches were failure points instead of thermally cut edge in this research. Grinding is usually made by hand compared to mechanized thermal cutting. If user error occurs during grinding process, the fatigue failure may localize to ground section instead of cut edge especially if the cutting quality is good. Fatigue crack on testing initiated even to small defects in ground section with stress concentration. Oxy-fuel cutting was not studied in this thesis but according to results of study, grinding should improve fatigue performance of oxy-fuel cut edges because softened material from cut surface is removed in grinding. Residual stress state of cut edge is dependent of working order. Bending and thermal cutting form tensile residual stresses while blasting induces compressive residual stresses. Finding the critical location on each application helps choosing the best after treatments to achieve a good fatigue performance. The fatigue strength of cut edge should never be weaker than fixing weld.

The detail design of welded structures has been highlighted on research and product development. The thermally cut edges geometries and surface finishing should also be noted at design phase. The crack initiation can be expected to high structural stress areas and they should be protected if outside damage possibility is present at operating environment. If possible, samples from cutting should be examined before production in critical details because literature review and research for this thesis have shown highly different fatigue performance for different cutting methods.

7.3 Future research objectives

Residual stress profile close to crack nucleation points should be measured from surface to 1 mm depth inside the specimen before testing, after $R = 0.1$ and after $R = 0.4$─0.5 testing and with few different cycle counts to understand the effect of residual stresses on the crack nucleation. Material delivery condition affected cut edge fatigue S690QL steel with shot blasted surface generated extra stress compared to rolled surface specimens. S1100 Plus sheet had smooth rolled surface but burr attachment at bottom of the cut removed possibility to compare smooth and blasted surface differences. Shot blasting affect the residual stress state of specimen inducing compressive residual stresses. Effect of work order should be researched and specimens shot blasted after cutting should be tested. Thermally cut edges are often bended in real structures. In bended parts there is a high peak of both compressive and tensile residual stresses. Generally working order should be researched to find optimal fatigue performance on complex structures. With fiber laser technology the 3D-cutting is available and cutting can also be done after bending, if necessary.

Assistant gas effect on fatigue performance should be researched. In this research, only nitrogen was used with fiber laser cutting but in the previous studies conducted at LUT University, oxygen cut specimens had significantly better fatigue capacity. Between different cutting systems also other parameters like focal point position influence the results. With low power oxygen cutting the focal point is usually close to top surface and cutting kerf on bottom of the cut is wider. On nitrogen cutting with high power laser focal point is set close to bottom of the cut to provide better surface quality but material removal challenging and burr can be attached to bottom of the cut although it would not be visible and only seen on microscopic images or felt by hand as a very sharp corner. The specimens

as prepared for customer with surface finish applied should also be tested to meet using conditions of existing structures.

The burr attachment in 12 mm thick fiber laser cut specimens was noted and fatigue testing was decided to perform without burr grinding while from 8 mm thick fiber laser cut specimens burr was not noted before fatigue testing and microscopic examination. Burr acts as initial crack on fiber laser cut edges similar to root side of weld. The removal of the burr did not increase the fatigue performance similar to CO_2 laser cut and defects under recast layer may behave similarly than burr but fatigue capacity was still increased with burr ground.

The developed 4R method application should be tested with specimens with curved sections and holes to widen and verify the method. The 4R method was constructed with FEA-implementation that allows stress estimation from 3D-model and then adding notch factor in addition to structural stress. For CO_2 laser cut edges the notch factor was easy to obtain from microscopic image and find the narrowest and still deep striation from top of the cut. Material hardening affects the notch factor because of crack initiation takes place in base material and notch factor should be reduced to base material with FEA.

Microscopic images, 3D-laser scanner and 3D-profilometer were used to estimate the notch effect. From 3D-scan only cross section data as a line could be used because of FEA-models from 3D-scanned data becomes heavy to process. Also scanning the burr was challenging because of the location on the edge and scanning process should have direct visibility to scanned object. Even if the burr was scanned correctly the processing should have needed 3D-solid element model instead of 2D-plate elements and pre-processing for scanned data with more advanced tools. The outward facing burr does not generally form notch stress but notch stress may be high inside the burr like on root side of weld. For developing FEM implementation for thermally cut edges the reliable method for analyzing full edge height should be studied. Vento (2018) proposed 3D-scanning of critical welds to recommended procedure to ensure weld quality. Similar scanning based quality control would be beneficial for cut edges on random samples and on cutting method suitability evaluation on critical details.

HCF as a phenomenon should be embedded to the 4R method to estimate run out levels above 300 MPa, as well plasticity of mild steel at high loading. With welded structures the run out level is estimated more correctly on HFMI-treated joint because of compressive residual stress assumption. The plasticity of mild steel have not been concerned in welded joints because the fatigue capacity of weld have not been competitive to base material on ASW joint. HFMI-treatment have been usually used for HSSs because of its more significant benefit.

Real time fatigue monitoring could be used with 4R method also for thermally cut edges. Fatigue testing for validating method and estimate suitable cumulative damage sum would be needed as it has been done for welded structures previously. On thermally cut edges the crack was extremely hard to find in visual inspection and on painted structure the inspection becomes even more difficult. On demanding application real time fatigue monitoring would offer possibility to prevent complete failures but still maximize lifetime of part.

8 CONCLUSIONS

Importance of thermally cut edges has been increasing along high strength materials usage and improved welding technology. Literature review focused on the hardness distribution, residual stress state, fatigue test results and fatigue estimation methods. In this thesis, four fatigue test series were tested. The main interest was on the S690QL steel which was cut with CO_2 laser, fiber laser and plasma process. For comparison, fiber laser cut UHSS S1100 Plus was tested. Fatigue of thermally cut edges were evaluated statistically from fatigue test results in previous researches. In this thesis, fatigue phenomena were researched besides test result analysing.

Metallurgy of thermally cut edges were researched and differences between laser cutting methods were found with SEM. In CO_2 laser cutting, oxygen was used as an assistant gas while nitrogen was used with fiber laser. Oxygen was found to react with alloying elements of steel and changed chemical composition significantly at 10 μm distance from cut edge but the transition distance of elemental composition was 50 μm. Nitrogen, as assist gas, did not change elemental composition as oxygen although small changes were possible. In the cutting with oxygen as an assist gas, the recast layer grain boundaries were not visible but close to surface a coarse grain area was found. Important finding from fiber laser, nitrogen as an assist gas, cut edges was the defects on turbulent gas flow area. The gas flow had turned inside molten material and formed defects which influenced fatigue strength.

Fracture surfaces of fatigue tested specimens were analyzed also with SEM. Importance of shot blasted surface defects was found. In CO_2 laser cut edges fatigue crack was initiated from shot blasted surface defect on base material or softened zone. In plasma cut edges, the fatigue failure point was not as clear as in the CO2 laser cut edges. Fatigue performance of plasma cut edges was lower than in CO_2 laser cut edges. In plasma cut edge fracture initiation was also influenced by burr attachment. In both fiber laser cut materials fracture had propagated from burr. When burr was removed the defect on cut surface become critical and restricted fatigue performance significantly.

Mean FAT value of 234 MPa with m = 4.10 was calculated from all test data. The CO_2 laser cut edges had the best fatigue performance on t = 12 mm S690QL specimens while fiber

laser cut edges had the worst performance. When thinner t = 8 mm fiber laser S1100 Plus specimen was tested it had better fatigue performance than CO_2 laser cut S690QL specimens. Test results in this thesis support that fiber laser cutting with nitrogen as an assist gas is more suitable to thin sheets although thick sheets can be cut with high power fiber laser.

Based on fracture surface and surface quality evaluation, the parameters for 4R method were estimated for different cutting methods. In CO_2 laser cut edges, the parameters of base material were used while on fiber laser cut edges the parameters of HAZ were used because of different failure location. The use of 4R method was found to result in accurate fatigue life estimations on at the LCF regime and below 10^6 cycles. Because high tensile residual stress state was estimated based on literature findings, the run out level was not estimated correctly on uniform cut quality edges.

Murakami's *area*-parameter based approach was found to estimate fatigue limit correctly on CO_2 laser and plasma cut edges with base material hardness and shot blasted defect size. Other application for hardness-based fatigue limit in this thesis, was estimating hardness of cut edge. When defect size and local stress were compared the very high hardness at bottom of the striations was estimated. This very high hardness area was also found in literature review where nano hardness was measured with SEM.

In future research the hardness and stress relation should be studied to obtain stress for 4R method and verification of results. Residual stress distribution measurement with small measurement area from rolled surface and inside cut edge should be considered. Based on this thesis, the fatigue estimation derived by local properties of cut edge is possible instead of fatigue testing with 4R method. Fatigue phenomena is highly local on thermally cut edges and micrometer size defects or metallurgical changes determines the fatigue estimation. The small scale properties are difficult to estimate and accurate 3D-scanning, micro- or nano hardness testing and SEM is needed for accurate fatigue parameter estimation. Fatigue testing with fiber laser cut edges should be re-tested after improved cutting parameters and quality. Fiber laser cutting with better gas flow would possible improve fatigue performance.

REFERENCES

Barmicho I. 2015. Fatigue Life Assessment of Cut Edges in High Strength Steel. [Master's Thesis] Royal Institute of Technology, Stockholm. pp. 34.

Björk, T, Samuelsson J & Marquis, G. 2008. The need for a weld quality system for fatigue loaded structures. [e-document] pp. 13.

Björk T, Ahola A, Skriko T. 2018. 4R method for consideration of the fatigue performance of welded joints – background and applications. [e-document]

Björk, T, Mettänen, H, Ahola, A, Lindgren, M & Terva, J. 2018. Fatigue strength assessment of duplex and super-duplex stainless steels by 4R method. [e-document] Welding in the World 62:1285–1300. pp. 15.

Cicero, S, Garcia, T, Álvarez, J.A, Martin-Meizozo, A, Bannister, A & Klimpel, A. 2016a. Definition of BS7608 fatigue classes for structural steels with thermally cut edges. [e-document] Journal of Constructional Steel Research. pp. 10.

Cicero, S, García, T, Álvarez, J.A, Martín-Meizoso, A, Bannister, A, Klimpel, A. 2016b. Fatigue behavior of high strength steel S890Q containing thermally cut straight edges. [e-document] Procedia Engineering. pp. 8.

Dabiri, M, Ghafouri, M, Rohani Raftar, H.R & Björk, T. 2017. Evaluation of Strain–Life Fatigue Curve Estimation Methods and Their Application to a Direct-Quenched High-Strength Steel. [e-document] pp. 15.

Diekhoff, P, Hensel, J, Nitschke-Pagel, T & Dilger, K. 2019. Fatigue strength of thermal cut edges—influence of ISO 9013 quality groups. Welding in the World. [e-document] pp. 14.

Dobosy, Á & Lukács. J. 2014. Fatigue resistance of welded joints of S690QL high strength steels. [e-document] pp. 11.

El Haddad, M.H, Smith K.N & Topper T.H. 1979. Fatigue Crack Propagation of Short Cracks. Engineering Materials and Technology.

European Union. High performance cut edges in structural steel plates for demanding applications (HIPERCUT). 2016. [e-book] ISSN 1831-9424. pp. 192.

Fridman, A. 2008. Plasma chemistry. United States of America: Cambridge University Press. [e-book] pp. 963.

Garwood, M.F, Zurburgand, H.H & Millan, J.F. 1951. Correlation of Laboratory Tests and Service Performance, Interpretation of Tests and Correlation with Service. ASM, Philadelphia, PA. pp. 1-77.

Górka, J and Poloczek, T. 2018. The influence of thermal cutting on the properties and quality of the cut surfaces toughened steel S960QL IOP Conf. Ser.: Mater. Sci. Eng. [e-document] pp. 10.

Hobbacher, A. 2007. The new IIW recommendations for fatigue assessment of welded joints and components – A comprehensive code recently updated. [e-document] pp. 8.

Hobbacher, A. 2013. The notch stress method for fatigue assessment of welded joints. Presentation in Theme Days of the HRO Design Forum 21.-22.8. 2013, Holiday Club Tampere Spa, Tampere, Finland.

University of Oulu. 2015. Laser- ja plasmaleikkausmenetelmän vaikutus väsymislujuuteen (Effect of Laser and plasma cutting on fatigue strength). In Finnish. [Powerpoint] Not available.

Khan U. 2018. Fatigue strength of laser CO_2, fiber laser and plasma cut edges made of S690QC and S1100. [Master's thesis] pp. 52.

Laitinen, R, Valkonen, I, Kömi, J. 2013. Influence of the base Material Strength and Edge Preparation on the Fatigue Strength of the Structures Made by High and Ultra-high Strength Steels. [e-document] Procedia Engineering 66. pp. 9.

Leitner, M, Khurshid, M & Barsoum, Z. 2017. Stability of high frequency mechanical impact (HFMI) post-treatment induced residual stress states under cyclic loading of welded steel joints. Engineering Structures 143. p. 589–602.

Lillemäe-Avi, I, Liinalampi, S, Lehtimäki, E, Remes, H, Lehto, P, Romanoff, J, Ehlers, S Niemelä, A. 2017. Fatigue strength of high-strength steel after shipyard production process of plasma cutting, grinding, and sandblasting. [e-document] pp. 11.

Mahrle, A & Beyer, E. 2009. Theoretical aspects of fiber laser cutting. Journal of Physics D: Applied Physics August 2009. [e-document] pp. 9.

Nykänen, T & Björk. T. 2015. Assessment of fatigue strength of steel buttwelded joints in as-welded condition -Alternative approaches for curve fitting and mean stress effect analysis. [e-document] Marine Structures 44. p. 288-310.

Nykänen, T, Mettänen, H, Ahola, A, Skriko, T, Hämäläinen, O.P, Björk, T. 2016. 3R-menetelmän käyttö vaihtuva-amplitudisesti kuormitettujen hitsausliitosten väsymisanalysoinnissa. Rakenteiden Mekaniikka Vol. 49, Nro 4. p. 176─201

Peippo J. 2015. A modified nominal stress method for fatigue assessment of steel plates with thermally cut edges. [Thesis] pp. 227.

Pessoa, D.F, Herwig, P, Wetzig, A & Zimmermann, M. 2017. Influence of surface condition due to laser beam cutting on the fatigue behavior of metastable austenitic stainless steel AISI 304. [e-document] Engineering Fracture Mechanics. Volume 185, November 2017. pp. 14.

Pirinen H. 2019. Fatigue strength of welded joints made of S1100 structural steel. [Master's thesis] pp. 91.

Rabb R. 2012. Todennäköisyysteoriaan pohjautuva väsymisanalyysi. Rakenteiden Mekaniikka Vol. 45, Nro 3, 2012, s. 162-187.

Riski J. 2017. Low-cycle fatigue of S960. [Master's thesis] pp.100.

Salo J. 2016. Fatigue strength of welded joints in super-duplex stainless steel. [Master's Thesis] pp. 93.

SFS-EN ISO 4288. 1998. Geometrical product specifications (GPS). Surface texture: profile method. Rules and procedures for the assessment of surface texture.

Skriko T. 2018. Dependence of manufacturing parameters on the performance quality of welded joints made of direct quenched ultra-high-strength steel. [Thesis] pp. 213.

SSAB 2006. Strenx 700 datasheet.

SSAB 2009. Strenx 700 MC Plus datasheet

Steen, W. 2010. Laser Material Processing. Fourth edition. Springer. ISBN 978-1-84996-061-8. pp. 58.

Stenberg, T, Lindgren, E, Barsoum, Z, Barmicho, I. 2017. Fatigue assessment of cut edges in high strength steel - Influence of surface quality. [e-document] Materials Science & Engineering Technology Volume 48, Issue 6 pp. 21.

Suresh, S & Ritchie, R.O. 1984. Propagation of short fatigue cracks. [e-document] International Metals Reviews Vol. 29, No 6. pp. 28.

Torres, M.A.S & Voorwald, H.J.C. 2002. An evaluation of shot peening, residual stress and stress relaxation on the fatigue life of AISI 4340 steel. International Journal of Fatigue 24 (2002) 877–886.

Vento, A. 2018. Poralaitteen puomin väsymiskestävyyden todentaminen laskennallisesti ja väsytystestaamalla. Hitsaustekniikka 3/2018. p. 21-24.

Wandera C. 2010. Performance of high power fibre laser cutting of thick-section steel and medium-section aluminum. [Thesis] LUT University. Digipaino. ISBN 952214973X, 9789522149732.

You, X, Wang, Z, Wang, Q, Cao, M, Shen, M & Huang, W. Effect of Shot Blasting on Fatigue Strength of Q345B Steel Plate with a Central Hole. [e-document] pp. 11.

Zanon, G, Bursi O.S, Scardi, P, D'Incau, M & Raso, S. 2017. Laser and mechanical cutting effects on the cut-edge properties of
steel S355N. Journal of Constructional Steel Research 133.

APPENDIX

$R_m := 1240$ Local hardness based value:

(HV hard (soft) / HV base material) * Rm base material

$H := 1.65 \cdot R_m = 2.046 \times 10^3$

$m_{ref} := 5.85$

$n := 0.15$

1. round

Notch factor from FEA or analytical calculation

Notch factor calculation

$t := 30$ Notch depth

$r := 100$ Notch radius

$$k_t := 1 + 2 \cdot \sqrt{\frac{t}{r}}$$

Notch factor selection on special cases
Small burr 1.3
Significant burr 1.5

Cut edge does not form over 1.5 notch factor with Rm > 780

Notch factor input from FEA

$k_{tfea} := 1.5$

$stress := 290$ Macrogeometrical stress FEA

$\Delta\sigma_k := stress \cdot k_{tfea}$ $R := 0.1$

$$\sigma_k := \frac{\Delta\sigma_k}{1 - R} = 483.333$$

Guideline for residual stress:

Base material	+fy, max 800 MPa
Cut edge measured or	200 MPa
Milled edge	250 MPa
Waterjet cutting	-300 MPa

Compressive or lovered residual stresses are possible from surface treatments

$\sigma_{res} := 200$ From cutting method and relative location to HAZ

$E := 207 \times 10^3$

$\sigma := 1$ $\Delta\sigma := 1$ GUESS

Given

$$\left[\left[\frac{\sigma}{E} + \left(\frac{\sigma}{H}\right)^{\frac{1}{n}}\right] - \frac{\left(\sigma_k + \sigma_{res}\right)^2}{\sigma \cdot E}\right] = 0$$

2. round

$\sigma_{max} := \text{Find}(\sigma) = 640.079$

Given

$$\frac{\Delta\sigma}{E} + 2\cdot\left(\frac{\Delta\sigma}{2\cdot H}\right)^{\frac{1}{n}} = \frac{\Delta\sigma_k^{\,2}}{\Delta\sigma\cdot E}$$

3. round

$\Delta\sigma := \text{Find}(\Delta\sigma) \rightarrow 434.93303487019805332$

$\sigma_{min} := \sigma_{max} - \Delta\sigma = 205.146$

$$R_{local} := \frac{\sigma_{min}}{\sigma_{max}} = 0.321$$

$C_{mean} := 10^{21.59}$ $C_{char} := 10^{20.83}$

$$N_f := \frac{C_{char}}{\left(\frac{\Delta\sigma_k}{\sqrt{1 - R_{local}}}\right)^{m_{ref}}} = 8.017 \times 10^4$$

$$N_{fl} := \frac{C_{mean}}{\left(\frac{\Delta\sigma_k}{\sqrt{1 - R_{local}}}\right)^{m_{ref}}} = 4.613 \times 10^5$$

Fatigue estimation with these values in case of surface crack initiation or under 10^6 cycles

Murakami hardness fatigue limit if fatigue crack initiation did not start from surface
If many possible defects choose defect with lower local hardness

$area := \sqrt{10}\cdot 30 = 94.868$ depth of defect, max 1000

$HV := 280$

$\alpha := 0.226 + HV\cdot 10^{-4} = 0.254$

$$\sigma_{limit} := \frac{[1.43(HV + 120)]}{(\sqrt{area})^{\frac{1}{6}}} \cdot \left[\left[\frac{(1 - R)}{2}\right]^{\alpha}\right] = 319.56$$

Modified 4R-method fatigue estimation result

If stress < σlimit then lifetime 10^7